Thesis for the degree
Doctor of Philosophy

Submitted to the Scientific Council of the
Weizmann Institute of Science
Rehovot, Israel

עבודת גמר (תזה) לתואר
דוקטור לפילוסופיה

מוגשת למועצה המדעית של
מכון ויצמן למדע
רחובות, ישראל

By
Hilla Afargan-Gerstman

מאת
הילה אפרגן-גרסטמן

השינוי העונתי בעוצמת הסופות בקווי הרוחב הבינוניים

The Seasonal Cycle of Midlatitude Storm Tracks

Advisor:
Prof. Yohai Kaspi

מנחה:
פרופ' יוחאי כספי

December 2017

טבת תשע"ח

Acknowledgments

First and foremost I would like to thank my advisor Yohai Kaspi, for his great inspiration, as a person and as a researcher, throughout my graduate studies. Working with Yohai has been an outstanding experience. I deeply appreciate his guidance throughout many hours of challenging and enlightening conversations over fundamental scientific problems, and always with a sense of humor. Thank you for standing by my side during difficult times and believing in my work.

I would like to thank my committee members Ilan Koren and Nili Harnik for their guidance throughout my PhD, and for motivating me to ask better scientific questions. I thank Orli Lachmy for enlightening scientific discussions and advice. I thank Orit Altaratz-Stollar for her guidance and support, and for her unique, optimistic point of view. Thanks to Ishai Dror for his advice and support, and for being a good listener. Thanks to Eli Galanti for his willingness to help.

Thanks to my colleagues and friends at the Weizmann Institute, Talia Tamarin, Janni Yuval, Rei Chemke, Marzia Parisi and Ilai Guendelman for many useful scientific discussions and help. Special thanks to Morgan E. O'Neill for motivating my scientific interest during the long hours in the office. Thanks to Nir Bluvshtein for helping me stay motivated.

I would like to express my appreciation to Professor Daniella Goldfarb and to the Weizmann Institute of Science for encouraging young women in science to pursue a scientific career and for providing useful leadership skills. Thanks to other members of the Department of Earth and Planetary Sciences at the Weizmann Institute for making my time in the department pleasant and joyful. I gratefully acknowledge the financial support provided by the Rieger Foundation graduate fellowship.

Thanks to everyone who believed in me. To my family, for teaching me that no matter what obstacles we encounter in life, we could overcome them if we are together. For my Mom and Dad, for allowing me to pursue my crazy dream to do a PhD in Atmospheric Sciences. The last six years have been a challenge for all of us, and I would not have made it as far without your support. To my Mom, for being my first teacher in life, for inspiring my interest in Mathematics and Science. For her willingness to travel more times than I can count between her home in Tiberias and wherever I was living, never complaining and always willing to help. To my dad, for inspiring my curiosity, my passion for knowledge and sense of independence. Thank you Harel, Racheli, Hod and Shani for being there for me whenever I needed, I would not have made it without all of you.

I would like to thank Uzi, my husband, for being the best person I have ever met. My achievements would not be possible without your patience, wisdom and generosity. I would also like to thank my daughters, Neta and Nitzan for being the light of my life. I have never imagined where this journey would take us, and I feel grateful every day.

This dissertation is dedicated to Hanan Einav-Levi.

"The answer, my friend, is blowin' in the wind" (Bob Dylan, 1962)

I hereby declare that this thesis summarizes my own independent research

Abstract

Midlatitude storm tracks are dominant features of the atmospheric circulation, transferring most of the heat, momentum and moisture in the extratropics. Despite their importance, the mechanisms controlling their seasonal variability are not fully understood. Over the North Pacific, transient eddy activity exhibits a distinct minimum during midwinter while reaching its maximum in late-fall and early-spring. This behavior occurs despite the enhanced jet and baroclinicity during midwinter, and is known as the Pacific midwinter minimum paradox. To explore the mechanisms that control the seasonal cycle of midlatitude storm tracks, we perform both observational analysis and numerical modeling. For the observational analysis, the seasonal cycle of storm tracks over the Pacific and Atlantic basins is explored using a 57-years reanalysis dataset. Particularly, the relationship between storm track intensity and the strength of the jet over the Atlantic is examined in years of a strong jet. It is found that in the Atlantic, similar to the well-known Pacific case, a midwinter minimum exists and is more pronounced when the jet is stronger. We find that in those years of a midwinter minimum the jet is more equatorward, resulting in less eddies, while for a more poleward eddy-driven jet, eddies tend to intensify. For the modeling study, we use an idealized moist atmospheric general circulation model (GCM) in which we implement an idealized seasonal cycle by varying the radiative parameters of the model. This allows to examine a wide range of climates, simulated by varying the top-of-atmosphere insolation. The model was used with several levels of complexity. First, the relationship between the strength of the subtropical jet (and the Hadley circulation) and storm track intensity in the zonally-symmetric model, without topography or land-sea contrasts, is investigated. We find that strengthening of the subtropical jet, which in the idealized GCM we explore by increasing the ocean heat flux, leads to baroclinic wave growth in the vicinity of the jet and to a weakening of near-surface baroclinicity in midlatitudes. In the next level of complexity, the response of the storm track seasonal cycle to changes in the strength of the subtropical jet in a zonally-asymmetric configuration is examined. We find that a midwinter minimum of storm track intensity occurs in the model when a Gaussian-shaped mountain is implemented in the idealized model. The minimum becomes more pronounced as the strength of the subtropical jet is increased. By analyzing the energy budget, we find that reduced storm track intensity in midwinter can be explained by increased barotropic energy conversion in the subtropics, leading to loss of eddy energy, together with an equatorward shift of the baroclinic and the barotropic conversion peaks, resulting in an additional eddy energy loss in midlatitudes. The midwinter minimum in the model occurs when the Gaussian mountain resembles the Tibetan Plateau (in terms of height, width and latitudinal position) and thus generating a “Pacific”-like storm track. When an “Atlantic”-like configuration is applied, the midwinter minimum is less pronounced, indicating the role of stationary features in controlling this phenomenon.

תקציר

סופות בקווי הרוחב הבינוניים הן רכיב מרכזי של הסירקולציה האטמוספירית, ואחראיות בין היתר על הסעת מרב החום, התנע והלחות בקווי הרוחב הבינוניים. על אף חשיבותם, המנגנונים השולטים בשינויים העונתיים של הסופות אינם מובנים במלואם. מעל לאוקיאנוס השקט, ישנה החלשות של פעילות הסופות במהלך החורף, בעוד במהלך עונת הסתיו והאביב ישנה התחזקות והם מגיעים לשיאם. תופעה זו מתרחשת על אף התחזקותו של זרם הסילון והתגברותה של הברוקליניות במהלך החורף, וידועה בשם "המינימום החורפי" של רצועת הסופות מעל האוקיאנוס השקט. במטרה לחקור את השינוי העונתי של הסופות בקווי הרוחב הבינוניים, אנו מבצעים אנליזה של תצפיות ומחקר באמצעות מודל נומרי. עבור האנליזה התצפיתית, אנו משתמשים במאגר נתונים של 57 שנים של רה-אנליזה על מנת לבחון את עוצמת הסופות מעל האוקיאנוס השקט ומעל האוקיאנוס האטלנטי. אנו מתמקדים בקשר שבין עוצמת הסופות ובין עוצמתו של זרם הסילון מעל האוקיאנוס האטלנטי בשנים של זרם סילון חזק. נמצא כי מעל האטלנטי, בדומה לאוקיאנוס השקט, קיימת החלשות חורפית של עוצמת הסופות, והיא נעשית מוגברת כאשר זרם הסילון חזק יותר. בנוסף, אנו מוצאים כי בשנים אלו מיקומו של זרם הסילון דרומי יותר. תופעה זו מציעה קשר בין היותו של זרם הסילון יותר סובטרופי בחורף, דבר הגורם להיחלשות הסופות. עבור המחקר הנומרי, אנו משתמשים במודל סירקולציה כללית (GCM) אידיאלי, בו יישמנו מחזור עונתי באמצעות שינוי פרמטרים קרינתיים של המודל. בשיטה זו אנו יכולים לבחון טווח רחב של אקלימים, תוך כדי שינוי של קרינת השמש בשכבות העליונות של האטמוספירה. אנו משתמשים במודל במספר רמות של מורכבות. בשלב ראשון, אנו חוקרים את הקשר בין עוצמת זרם הסילון הסובטרופי (וסירקולצית האדלי) ועוצמת הסופות בעזרת מודל בעל סימטריה זונאלית, ללא טופוגרפיה וללא יבשות, ומבצעים השוואה בין תוצאות המודל לתצפיות. אנו מוצאים כי התחזקותו של זרם הסילון הסובטרופי מביאה להתחזקות הסופות בקרבת זרם הסילון, ולהיחלשות של הברוקליניות בקווי הרוחב הבינוניים. בשלב הבא, השינוי במחזור העונתי של הסופות בתגובה לשינויים בעוצמת זרם הסילון הסובטרופי נחקרת במודל א-סימטרי, אליו הוספנו טופוגרפיה בעלת מבנה גאוסיאני. מצאנו שתופעת המינימום החורפי מתרחשת במודל הא-סימטרי האידיאלי. המינימום נעשה יותר משמעותי ככל שעוצמת זרם הסילון מתגברת, תהליך אשר ניתן לשלוט בו על ידי חיזוק מעבר החום בין האוקיאנוס לאטמוספירה באזור הטרופי. באמצעות אנליזה של מעברי האנרגיה בין הסופות לבין זרם הסילון, אנו מוצאים שבעונת החורף ישנה הסטה דרומה של מעברי האנרגיה הברוקלוניים והברוטרופיים, ביחס לסתיו ולאביב, והסופות מאבדות יותר אנרגיה קינטית בעיקר באזור הסובטרופי ובקווי הרוחב הגבוהים, דבר אשר משפיע על המחזור העונתי של עוצמתן. תופעת המינימום החורפי של עוצמת הסופות מתרחשת במודל כאשר ממדי ההר הגאוסיאני דומים לממדי הרמה הטיבטית (במושגים של גובה, רוחב ומיקום), ועל כן יוצרים רצועת סופות אשר דומה לרצועת הסופות מעל האוקיאנוס השקט. כאשר אנו משנים את ממדי ההר על מנת ליצור רצועת סופות "אטלנטית", תופעת המינימום החורפי נעלמת כתוצאה מהשינוי, דבר המעיד על חשיבותם של הגלים הסטציונרים (והאינטרקציה בין זרם הסילון הסובטרופי לטופוגרפיה) בהתהוותו של המינימום החורפי בקווי הרוחב הבינוניים.

Contents

1 Introduction **9**

1.1 Motivation 9

1.2 Basic aspects of midlatitude climate 10

1.3 Seasonal variability of midlatitude storm track 12

2 The Atlantic storm track midwinter minimum **17**

2.1 Motivation 17

2.2 Data and methodology 17

2.3 The Atlantic midwinter minimum in climatology 18

2.4 The relation between jet intensity and the storm track minimum 22

2.5 The relation between the storm track minimum and NAO variability 26

2.6 The relation between jet latitude and the storm track minimum 28

2.7 Discussion and conclusions 30

2.8 Appendix A: Statistical significance 33

2.9 Appendix B: Comparison with the previous studies of Nakamura (1992) and Penny et al. (2010) 34

3 The seasonal cycle of midlatitude storm tracks. Part I: zonally-symmetric idealized GCM **36**

3.1 Introduction 36

3.2 Model description 37

3.3 Development of the seasonal model 37

3.3.1 Seasonally-varying solar radiation 37

3.3.2 Top of the atmosphere albedo 38

3.3.3 Seasonally-varying longwave absorption 39

3.3.4 Surface heat capacity 41

3.3.5 Prescribed seasonally-varying ocean heat flux 41

3.4 Surface temperature response to seasonal radiative forcing 41

3.4.1 Equator-to-pole surface temperature structure . . . 43
3.5 Model climatology . . . 45
3.5.1 Reference climate . . . 47
3.6 Series of simulations . . . 48
3.7 Storm track response to variations in subtropical jet strength . . . 49
3.7.1 Model description . . . 49
3.7.2 Simulated storm track seasonal cycle . . . 51
3.7.3 Seasonal variation of baroclinicity, shear and static stability . . . 55
3.8 Model simulations with longer orbital period . . . 57
3.9 Discussion . . . 60

4 The seasonal cycle of midlatitude storm tracks. Part II: zonally-asymmetric idealized GCM 62
4.1 Introduction . . . 62
4.2 Idealized GCM with a Gaussian mountain . . . 63
4.2.1 Sensitivity to the longitudinal width of the mountain . . . 64
4.2.2 Sensitivity to the latitudinal position of the mountain . . . 66
4.3 Storm track response to variations in subtropical jet strength . . . 67
4.4 Eddy-mean flow energy cycle . . . 69
4.5 Atlantic storm track response . . . 75
4.6 Discussion . . . 77
4.7 Appendix A: MWM Index and subtropical jet strength . . . 78
4.8 Appendix B: Seasonal variability of lower-level baroclinicity . . . 78
4.9 Appendix C: Seasonal variation of the EP Flux . . . 80

5 Summary and conclusions 82

List of Abbreviations

Acronym	Definition
GCM	General Circulation Model
NH	Northern Hemisphere
SH	Southern Hemisphere
EKE	Eddy Kinetic Energy
EMFC	Eddy Momentum Flux Convergence
NCEP	National Centers for Environmental Prediction
ECMWF	European Centre for Medium-Range Weather Forecasts
MWM	Midwinter Minimum
SON	September-November
DJF	December-February
MAM	March-May
JJA	June-August
JFM	January-March
BC	Baroclinic
BT	Barotropic

Chapter 1

Introduction

1.1 Motivation

The main goal of my PhD was to better understand the mechanisms controlling the seasonal cycle of midlatitude storm tracks, and their response to changes in forcing. Despite their importance to midlatitude weather and climate, the mechanisms controlling storm track seasonal variability are not fully understood. Linear theories of baroclinic instability (e.g., Charney, 1947; Eady, 1949) provided significant insights on the influence of the zonal mean flow on generation of baroclinic eddies. According to these theories, midlatitude baroclinic eddies should reach their maximum amplitude when the meridional temperature gradients and jet are maximized. However, in the Northern Pacific transient eddy activity (expressed using either Eulerian or Lagrangian measures) exhibits a relative decrease during the winter season (Nakamura, 1992; Penny et al., 2010) and contradicts linear theory predictions. The goal of this work is to study this midwinter suppression of storm track eddy activity and its sensitivity to changes in the strength of the subtropical jet. Its complexity involves multiple time scales - seasonal and interannual, as well as zonal asymmetries due to topographic features and land-ocean interactions.

While some modeling studies have been able to reproduce the midwinter suppression using full comprehensive general circulation models (GCMs), identifying and isolating mechanisms from those is rather complex. Here, in attempt to better understand the mechanisms controlling the midwinter minimum, we use an idealized GCM in which we can vary systematically some of the properties of the general circulation. Despite the idealized model lacking the complexity of the full GCMs, we show that it is able to simulate the midlatitude storm tracks, and in particular it captures the seasonal variability of the Pacific storm track, including a midwinter suppression of eddy activity under certain conditions.

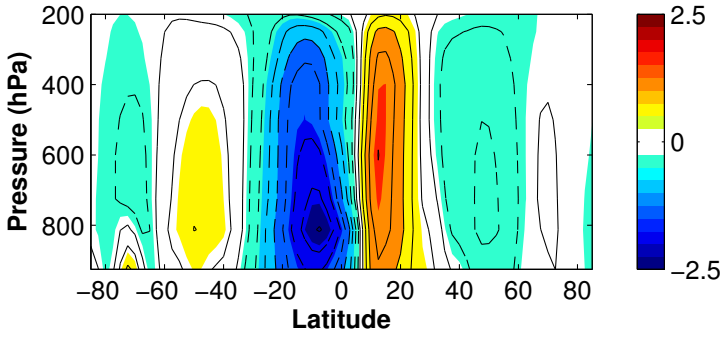

Figure 1.1: Annual mean meridional circulation (filled contours, kg s^{-1}, contour interval 1×10^9 kg s^{-1}). Data is based on NCEP reanalysis, averaged between 1958-2014.

1.2 Basic aspects of midlatitude climate

Atmospheric motions are generated by the variations in heating of Earth's surface due to the meridional gradients of insolation, albedo and other factors. By transporting energy, the winds acts to reduce the effects of these heating variations in the atmosphere. The distribution of the zonal mean wind indicates that the zonal wind is westerly throughout most of the atmosphere, and peaks in the subtropical jet stream around latitude 30° and at altitude of about 12 km (∼250 hPa). At the surface, the zonal wind is westerly at most latitudes between 30°-70°N, except in the tropics (30°S - 30°N) where easterly wind prevails.

The mean meridional circulation can be described using the zonal-mean meridional and vertical wind velocities, as the mass streamfunction

$$\psi(\phi,\mathrm{p}) = 2\pi\mathrm{a}\int_0^{\mathrm{p}} \mathrm{v}\cos(\phi)\,\frac{\mathrm{dp}}{\mathrm{g}}, \tag{1.1}$$

where ϕ is latitude and a is the radius of the Earth, v is the meridional wind speed and p is pressure level.

The mean meridional circulation in each hemisphere is dominated by a large circulation cell, known as the Hadley cell (Fig. 1.1). The Hadley cell is a thermally direct cell, in which warm air rises near the equator, moves poleward (in the winter hemisphere) at the upper levels, and descends in the subtropics. At the surface, the mean meridional winds bring air back toward the equator. In winter, the upward branch is shifted slightly into the summer hemisphere, forming a cross-equatorial Hadley cell (Fig. 1.2). In equinox seasons, the mean meridional circulation consists of two Hadley cells located at each side of the equator. Within the Hadley cell, the poleward flowing air conserves its angular momentum, leading to zonal wind that increases away from the equator, before it sinks in the subtropics.

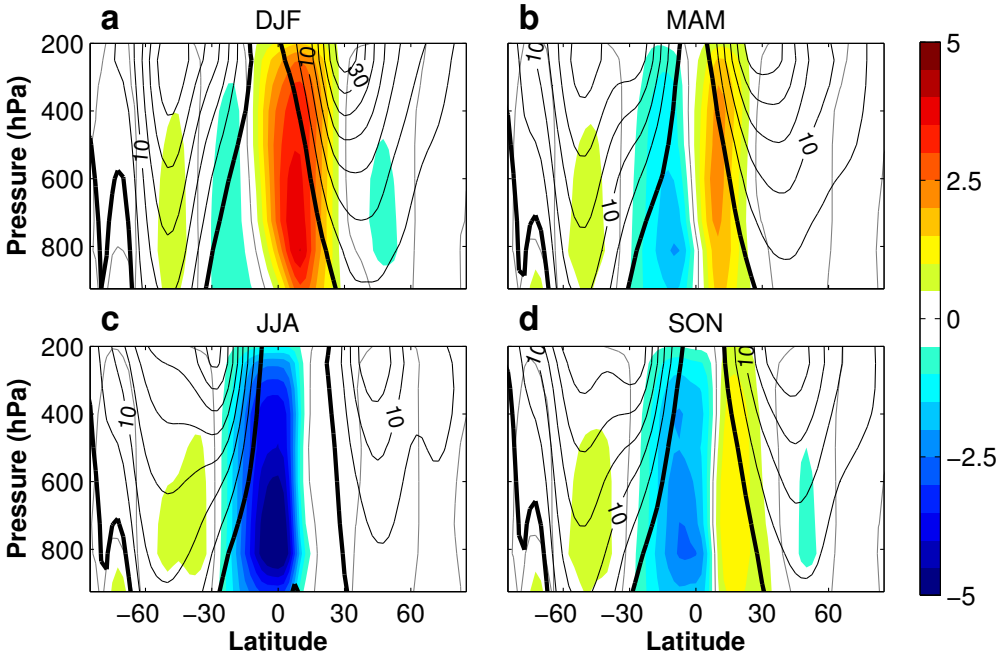

Figure 1.2: Seasonal variation of the mean meridional circulation (filled contours, kg s^{-1}, contour interval 1×10^9 kg s^{-1}, zero value is denoted in gray) and zonal winds (black contours, contour interval 5 m s^{-1}). Data is based on NCEP reanalysis, averaged between 1958-2014.

In the midlatitudes, weaker cells called the Ferrel cells exist. In these cells the overturning circulation is reversed, with rising of colder air at around 60°N and sinking in the subtropics. The Ferrel cells are considered thermally indirect, as they transport air from cold temperature into warm temperature areas. The Ferrel cells balance the eddy momentum flux convergence in midlatitudes, and are driven by midlatitude eddies. These eddies are the deviations from the time or the zonal mean, and are important features of the atmospheric circulation.

Weather variations in the midlatitudes (i.e., cyclones and anticyclones) can be expressed as deviations from the time mean (i.e., "transient eddies").

$$u' = u - \overline{u}, \tag{1.2}$$

These disturbances are associated with rapidly developing (and decaying) weather systems, with typical synoptic timescale of less than 10 days. Other variations are associated with stationary features, such as continents, topography and oceans, and can be expressed as the deviations of the time mean from its zonal average (i.e., "stationary eddies").

$$\overline{u}^* = \overline{u} - [\overline{u}], \tag{1.3}$$

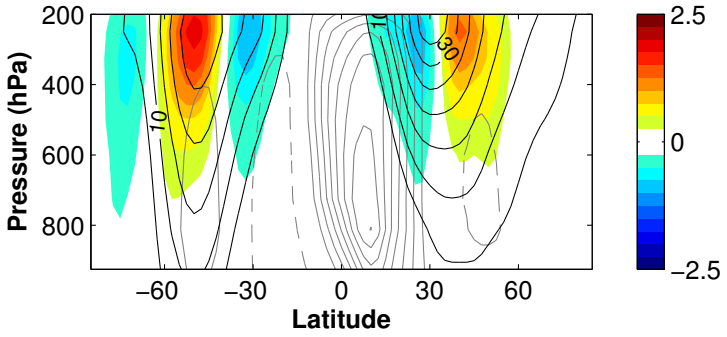

Figure 1.3: DJF transient eddy momentum flux convergence (color contours, 10^{-5} m s^{-2}) and zonal wind (black contours, contour interval 5 m s^{-1}). Mean meridional circulation is denoted in gray contours (kg s^{-1}, contour interval 1×10^{9} kg s^{-1}). Data is based on NCEP reanalysis, averaged between 1958-2014.

Historically, the preferred regions of storm (cyclone) activity, also known as the storm tracks, where defined by tracking midlatitude disturbances (Chang et al., 2002). Blackmon (1976) and Blackmon et al. (1977) showed that time filtering of weather maps to isolate disturbances with periods of 2-6 days captures the O(1000 km) spatial-scale synoptic systems, and provides an alternative definition of storm tracks as "geographically localized maxima in bandpass transient variance" (Chang et al., 2002). An example of the midlatitude storm track is shown in Fig. 1.4c,d, where the storm track appear as a band of enhanced eddy kinetic energy (EKE) averaged over the Pacific and the Atlantic basins, respectively. EKE is computed using a 3-10 days bandpass filter of daily zonal and meridional winds (see Fig. 1.4 caption).

If we look more closely at the mean zonally-averaged wind in Fig. 1.2 we can identify hints of two jets in each hemisphere, particularly in northern hemisphere winter (JJA). One is the subtropical jet, located around latitude 30° and associated with the strong meridional temperature gradient at the edge of the Hadley cell and has a relatively baroclinic structure. The second jet is located in midlatitudes, it has a more barotropic structure with less vertical shear than the subtropical jet, and is driven by momentum flux convergence by transient eddies, and is known as the eddy-driven jet. A third type of jet is a "merged jet" (Lachmy and Harnik, 2014), a single jet inside the Ferrel cell that is created by a merging of the subtropical and eddy-driven jets (an example of such a jet is the zonally-averaged jet in the northern hemisphere, shown in Fig. 1.3).

1.3 Seasonal variability of midlatitude storm track

In midlatitudes, storm tracks are dominant features of the atmospheric circulation, transferring heat, momentum and moisture to the extratropics. According to linear theories of baroclinic instability,

baroclinic growth of eddies is associated with regions of strong vertical shear of the westerly winds (e.g., Charney, 1947; Eady, 1949). These linear theories have made significant contribution to our understanding of the influence of the zonal mean flow on the generation of baroclinic eddies. However, eddy activity observed over the Northern Pacific during the winter season contradicts linear theory predictions, and suggests that the relationship between the mean flow and the eddies within the storm tracks may not be as straightforward as predicted. As shown by Nakamura (1992), baroclinic wave activity over the Northern Pacific is reduced in midwinter, relative to late-fall and early-spring, despite the enhanced baroclinicity and stronger westerlies. This reduction is referred to as the Pacific midwinter minimum (Fig. 1.4c). Recent studies have suggested that such a midwinter suppression of eddy activity may occur in other regions as well. A midwinter minimum has been observed in the upstream region over East Asia (Penny et al., 2010; Ren et al., 2010), and a weak signal of winter suppression has been identified in the North Atlantic (Ren et al., 2014).

The relation between the observed strengthening of the Pacific jet during midwinter and the associated decrease in eddy activity has been discussed in several studies. Nakamura (1992) has shown that on the interannual, as well as on the seasonal time scales, a positive correlation between the intensity of the storm track and the strength of the jet exists as long as the speed of the jet is below $\sim$45 m s^{-1}. Above this threshold, the correlation becomes negative and storm track intensity is decreased as the jet strengthens (see also Christoph et al., 1997). In addition, observational studies indicate that strengthening of the jet is not necessarily associated with intense baroclinic growth, as occurs in the southern hemisphere, where baroclinic growth has been shown to be weaker along an intense subtropical jet (Nakamura and Shimpo, 2004). In addition, Sampe et al. (2010) suggests that storm tracks (particularly in the lower levels of the atmosphere) tend to coincide with oceanic frontal zones with sharp SST gradients, rather than with the intense subtropical jet, as also shown by the simulations of Brayshaw et al. (2008).

It has been suggested that increased advection by the strong westerlies may suppress eddy growth, by causing the eddies to move fast out of the baroclinic region before they reach large amplitudes (Nakamura, 1992; Chang, 2001). Moreover, the strong westerlies also lead to a less efficient energy conversion from the mean flow to the eddies (Chang, 2001; Nakamura et al., 2002). Nakamura and Sampe (2002) showed that winters of pronounced midwinter minimum are associated with stronger jets, suggesting that the intensified jet suppresses baroclinic growth by trapping the upper-level disturbances within the subtropical jet, meridionally away from the surface baroclinic zone. Other studies have focused on variations in the jet structure and their relation to storm track activity. Harnik and Chang (2004) examined the effects of variations in the jet width on the growth of baroclinic waves, and showed that weakening of the storm tracks during periods of strong jets can be related to the narrowing of the jet during that time. However, while this effect may be important for interannual variability, they showed that the seasonal changes in the width of the jet are relatively small and cannot

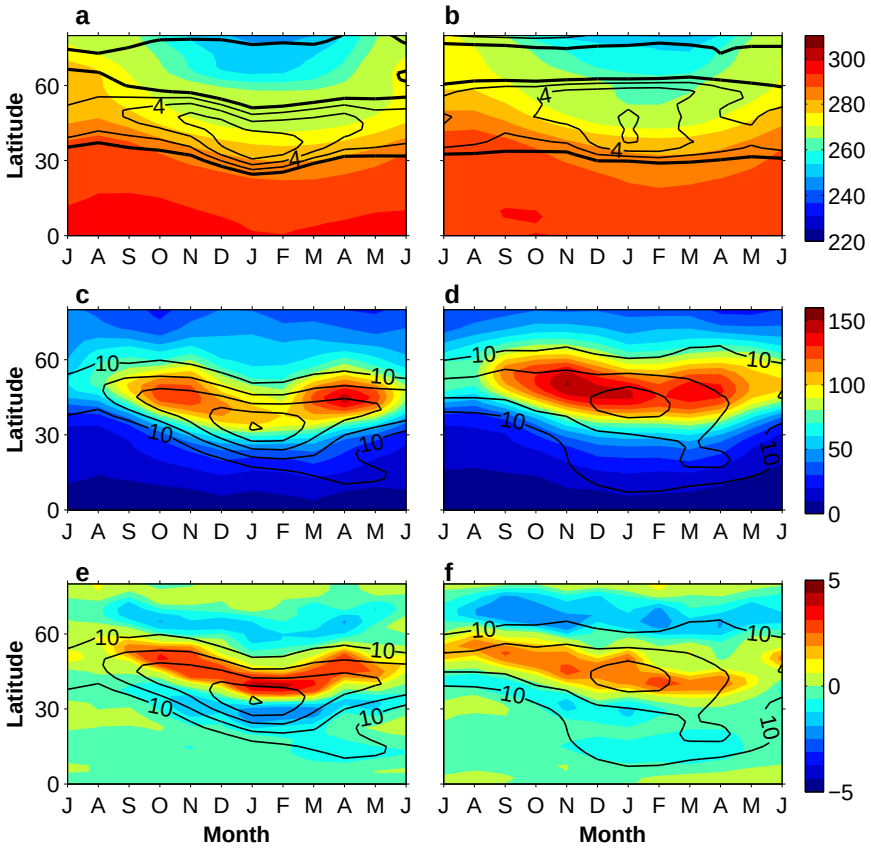

Figure 1.4: Observed zonally-averaged surface temperature (color contours, K) and near-surface zonal wind (black contours, m s^{-1}) zonally-averaged over (a) the Pacific (160°E-160°W) and (b) the Atlantic (30°-70°W) basins. (c-d) EKE at 300 hPa ($\frac{1}{2}(\overline{u'^2} + \overline{v'^2})$, color, m^2 s^{-2}) and upper-level zonal wind (black contours, m s^{-1}) at the same vertical level, averaged over the (c) Pacific and (d) Atlantic basins. (e-f) 300-hPa eddy momentum flux convergence (color, 10^{-5} m s^{-2}) and 300-hPa zonal wind (black contours, m s^{-1}) averaged over the (e) Pacific and (f) Atlantic basins. Data is based on NCEP reanalysis, averaged between 1958-2014. Similar seasonal patterns are observed for vertically-integrated EKE (see Fig. 2.1).

account for the midwinter suppression. Deng and Mak (2005) suggested that a midwinter suppression could be a result of a significant increase in the shearing and stretching deformation of the jet over the North Pacific in midwinter, resulting in a barotropic governor type mechanism (James, 1987), where reduction in the growth rate of baroclinic waves could be a result of increased barotropic shear within the wintertime jet. Yuval and Kaspi (2016) showed that the reduction in Pacific eddy kinetic energy (EKE) during midwinter might be related to differences in the vertical structure of baroclinicity between midwinter and the shoulder seasons.

More recent studies explored the effect of topography and stationary waves on the seasonal cycle of the storm tracks (Park et al., 2010; Lee et al., 2013; Penny et al., 2010). In particular, a reduction in

the seeding of baroclinic waves propagating to the Pacific storm track from midlatitude Asia has been proposed as a mechanism for the midwinter suppression (Penny et al., 2010, 2011, 2013). However, other studies found a lack of a clear relation between interannual variability of the storm track and variability of upstream seeding in the Asian source region (Chang and Guo, 2011, 2012), suggesting a less dominant role of upstream seeding in controlling the midwinter minimum.

Park et al. (2010) found that the presence of central Asian mountains in GCM simulations suppress storm track intensity in the North Pacific during midwinter. They relate the suppression to a decreasing baroclinic energy conversion over eastern Asia, which reduces the number of disturbances entering the North Pacific. In addition, mountains modify stationary waves that change the zonal propagation of wave packets, causing them to be refracted more equatorwards, and therefore weakening the downstream development of the eddies. Penny et al. (2010) employed feature-tracking techniques to locate the source of the midwinter suppression. They found that disturbances entering the Pacific storm track from midlatitude Asia have a reduced frequency and amplitude. They suggest three possible mechanisms for the midwinter suppression, including seasonal changes in static stability over Asia that lead to trapping of the eddies into the jet core (in consistency with Nakamura and Sampe, 2002), a shift of the strong temperature gradients to the south, and interaction between upper-level waves and topography. In response, Chang and Guo (2011) have shown the lack of a clear relation between interannual variability of the storm tracks and variability in the Asian source region.

Lee et al. (2013) reproduced the seasonal cycle of the Pacific storm track using a full GCM, with realistic orography, and related the suppression during midwinter to the presence of the Tibetan Plateau, despite the fact that it strengthens baroclinicity along the Pacific jet. They identify three major factors for the midwinter minimum caused by the Tibetan Plateau. First, similar to Nakamura (1992), they found a negative correlation between the jet speed and eddy activity when the jet is stronger than 40 m s^{-1}. They relate the strengthening of the jet to a decrease in the barotropic energy conversion from the mean flow to the eddies. They suggest that this decrease is associated with the barotropic governor effect and to changes in the meridional shear which has been proposed by James and Gray (1986); James (1987). Second, consistent with Penny et al. (2010), they suggest that strong static stability and weak wind shear in January lead to a minimum in Eady growth rate and baroclinicity over the northern part of the Tibetan Plateau. Third, enhanced moist static energy due to sea surface temperatures increase, particularly in March, may result in strengthening of the storm tracks.

These studies have provided significant insight to the dominant processes controlling the Pacific midwinter minimum. Yet, a distinct mechanism has yet to emerge. While modeling studies using full comprehensive GCMs have been able to reproduce the midwinter suppression, identifying and isolating mechanisms from those is rather complex. Here, in attempt to better understand the mechanisms controlling the midwinter minimum, we use an idealized GCM in which we can systematically vary some of the properties of the general circulation. Despite the understanding that the idealized model

lacks the complexity of the full GCMs, we show that it is able to simulate the midlatitude storm tracks, and in particular it captures the seasonal variability of the Pacific storm track, including a midwinter suppression of eddy activity.

This thesis is organized as follows. In chapter 2, we present an analysis of the observed storm track seasonal cycle over the Pacific and the Atlantic oceans. Specifically, we focus on the occurrence of a midwinter minimum of storm track activity over the Atlantic domain and the relation between years of strong jet and a midwinter minimum of EKE. Chapter 3 describes the model, an idealized moist GCM with a seasonally-varying forcing. The zonally-symmetric model configuration is described, and the model ability to reproduce a realistic climate is demonstrated. In chapter 4, the zonally asymmetric storm track is examined and storm track response to variations in the strength of the subtropical jet (and the Hadley circulation) is explored. The results of this work and final concluding remarks are summarized in chapter 5.

Chapter 2

The Atlantic storm track midwinter minimum

2.1 Motivation

In this study, we examine the relation between jet strength and the seasonal cycle of the Pacific and Atlantic storm tracks, and demonstrate how a weak, yet statistically significant, midwinter minimum in storm track intensity can be found over the Atlantic as well. We show that winters with a stronger jet are associated with a more pronounced midwinter minimum in both the Pacific and the Atlantic storm tracks.

2.2 Data and methodology

We use daily reanalysis data over a 57-year period from January 1st 1958 to December 31st 2014 provided by NCEP/NCAR (National Centers for Environmental Prediction/National Center for Atmospheric Research). The full dataset consists of Reanalysis 1 between 1958-1980 (Kalnay et al., 1996) and Reanalysis 2 between 1981-2014 (Kanamitsu et al., 2002). The data has a horizontal spatial resolution of 2.5° $\times$ 2.5°. Storm track transient eddies are commonly represented by bandpass time filtering of atmospheric fields (Blackmon et al., 1977). We implement a Butterworth bandpass filter with a 3-10 days cutoff period, chosen to match the typical timescale of synoptic cyclones in midlatitudes. This bandpass filter is applied on daily horizontal winds to calculate the storm track EKE. The existence of the Pacific midwinter minimum of eddy activity is not sensitive to the choice of the bandpass cutoff frequencies (Christoph et al., 1997), nor is it sensitive to choosing only the NCEP Reanalysis 2 data set (1981-2014). Analysis is performed on eddy quantities and mean flow for both the Pacific (160°E-160°W) and Atlantic basins (30°-70°W). All eddy quantities are computed

using the same 3-10 days bandpass filter.

2.3 The Atlantic midwinter minimum in climatology

Over the Northern Pacific, the jet stream exhibits a pronounced seasonal cycle, with a strong, equatorward jet during winter, and a weaker, poleward jet during spring and fall (Fig. 2.1a). As found by Nakamura (1992), the associated EKE over the Northern Pacific is weaker in midwinter relative to fall and spring, decreasing by approximately 30% (Fig. 2.1a). The longitudinal distribution of 250-hPa EKE, meridionally-averaged between 20°-70°N (Fig. 2.2a), indicates that in addition to the well-documented Pacific midwinter minimum (160°E-160°W), it is possible to identify a midwinter decrease in EKE over the Atlantic as well (30°-70°W).

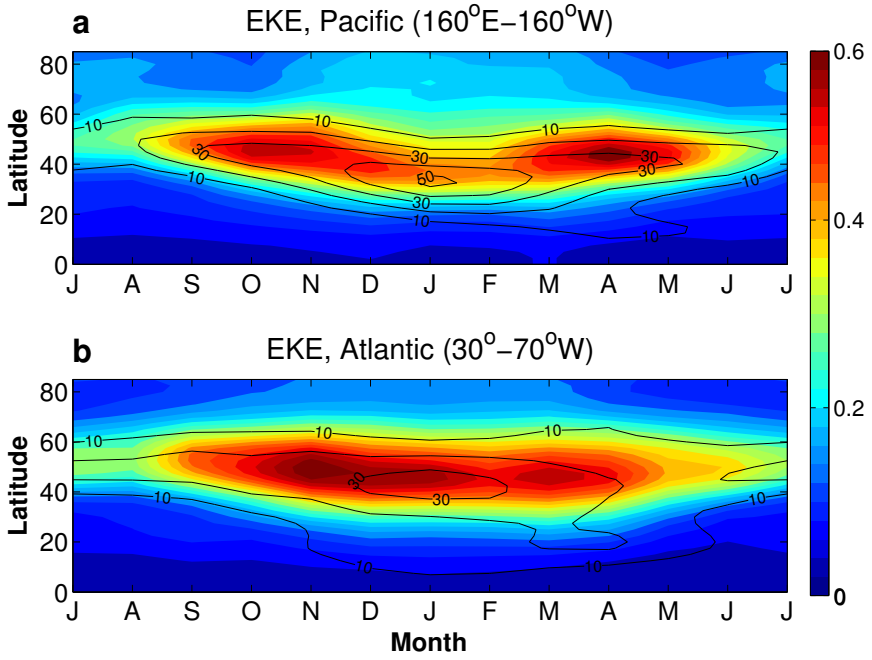

Figure 2.1: Observed zonally-averaged zonal wind (black contours, m s^{-1}), and EKE, vertically-integrated from the surface to 100 hPa ($\frac{1}{2g}\int(\overline{u'^2}+\overline{v'^2})dp$, color, MJ m^{-2}), zonally-averaged over (a) the Pacific (160°E-160°W) and (b) the Atlantic (30°-70°W) basins. Data is based on NCEP reanalysis, averaged between 1958-2014. Similar seasonal patterns are observed for upper level EKE (see Fig. 1.4).

The main contribution to the midwinter minimum, shown in Fig. 2.2a, comes from midlatitudes (40°-60°N), where eddy activity is decreased in midwinter over both the Pacific and the Atlantic basins (Fig. 2.2b). While the Pacific seasonal cycle is comprised of two distinct peaks, in November and in April, the seasonal cycle of the Atlantic storm track reaches its maximum EKE in November-

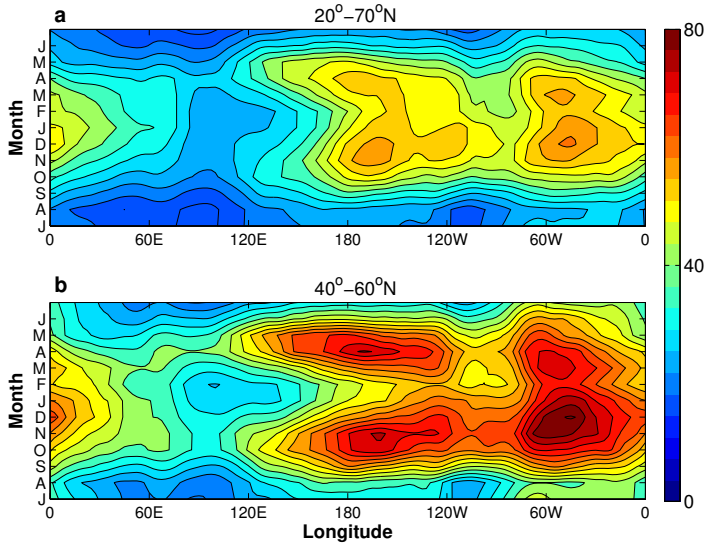

Figure 2.2: The longitude-temporal variation of 250-hPa EKE (m^2 s^{-2}) averaged between latitudes: (a) 20°-70°N, and (b) 40°-60°N.

December, followed by a minimum of nearly 10% during February, and a second maximum around March. Furthermore, a midwinter minimum can be found over Asia, upstream of the Pacific storm track (60°-120°E), in agreement with feature-tracking analysis (Penny et al., 2010).

The interannual variability of the Pacific and Atlantic storm tracks between 1981-2014 (Fig. 2.3) reveals that while over the Pacific the seasonal cycle tends to have a midwinter minimum in most years, as can also be seen in its climatology, over the Atlantic the year-to-year variability is larger, and a midwinter minimum is less prominent. In addition to the interannual variability of the storm track, there are notable changes in the relative intensity of the storm track over the seasonal cycle (Fig. 2.4). Midwinter suppression of EKE occurs in the upper-levels of the atmosphere, and is most apparent during January-February in the Pacific (relative to December and March). The Atlantic midwinter minimum during February, relative to the January and April, is clear in midlatitudes. Over both the Pacific and the Atlantic sectors, the jet shifts equatorward during January-February, and the vertical shear is largest then (Fig. 2.4).

The similarity of the storm track seasonal cycle between the Atlantic and the Pacific storm track seems to occur despite the differences in the jet characteristics. While the Pacific jet in mid-winter is more subtropical, the Atlantic jet is eddy-driven, forced by convergence of eddy momentum flux (e.g., Lee and Kim, 2003) and linked to the dominant modes of variability in the North Atlantic region such as the North Atlantic Oscillation (NAO). In the shoulder seasons, when the Hadley cell is weaker, the Pacific jet is more poleward (Fig. 2.1a), and more eddy-driven. The stronger eddies in the shoulder seasons may be associated with the different character of the jet or its more poleward location (Yuval and Kaspi, 2017). The fact that the Atlantic jet has less of a seasonal variation (Fig. 2.1b), and is

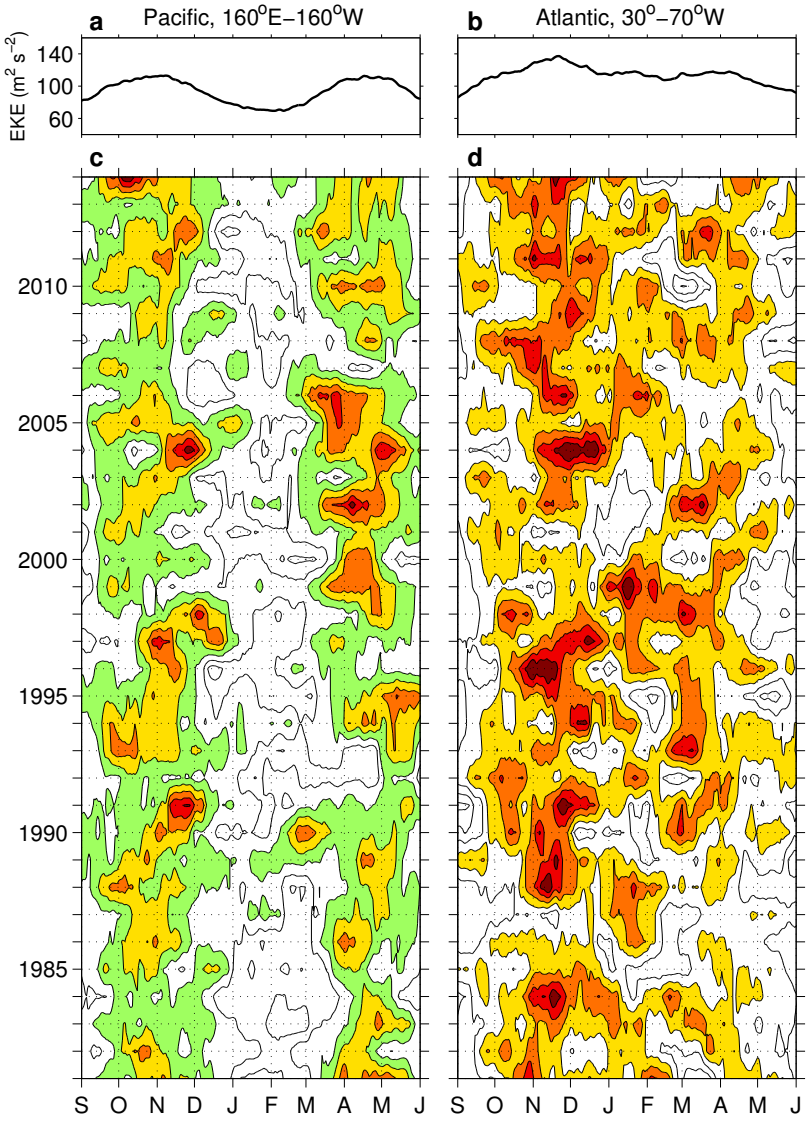

Figure 2.3: Year-month diagram of daily climatological (a,c) North Pacific and (b,d) North Atlantic storm tracks, shown by the 250-hPa EKE ($m^2\ s^{-2}$, contours every 20 $m^2\ s^{-2}$) between the years 1981-2014. EKE is averaged between latitudes 40°-60°N. Color contours start where the value exceeds 90 $m^2\ s^{-2}$ for the Pacific, and 110 $m^2\ s^{-2}$ for the Atlantic (color contours every 20 $m^2\ s^{-2}$, color coding is the same in both panels). Climatology for the entire period is shown in panels (a) and (b) for the Pacific and Atlantic domains, respectively. Results are smoothed using a 31-day running average.

generally weaker, may therefore lead to the midwinter minimum being less pronounced (Fig. 2.2 and Fig. 2.4). Lachmy and Harnik (2014) have shown that efficiency of eddy amplification is suppressed at lower latitudes, meaning that a stronger jet and more baroclinicity do not necessarily correlate with more eddies, a result which is consistent with the simulations of Brayshaw et al. (2008) and Sampe et al. (2010). In the Pacific, these conditions of strong jet and enhanced baroclinicity exist over most

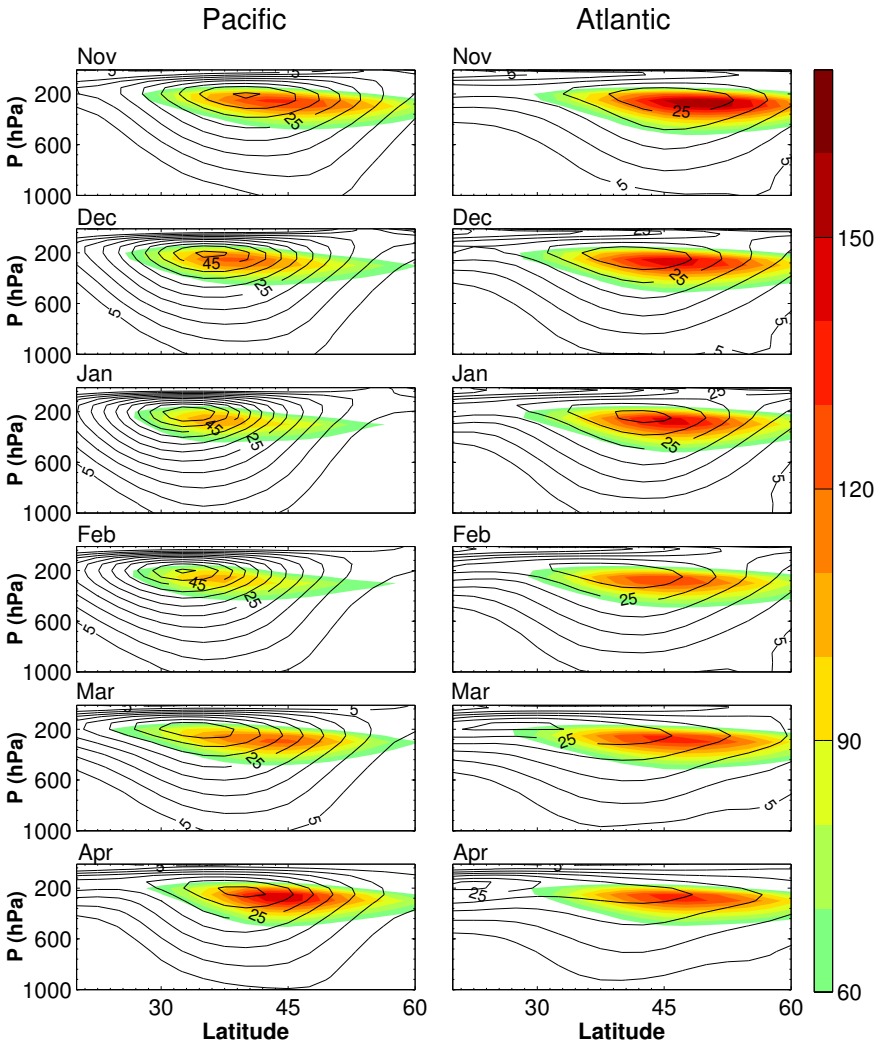

Figure 2.4: Zonally-averaged EKE (color, $m^2\ s^{-2}$, contour interval 10 $m^2\ s^{-2}$), and zonally-averaged zonal wind (black contours, m s^{-1}, contour interval 5 m s^{-1}) as a function of latitude and pressure averaged over the Northern Pacific and Northern Atlantic basins during each month between November and April.

years, possibly leading to a midwinter minimum; here, we show that in years when the Atlantic jet is stronger (and typically more equatorward) a midwinter minimum occurs over the Atlantic as well.

In the following section, we investigate the existence of a midwinter minimum in the Atlantic storm track, and examine how the strength of the Atlantic jet influences the storm track intensity throughout the seasonal cycle by performing an analysis based on years of strongest and weakest wintertime jet over the Atlantic. For comparison, we perform the same type of analysis for the Pacific as well, where the relationship between storm track intensity and jet strength is consistent with previous studies (e.g., Nakamura, 1992; Nakamura and Sampe, 2002; Penny et al., 2013). For the Atlantic such a relation has not been identified before.

2.4 The relation between jet intensity and the storm track minimum

Over the Pacific, winters of reduced eddy activity (and most pronounced minimum) are associated with a strong jet, which is nearly 10 m s^{-1} stronger relative to winters of increased eddy activity (Nakamura and Sampe, 2002). In order to examine the effect of this intensified jet on the seasonal cycle of the storm track we compare between 7 years of the strongest jet and 7 years of the weakest jet (hereafter referred to as "strong jet" and "weak jet" winters, respectively) in the North Atlantic and North Pacific domains. The criterion used for this analysis determines the strength of the jet according to the maximum intensity of the zonally-averaged 250-hPa zonal wind, averaged over the domain between January-March. The results are not sensitive to this height nor to the exact number of years chosen. For both sectors, the differences between years of strong and weak jet are statistically significant in midwinter, with over 90% confidence level.

Fig. 2.5a-d shows the seasonal cycle of EKE at 250 hPa for these two types of winters. To indicate the position of the jet, as well as its intensity, the 250-hPa zonally-averaged zonal winds are displayed. As expected, in years of strong jet over the Pacific (1970, 1978, 1981, 1983, 1984, 1995 and 2003), the midwinter suppression of EKE is more prominent relative to years of weak jet (1969, 1972, 1982, 1989, 1990, 2006 and 2009). Specifically, the minimum is more pronounced during January-February, when the jet is strongest. We note that EKE in midwinter is weaker relative to spring and fall also in years of weak Pacific jet (Fig. 2.5b), suggesting that the characteristics of the Pacific jet are favorable for a midwinter suppression even in those years of relatively weak jet in the subtropics.

A similar analysis of the Atlantic domain (Fig. 2.5a,c) reveals that in years of strong jet (1960, 1964, 1974, 1977, 1989, 2010 and 2014) EKE decreases in midwinter by nearly 30% relative to spring and fall, similar to the observed midwinter minimum in the Pacific. Such seasonal variations in EKE are not observed during years of weak jet over the Atlantic (1968, 1973, 1983, 1995, 1998, 2000 and 2012), in which the eddies reach their maximum intensity in winter. In years of strong jet, the jet is significantly more equatorward than years of weak jet (Fig. 2.5a,c). These differences in the jet and the storm track, between years of strong and weak jet, are statistically significant during midwinter, with over 90% confidence level.

To identify the position of the eddy-driven component of the jet, in which eddy momentum fluxes contribute to eastward flow, we examine the seasonal evolution of eddy momentum flux convergence over the Pacific and Atlantic basins (Fig. 2.5e-h). Over both domains eddies converge momentum in midlatitudes. However, over the Pacific, eddy momentum flux convergence occurs poleward of the jet during midwinter (around latitude 40°N), while over the Atlantic the maximum zonal wind coincides with regions of eddy momentum flux convergence throughout the year, except for periods when there is not a clear separation between subtropical and the eddy-driven jets (i.e., during March-April). In

years of strong jet, the eddy momentum flux convergence is stronger in the shoulder seasons (October-December, March-May) (Fig. 2.5g), leading to enhanced EKE in those seasons, while in midwinter (January-February), when the jet is more equatorward there are less eddies. Over the Pacific, though, eddy momentum flux convergence is maximal in midwinter, particularly in years of strong Pacific jet (Fig. 2.5h). Recently, Robert et al. (2017) have shown that the effect of strong shear by the mean flow may lead to a decrease of eddy energy through strong barotropic decay. This effect may explain the decrease in EKE during periods of strong jet (Fig. 2.5h).

EKE anomalies in years of strong and weak Atlantic jet To further explore the relation between the jet strength and the eddies, a composite map of zonal wind and EKE anomalies for winters of weak jet is shown in Fig. 2.6a,b and strong jet in Fig. 2.6c,d. Anomalies are computed relative to climatology averaged between the years 1958-2014. Both zonal wind and EKE are averaged between February-March, during the period of the most pronounced decrease in EKE. While in winters of weakest jet over the Atlantic, EKE is increased in midlatitude by nearly 30 m^2 s^{-2}, in winters of strongest jet EKE is decreased by about 20%. This inverse relation between the jet strength and eddies intensity is similar to what was found for the Pacific basin (Nakamura, 1992; Nakamura and Sampe, 2002; Penny et al., 2013), suggesting that similar mechanisms could be responsible for this behavior.

Zonally-averaged zonal wind, shown in Fig. 2.6, indicates that in years of weak jet in midlatitude, the zonal wind forms a double jet structure, with a stronger-than-average jet poleward of latitude 60°N, and another jet at latitude 40°N. This structure is consistent with the northern jet pattern described by Woollings et al. (2010)). In contrast, in winters of strong jet, the jet is located in the central Atlantic, with maximal zonal wind around latitude 45°N. We further investigate the role of jet latitude, associated with the North Atlantic Oscillation (NAO), the leading mode of variability in the North Atlantic, and storm track intensity in Section 2.5.

Eliassen-Palm (EP) flux in years of strong and weak Atlantic jet We calculate Eliassen-Palm (EP) flux vectors in the 3-10 days filtered fields. The horizontal components of the EP-vector is $E_h = (\overline{v'^2} - \overline{u'^2}, -\overline{u'v'})$ is plotted in Fig. 2.7. During winters of weak Atlantic jet (Fig. 2.7a), the EP vectors point dominantly eastward, indicating the main direction of wave propagation. The strongest divergence of the EP vectors (and convergence of the eddy momentum flux) occurs in the midlatitudes and in the downstream region of the storm track, indicating acceleration of the jet in these regions. However, in winters of strong jet (Fig. 2.7b), the main divergence occurs more equatorward. The eddies act to reinforce the jet in the downstream region, creating a more zonal and eastward-extended jet. Penny et al. (2013) have found similar differences between months of strong-core and weak-core jets over the Pacific domain; eddies maintain a stronger, eastward-extended and more subtropical jet

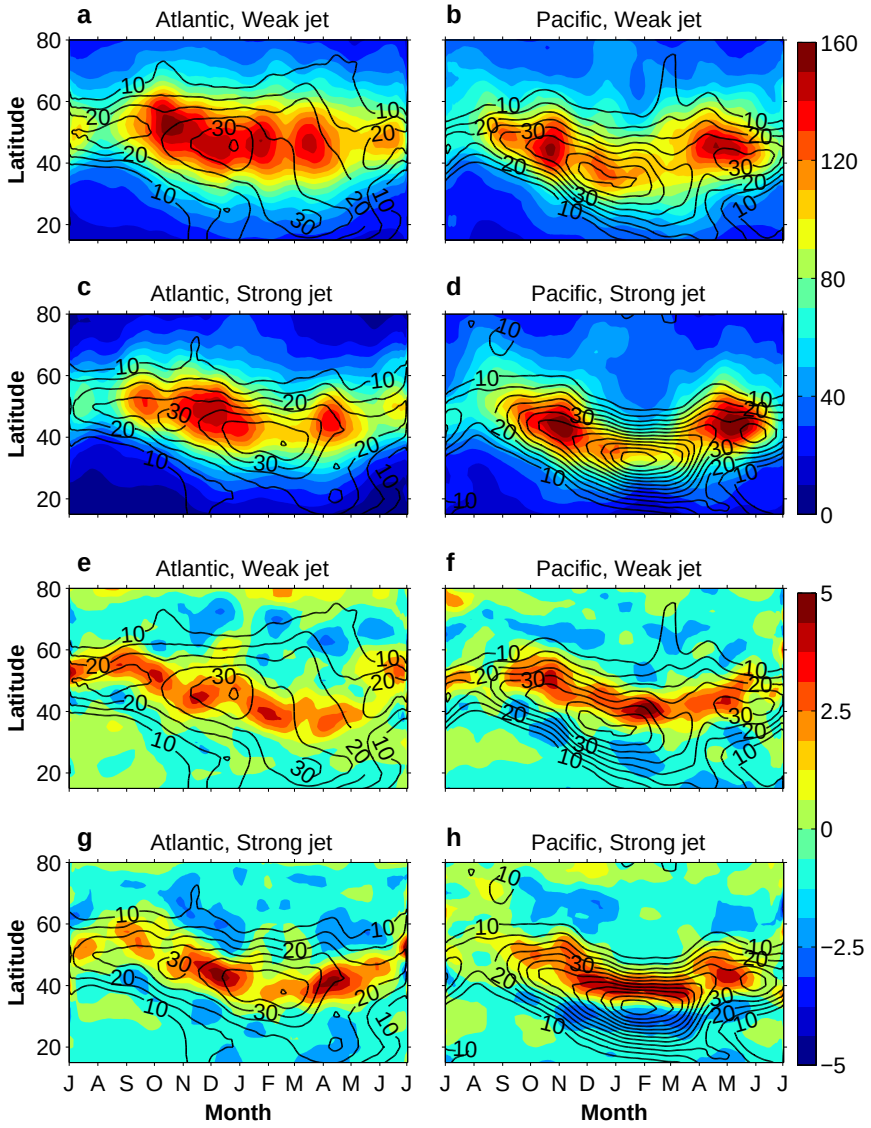

Figure 2.5: (a-d) 250-hPa daily EKE (color, $m^2\ s^{-2}$) and zonally-averaged zonal wind at 250 hPa (black contours, $m\ s^{-1}$) averaged over years of (a,b) weak jet, and (c,d) strong jet, over the Pacific and Atlantic domains. Results in midlatitudes for the months of November-March are statistically significant with 95% confidence level. Statistical significance was determined with Student's t-test. (e-h) Eddy momentum flux convergence at 250-hPa (color, $10^{-5}\ m\ s^{-2}$), and 250-hPa zonally-averaged zonal wind (black, $m\ s^{-1}$) in years of (e,f) weak jet, and (g,h) strong jet. Results are smoothed using a 31-day running average.

in winters of strong jet, with a weaker amplitude of eddy propagation. Nevertheless, as was also noted by (Penny et al., 2013), eddy forcing provides only a partial explanation to the differences in the jets between years of strong and weak jets, and on the interannual time scale, other factors, such as tropical diabatic heating, should also be taken into account (Seager et al., 2003, 2010).

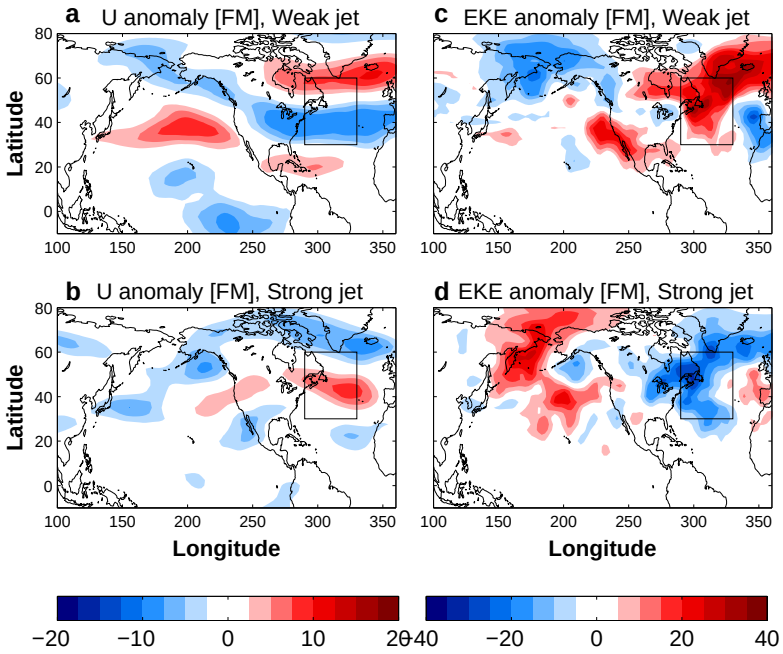

Figure 2.6: Anomalies from climatology of (a,b) 250-hPa zonal wind (m s^{-1}) and (c,d) EKE (m^2 s^{-2}) over the North Atlantic during winters of (a,c) weak and (b,d) strong Atlantic jet. Both fields are taken daily and averaged between February-March. The rectangle marks the boundaries of the Atlantic domain in Fig. 2.5.

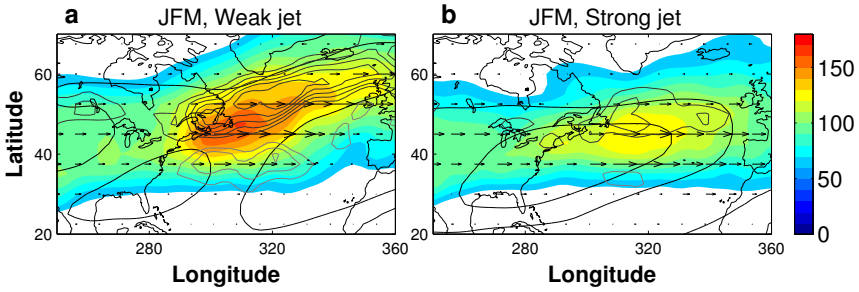

Figure 2.7: Horizontal component of the EP vectors at 250-hPa (arrows) and divergence of EP vectors (dark gray contours every 0.02 m s^{-1}) and convergence (light gray) during winters of (a) weakest jet and (b) strongest jet over the North Atlantic. Color contours show 250-hPa EKE (m^2 s^{-2}). Contours of 20 and 30 m s^{-1} upper-level zonal wind are indicated by black lines. The EP vectors are plotted every 7.5°. We use daily data averaged between January-March).

On the interannual time-scale, the strength of Atlantic storm track eddies and zonal wind speed are positively correlated for weaker wind speeds, and negatively correlated for stronger winds (Fig. 2.8). Storm track intensity tends to increase with jet strength for upper-level wind below 30 m s^{-1}, but decrease when the wind speed is higher than this threshold. This correlation resembles the complex relationship that was found for the Pacific (Nakamura, 1992; Christoph et al., 1997). However, for the

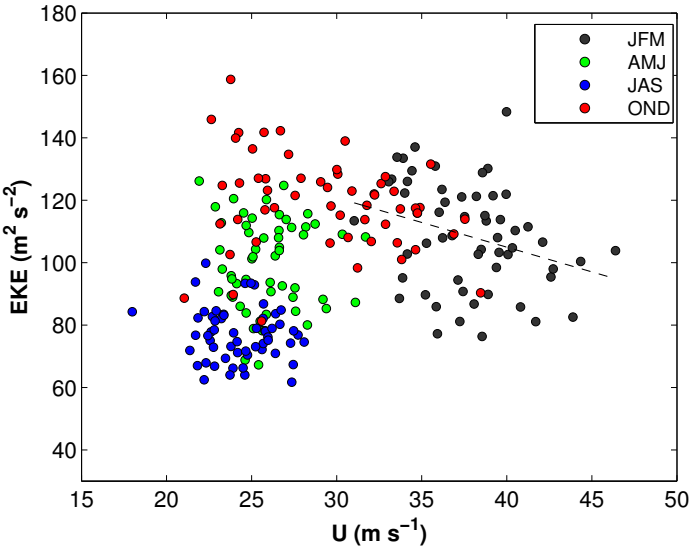

Figure 2.8: The relation between 250-hPa EKE (m^2 s^{-2}), averaged between 40°-60°N over the Atlantic, and the strength of the jet (m s^{-1}) at the latitude of maximum monthly-averaged zonal wind. A linear fit (dashed) indicates a negative slope of -1.5 m s^{-1}, with corresponding R^2 value of 0.15.

Pacific the peak is estimated around 45 m s^{-1}, and since zonal wind speeds over 45 m s^{-1} are rare over the Atlantic, it remained unclear if the negative correlation is a unique feature of the Pacific or if the same kind of complex relationship can be found in both basins (Christoph et al., 1997). Interestingly, we find that over the Atlantic the negative correlation mostly occurs during JFM (January to March), when the wind speed is more intense relative to the other seasons.

2.5 The relation between the storm track minimum and NAO variability

Over the North Atlantic, the dominant mode of atmospheric variability is the North Atlantic Oscillation (NAO), which is associated with a latitudinal displacement of the jet where positive and negative phases correspond to a poleward and equatorward shift of the jet, respectively (e.g., Hurrell, 1995; Thorncroft et al., 1993; Lee and Feldstein, 1996; Orlanski, 2003; Riviere and Orlanski, 2007; Woollings et al., 2010). We analyze the Atlantic storm track seasonal cycle in years of positive and negative NAO phases. For each composite, we choose seven years of strongest positive (negative) NAO index (by the CPC, http://www.cpc.ncep.noaa.gov/) averaged between January and March, respectively. As expected, in winters of negative NAO the jet position is relatively equatorward, around latitude 35°N, while in winters of positive NAO the jet is located nearly 10° poleward (Fig. 2.9). In terms of the wind speed, it is weakest in the negative NAO and highest in the positive NAO case.

Examining the storm track intensity reveals that in years of negative NAO the storm track seasonal cycle consists of a single maximum in fall, around November-December, and relatively weaker EKE during winter and spring (Fig. 2.9). This seasonal pattern of EKE is distinctively different than in years of positive NAO phase, in which EKE is relatively stronger throughout the year (fall to spring) with a slight decrease in January-February, similarly to the midwinter minimum pattern discussed above.

A composite map of the eddies intensity, shown in Fig. 2.10, indicates that during winters of negative NAO, when the jet is located further equatorward, the eddies are weaker relative to climatology in most of the North Atlantic sector, with a slight increase in EKE equatorward of latitude 40°N. In contrast, winters of positive NAO (Fig. 2.10c) are associated with the opposite pattern, with a decrease of EKE equatorward of latitude 40°N, and an increase of EKE more poleward. Yet, this pattern is less pronounced, resulting in only a slightly weaker EKE anomaly in the North Atlantic sector during winters of positive NAO phase.

Therefore, winters of equatorward jet position, associated with a negative phase of the NAO, show a stronger decrease in EKE in midlatitudes during winter (Fig. 2.10c), compared to winters of positive NAO (Fig. 2.9b). Yet, their seasonal cycle cannot be related with a midwinter minimum due to the absence of a second maximum of storm track activity in spring (Fig. 2.9a). On the other hand, winters of poleward jet position associated with a positive NAO phase show a clear midwinter minimum pattern (Fig. 2.9b), however this response is relatively small, suggesting that the midwinter minimum in years of positive NAO is only slightly more pronounced than in climatology (Fig. 2.2). Stronger differences are found during spring (March-April, not shown).

These findings suggest that a more pronounced suppression of storm track intensity is more likely to occur in the Atlantic during winters of negative NAO, when the jet shifts further equatorward. Consistently, Harnik et al. (2014) shows that eddy fluxes similar to those found during a negative NAO state are associated, together with changes in diabatic heating, with a regime transition of the eddy-driven Atlantic jet to a mixed thermally-eddy-driven jet, as found in the Pacific.

This relation between the jet latitude and midwinter weakening of eddy intensity implies a potential link to the Pacific storm track variability. Nakamura and Sampe (2002) explain the midwinter suppression of storm track intensity for the Pacific by the tendency of equatorward eddies to be trapped within the jet core, reducing the interaction with the lower level potential vorticity, and therefore reducing eddy amplification (see also Nakamura and Shimpo (2004)). Consistently, Lachmy and Harnik (2014) show that the efficiency for eddy amplification is suppressed at lower latitudes.

Analysis of EP fluxes over the Atlantic in winters of negative and positive NAO phases (Fig. 2.11) shows that in both cases the eddies act to converge momentum in the midlatitudes, and accelerate the eastward flow. However, the location of the strongest EP flux divergence (gray contours in Fig. 2.11) varies between positive and negative NAO phases. In years of positive NAO, eddies reinforce the jet

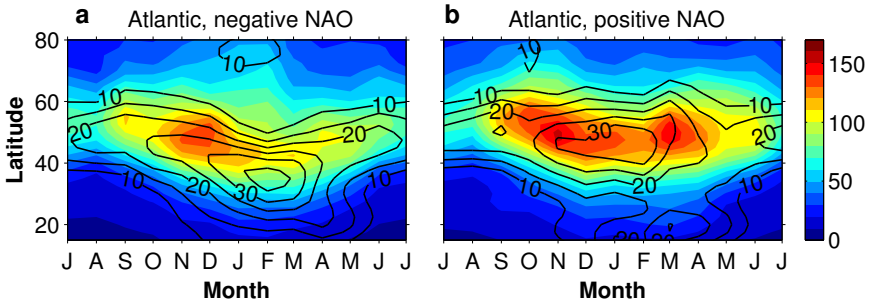

Figure 2.9: EKE ($m^2\ s^{-2}$) at 250-hPa (color, 10^{-5} m s^{-2}), and zonally-averaged zonal wind at the same level (black, m s^{-1}) over the Atlantic in years of (a) negative NAO and (b) positive NAO phases. NAO phase is determined by the average NAO index for the months January to March. Results in midlatitudes for winter months are statistically significant with 95% confidence level (not shown).

mostly in the midlatitudes, between 40°N to 60°N, and divergence is strongest near the storm track entrance region, around longitude 60°W. We also note that in years of positive NAO the EP fluxes divergence occurs along a southwest-northeast axis, which coincide with the strong poleward tilt of the zonal wind.

In contrast, in years of negative NAO (Fig. 2.11a), divergence is much weaker and mostly concentrated along latitude 40°N, indicating reinforcement of the jet in lower latitudes compared to the positive phase of the NAO. In addition, the divergence occurs further eastward, near the downstream end of the storm track. In both cases convergence of momentum fluxes contributes to the eastward acceleration of the flow, however there are major difference in the spatial distribution. Winters of positive NAO are characterized with a more poleward divergence, supporting a northeastward tilted jet, while a more equatorward and eastward divergence occurs in winters of negative NAO, maintaining a more zonal, equatorward jet.

2.6 The relation between jet latitude and the storm track minimum

Lee and Kim (2003) have showed that forcing of a strong subtropical jet in an idealized model leads to baroclinic wave growth in the region of the subtropical jet, while weaker subtropical jet results in baroclinic wave growth primarily in the midlatitudes, forming an eddy-driven jet, well-separated from the subtropical jet (Son and Lee, 2005; O'Rourke and Vallis, 2013). Thus, changes in the jet characteristics (driven by subtropical jet strengthening/weakening) are also associated with changes in jet latitudinal position, where a subtropical jet is found more equatorward and an eddy-driven jet is found in higher latitudes (Lachmy and Harnik, 2014; Yuval and Kaspi, 2017).

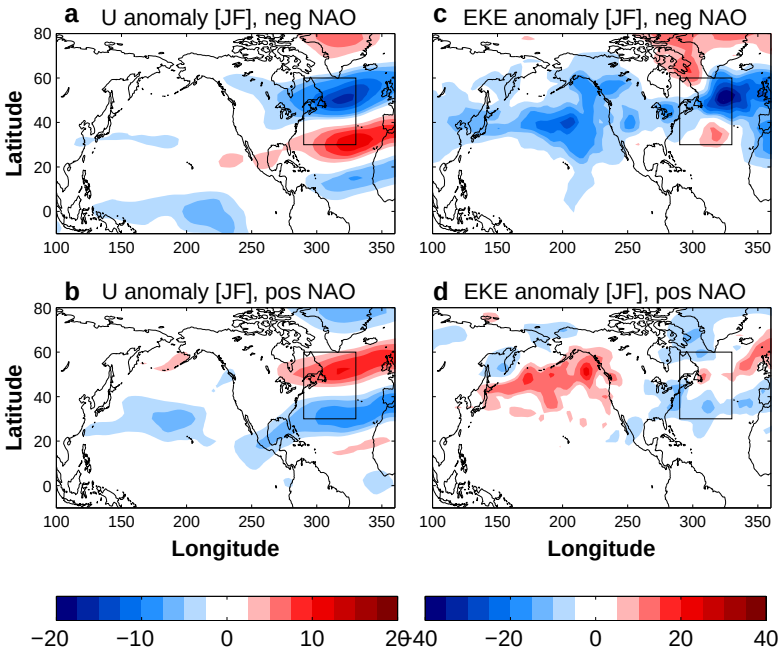

Figure 2.10: Anomalies from climatology of (a,b) 250-hPa zonal wind (m s^{-1}) and (c,d) EKE (m^2 s^{-2}) over the North Atlantic during winters of (a,c) negative and (b,d) positive NAO phases. Both fields are taken daily and averaged between January-February.

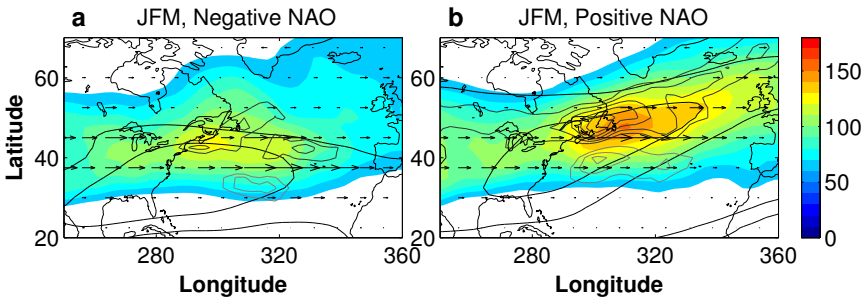

Figure 2.11: Horizontal component of the EP vectors at 250-hPa (arrows) and divergence of EP vectors (dark gray contours every 0.02 m s^{-1}) and convergence (light gray) during winters (a) negative NAO and (b) positive NAO. Color contours show 250-hPa EKE (m^2 s^{-2}). Contours of 20 and 30 m s^{-1} upper-level zonal wind are indicated by black lines. The EP vectors are plotted every 7.5°. We use daily data averaged between January-March).

Similar variations also occur throughout the seasonal cycle of the Pacific jet. During winter, the Pacific jet is found at low latitudes, and resembles a mixed or subtropical jet. On the other hand, during transition seasons, the jet is found at higher latitudes and resembles an eddy driven-like jet. Recently, Yuval et al. (2018) have found that both in reanalysis data and in idealized simulations the seasonal differences in jet characteristics play an important role in the occurrence of the midwinter minimum. It is found that when a zonally-symmetric Pacific temperature distribution is simulated,

a midwinter minimum-like behavior, which resembles reanalysis data, is obtained. Furthermore, it is found in simulations that a poleward shift of the subtropical jet in January leads to an increase in EKE.

These results are supported by observations of the Pacific storm track (Fig. 2.12). In years of a more equatorward jet position in midwinter (Fig. 2.12c), storm track intensity is decreased in winter relative to years of a more poleward jet (Fig. 2.12a), resulting in a more pronounced midwinter minimum in years of equatorward jet. The seasonal variation of jet latitude also demonstrates the same behavior, where a more poleward jet (as observed in the shoulder seasons) is associated with stronger EKE relative to a more equatorward jet position (as observed in midwinter). In addition to the variation in the jet position, there are also changes in the jet characteristics, as demonstrated by eddy momentum flux convergence (Fig. 2.12b,d). It is found that in the transition seasons, eddy momentum flux convergence coincides with the latitude of the maximum zonal wind both in years of equatorward or poleward jet position, indicating the eddy-driven characteristics of the jet. However, in winter there is a difference between the two composites; while in winters of poleward jet position eddy momentum flux convergence maximizes in the vicinity of the jet, indicating its eddy-driven character, in winters of equatorward jet eddy momentum flux convergence maximizes poleward of the jet and is less intense (Fig. 2.12d), suggesting a more subtropical or mixed jet state.

Further comparison of the relation between storm track intensity and jet latitude is made in Fig. 2.13. For each year, EKE was averaged over all the days during the winter season in which the jet was located at a certain latitude (latitudes are equally-spaced every 2.5° due to the horizontal resolution of the Reanalysis data). It is found that poleward of latitude 30°N, storm track intensity is increased as the jet is more poleward. These results indicate a linear relationship between EKE and jet latitude, suggesting that the midwinter suppression of Pacific storm track intensity could be explained by an equatorward shift of the jet.

2.7 Discussion and conclusions

In this study, we show that a midwinter minimum in EKE occurs over the Atlantic ocean, similar to the well known Pacific midwinter minimum. The Atlantic midwinter minimum is more mild on average compared to the Pacific, with a midwinter decrease in EKE of only 10% relative to fall or spring (the Pacific EKE decrease is nearly 30%). However, our analysis suggests that the Atlantic midwinter minimum is more pronounced in years of stronger jet.

The climatological characteristics of the Pacific and Atlantic jets may account for the frequency and strength of the midwinter suppression in these sectors. While the average intensity of the Atlantic jet in winter is around 35 m s^{-1}, the Pacific jet is stronger, reaching 60 m s^{-1}, and therefore may represent more favorable conditions for a midwinter suppression. According to our analysis, when

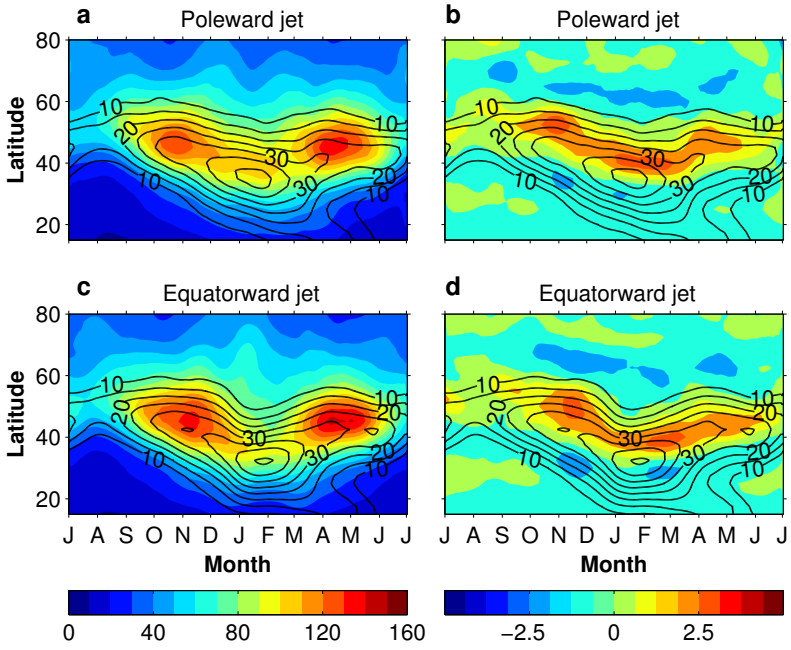

Figure 2.12: (a,c) 250-hPa daily EKE (color, $m^2\ s^{-2}$) and zonally-averaged zonal wind at 250 hPa (black contours, $m\ s^{-1}$) averaged over years of a more (a) equatorward jet, and (c) poleward jet over the Pacific (160°-222.5°E). Results for the months of November-March are statistically significant with 90% confidence level. (b,d) Eddy momentum flux convergence at 250-hPa (color, $10^{-5}\ m\ s^{-2}$), and 250-hPa zonally-averaged zonal wind (black, $m\ s^{-1}$) for the same composites as in (a) and (c). Daily fields are smoothed using a 31-day running average.

the jet is stronger over the Atlantic, then a midwinter minimum can be observed over the Atlantic as well. Furthermore, the Pacific midwinter minimum is also more pronounced in years when the jet is stronger (Nakamura, 1992; Nakamura and Sampe, 2002; Penny et al., 2013).

The Atlantic storm track is characterized by a weaker baroclinicity relative to the Pacific, yet the storm track is stronger than the Pacific. Penny et al. (2013) suggested that the cause for this difference in storm track intensity is not local, but due to the fact that the Atlantic storm track is more strongly seeded than the Pacific. The arguments above imply that the Atlantic storm track can also be affected by the strength of upstream storms and their propagation path.

Over the North Atlantic, the dominant mode of atmospheric variability is the North Atlantic Oscillation (NAO), which is associated with a latitudinal displacement of the jet where positive and negative phases correspond to a poleward and equatorward shift of the jet, respectively (e.g., Hurrell, 1995; Thorncroft et al., 1993; Lee and Feldstein, 1996; Orlanski, 2003; Riviere and Orlanski, 2007; Woollings et al., 2010). We find that winters associated with a negative phase of the NAO are related to reduced EKE over the Atlantic, suggesting that a midwinter minimum is more likely to occur in the Atlantic during years of negative NAO. Gerber and Vallis (2009) proposed that the variability of the

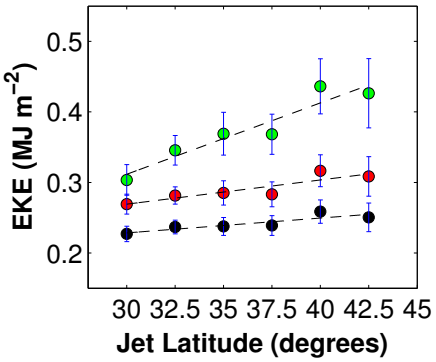

Figure 2.13: The relation between the vertically-integrated EKE (10^6J s^{-2}), averaged over a $\pm 10°$ latitude interval centered on the latitude of zonally-averaged jet maximum (green markers), and the latitude of the jet maximum (m s^{-1}) over the Pacific domain (160°-222.5°E). For each year between 1981-2014, EKE was averaged over all the days during DJF in which the jet was located at a certain latitude. A confidence interval of 95% is marked in blue. A linear fit (dashed) indicates a positive slope of 0.01 MJ s^{-2} degree^{-1}, with corresponding R^2 value of 0.95. Vertically integrated EKE averaged over the entire northern hemisphere and between 20°-70°N are denoted by black and red markers, respectively.

North Atlantic region can be viewed as the interaction of two jets: the subtropical jet, at the edge of the Hadley cell, and the eddy-driven jet in the midltitudes. A positive phase of the NAO corresponds to a splitting of these jets, while a negative phase related to merging of the jet into a single jet. Eichelberger and Hartmann (2007) found that larger variability of the eddy-drive jet exists when the jets are separated. In contrast, over the Pacific the jet is considered more steady and less variable (Ambaum et al., 2001). Our findings suggest that equatorward, merged jet, as observed in the Atlantic in winters of negative phase of the NAO, may resemble the merged Pacific jet and to its associated midwinter minimum of storm track activity.

In summary, a midwinter minimum of EKE occurs over the Atlantic when the wintertime jet strengthens, possibly related to the Atlantic jet being more equatorward in winter with characteristics more similar to the Pacific jet. The occurrence of the midwinter minimum in winters with a strong Atlantic jet is consistent with a midwinter minimum being more prominent in the Pacific, where the jet is naturally stronger.

The Atlantic midwinter minimum in 2-6 days bandpass data While previous studies have shown that the midwinter minimum is a robust feature of the atmospheric circulation over the North Pacific storm track, they found no or weak evidence for the existence of a midwinter suppression over the Atlantic (e.g., Nakamura, 1992; Christoph et al., 1997; Penny et al., 2010; Ren et al., 2014). Others note briefly that when the Atlantic jet is strong, the Atlantic storm track is weak (Penny et al., 2013). To further evaluate the Atlantic midwinter minimum, we examine the sensitivity of our results to

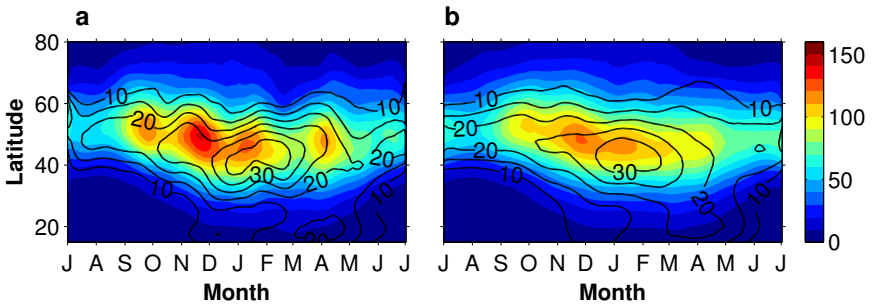

Figure 2.14: (a) 'Strong jet' composite of zonally-averaged 2-6 days bandpass filtered EKE at 250 hPa (color, $m^2\ s^{-2}$, contour interval 10 $m^2\ s^{-2}$), and zonally-averaged zonal wind (black contours, m s^{-1}, contour interval 5 m s^{-1}), averaged over 7 years of strong Atlantic jet, selected according to the maximum zonal wind averaged over JFM. (b) Climatology of 2-6 days bandpass filtered EKE, zonally averaged over the Atlantic domain.

the dataset, period of averaging and measure of eddy activity, and compare to the original study of Nakamura (1992). For consistency, we use National Centers for Environmental Prediction (NCEP, formerly the National Meteorological Center (NMC)) datasets. All fields were averaged over the same period as in Nakamura (1992) (1965-1984), and are zonally-averaged over the same domain boundaries as in Nakamura (1992). Averaging over an earlier period produces qualitatively similar results to the more recent dataset used in our study (NCEP reanalysis 2, averaged between 1981-2014), with a shallow midwinter minimum in EKE over the Atlantic domain. This analysis suggests that the choice of data and period of averaging do not seem to explain the differences between previous studies. Therefore, the lack of a midwinter minimum in Atlantic climatology in Nakamura (1992) may be a result of how the eddy fields are defined. When a 2-6 day bandpass filter is used to represent eddy fields, the midwinter suppression over the Atlantic is less pronounced in EKE, yet appears clearly in geopotential height variance (Penny et al., 2010), and appears when choosing the years of the strongest jet.

2.8 Appendix A: Statistical significance

In Fig. 2.15, we show the statistical significance of the differences in zonal wind and EKE between composites of years with strong jet and years of weak jet during midwinter, which are analyzed in Section 2.4. Results are statistically significant in midlatitudes over both the Pacific and Atlantic sectors, with over 90% confidence level. Statistical significance was determined with Student's t-test (p-value<0.05), computed in the following way: First, EKE and zonal wind are zonally-averaged over the relevant basin (Atlantic or Pacific). Second, for each latitude and for each month we compute the statistical significance between the values of the two composites (years with strong jet and years of

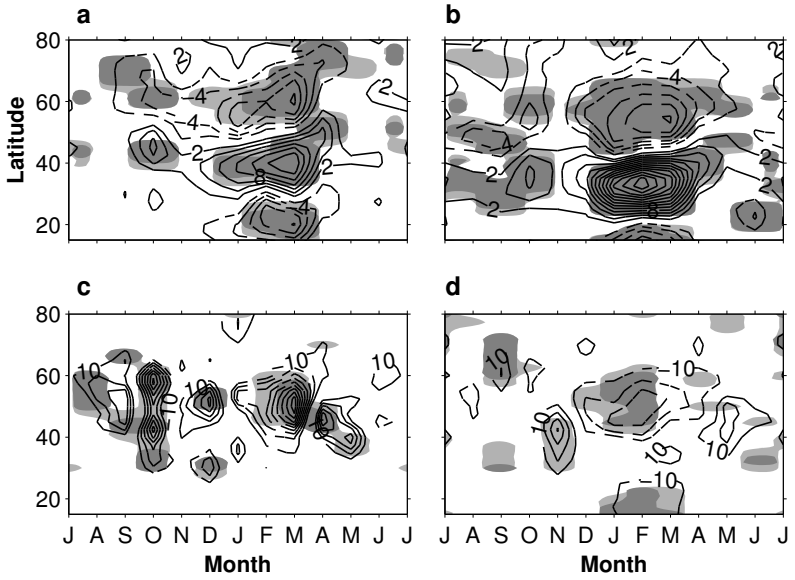

Figure 2.15: (a,b) 250-hPa zonal wind difference (m s^{-1}, contour interval 2 m s^{-1}) between years of strong and weak wintertime jet composites (positive values are solid contours, negative are dashed and zero lines are omitted) for (a) the Atlantic and (b) the Pacific basins. Shaded lightly and heavily is where the difference exceeds the 90% and 95% confidence levels, respectively. Statistical significance was determined with Student's t-test (p-value$<$ 0.05). (c,d) Similar analysis as in (a,b), for the 250-hPa EKE (m^2 s^{-2}, contour interval is 5 m^2 s^{-2} and 10 m^2 s^{-2}, respectively) for (c) the Atlantic and (d) the Pacific basins.

weak jet). We repeat this procedure for two confidence levels: 90% and 95%, and consider only results with p-value less than the significance level.

2.9 Appendix B: Comparison with the previous studies of Nakamura (1992) and Penny et al. (2010)

The sensitivity of the Atlantic midwinter suppression is further examined by applying the same analysis to reanalysis dataset of the same period as in Nakamura (1992) (1965-1984). For consistency we use National Centers for Environmental Prediction (NCEP, formerly the National Meteorological Center (NMC)) datasets. All fields are zonally-averaged over the Pacific and the Atlantic domains, as in Nakamura (1992), Fig. 2) domains. Results shown in Fig. 2.16 below indicate that averaging over an earlier period produces qualitatively similar results to the more recent dataset used in our study (NCEP reanalysis 2, between the years 1981-2014). A shallow midwinter minimum in EKE appears over the Atlantic domain. This analysis suggests that the choice of data and period of averaging do not seem to explain the differences between previous studies. Therefore, it seems that if the measure

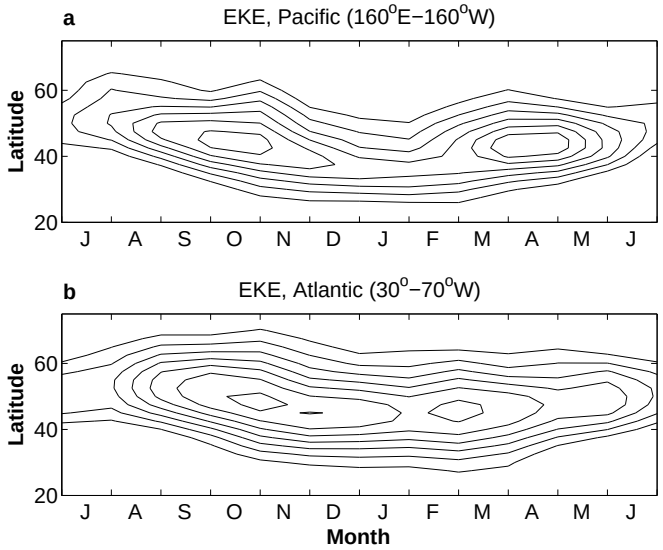

Figure 2.16: Observed 250-hPa zonally-averaged 3-10 days filtered EKE ($m^2\ s^{-2}$, contoured every 15 $m^2\ s^{-2}$ starting at 60 $m^2\ s^{-2}$), zonally-averaged over (a) the Pacific and (b) the Atlantic basins. Data is based on NCEP reanalysis, averaged between 1965-1984, the same period as in Nakamura (1992).

Name of Study	Dataset	Period	Measure of eddy activity	Time Filter
Nakamura, 1992	NMC (NCEP)	1965-1984	Wave amplitude in Z at 250 hPa	6-day highpass
Penny, 2010	ERA-40	1958-2001	Variance in Z at 300 hPa	2-6 days
Current study	NCEP	1958-2014	EKE at 300 hPa	3-10 days

Table 2.1: Comparison between studies in terms of period, measure of eddy activity, time filter. All three studies use the same longitudinal sector of the Atlantic (30°-70°W).

of eddy activity and the filtering method in Nakamura (1992) is not the same, this could account for the lack of midwinter minimum in Nakamura (1992).

Furthermore, Penny et al. (2010) present an update of Fig. 2 in Nakamura (1992) for ERA-40 dataset between 1958-2001. They use variance in geopotential height at 300 hPa as their measure of eddy activity. Their results also indicate a slight minimum in the Atlantic storm track (particularly during January-February), however as far as we know it is not discussed in the text. We have also verified our findings with the ERA-INTRIM dataset between the years 1981-2014. Results are qualitatively the same.

Chapter 3

The seasonal cycle of midlatitude storm tracks. Part I: zonally-symmetric idealized GCM

3.1 Introduction

On Earth, the seasonal cycle of storm tracks in the Northern Hemisphere varies between the Atlantic and the Pacific basins. While the storm track activity over the Atlantic reaches its maximum in winter (in most of the years, see section 2.3 for detailed discussion), the strongest activity over the Pacific is observed in late autumn and early spring, with a suppression in midwinter. To study midlatitude storm track seasonal cycle, we use a zonally-symmetric framework of an aqua-planet GCM. To generate a full seasonal cycle, we apply a realistic time-dependent solar insolation, unlike other modeling studies with zonally-symmetric configurations in which the desired climatology is obtained by variations in thermal forcing (Son and Lee, 2005; Brayshaw et al., 2008). Using the seasonal model we are able to examine the atmospheric response to a continuous, seasonally-varying forcing, rather than the response to forcing of the monthly mean conditions.

In the idealized GCM, the complexity of Earth's climate is controlled by idealized representation of realistic forcing. Here, we try to capture Earth-like climate and its seasonal variability using a combination of three parameters, which control the model radiative forcing: (a) seasonally-varying incoming solar radiation, (b) TOA albedo and (c) atmospheric absorption coefficient (optical thickness) which represents the effect of water vapor concentration Frierson et al. (2006). The forth parameter is ocean heat flux (Q-flux) which can be used to control the strength of the subtropical jet (and the Hadley cell). By varying each of these parameters and examining its influence, we obtain the reference climate. We further examine the sensitivity of the storm track seasonal cycle to changes in the

incoming radiation profile and to changes in the strength of the jet.

3.2 Model description

We use an idealized GCM with a representation of seasonal cycle to simulate midlatitude storm tracks. The model is based on the Flexible Modeling System (FMS) developed at GFDL. It solves the primitive equations for an ideal-gas atmosphere, using spectral transform in the horizontal and finite differences in the vertical. The idealized GCM is similar to that described and used by Frierson et al. (2006) and O'Gorman and Schneider (2008).

3.3 Development of the seasonal model

Obtaining a realistic seasonal cycle in the idealized GCM requires several adaptations to the original code (set to run in perpetual equinox conditions). We developed and added the following features:

- Seasonally-varying incoming solar radiation at the top of the atmosphere
- Top of the atmosphere albedo, with dependence on latitude
- Seasonally-varying ocean heat flux, with dependence on latitude and time

In addition, we made adaptations to the constant meridional profile of longwave absorption (Frierson et al., 2006), such that it depends on latitude and time. The model is run with spectral resolution of T42, corresponding to horizontal resolution of about 2.5°× 2.5°, and 30 discrete sigma-coordinate levels in the vertical ($\sigma = p/p_s$). We use a zonally symmetric configuration of the idealized GCM, without zonal asymmetries such as topography and land-sea contrast. For simplicity, it also omits details such as sea-ice and cloud-radiative feedbacks. Below, we describe the main seasonal features introduced to the model.

3.3.1 Seasonally-varying solar radiation

While some of the previous studies of the seasonal storm tracks variability have used perpetual conditions in their model simulations (e.g., Zhang and Held, 1999; Brayshaw et al., 2008), we run a model with a full seasonal cycle. Solar radiation at the top of the atmosphere is prescribed, varying with daily, seasonal and latitudinal distribution (Hartmann, 1994). The average daily insolation per unit surface area is given by

$$\overline{\mathrm{Q}} = \frac{\mathrm{S}_0}{\pi} \left(h_0 \sin\phi \, \sin\delta + \cos\phi \, \cos\delta \, \sin h_0 \right), \tag{3.1}$$

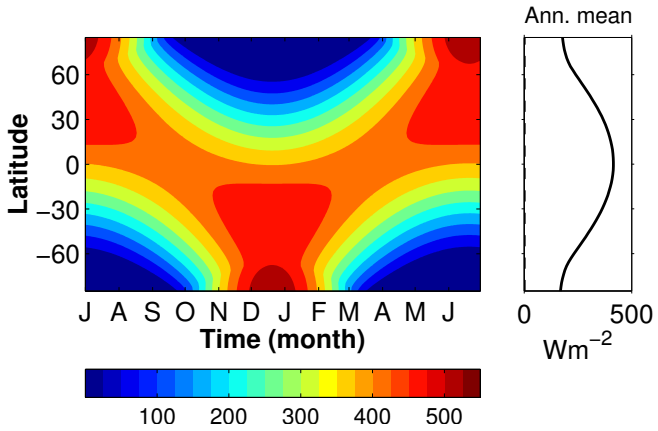

Figure 3.1: Left: Daily incoming solar radiation (W m^{-2}) at the top of the atmosphere as a function of latitude and time (Hartmann, 1994). This insolation is used as forcing in idealized model simulations. Right: zonally-averaged annual mean of solar insolation.

where S_0 is the solar constant, ϕ is latitude of the solar zenith angle, δ is the declination angle determined by the day in the year and h_0 is the hour angle at sunrise and sunset. The eccentricity of Earth's orbit is not taken into account in our simulations. For each day of the year, the model is forced by the daily insolation profile, as shown in Fig. 3.1.

3.3.2 Top of the atmosphere albedo

At the top of the atmosphere, the downward radiation is multiplied by $(1 - A_0)$, before decaying exponentially with pressure. Albedo at the top of the atmosphere varies with latitude

$$A_0(\phi) = A_{pole} + (A_{eq} - A_{pole}) \exp(-\phi^2) \tag{3.2}$$

where ϕ is latitude. $A_{eq} = 0.15$ and $A_{pole} = 0.85$ are the albedo values at the equator and poles, respectively, and mostly come to represent the effect of reflection by clouds. On Earth, the meridional temperature gradient is partly determined by the meridional distribution of clouds and their associated radiative forcing (e.g., Merlis, 2012). In the extratropics, clouds have a net cooling effect (e.g., Hartmann, 1994). Therefore, without a simplified form of cloud radiative forcing in the exstratropics the equator-to-pole temperature difference will be weaker compared to observations. In addition, at high latitudes a large part of the incoming radiation is reflected back to space due to the large incident angle, as well as due to snow and ice converge (e.g., Peixoto and Oort, 1992). At the surface, albedo is fixed in space and in time with a constant value of 0.38.

Prescribed incoming solar radiation profiles, multiplied by the TOA albedo, are shown in Fig. 3.2. When TOA albedo of 85% is applied at the poles and 35% is applied at the equator (green curve in

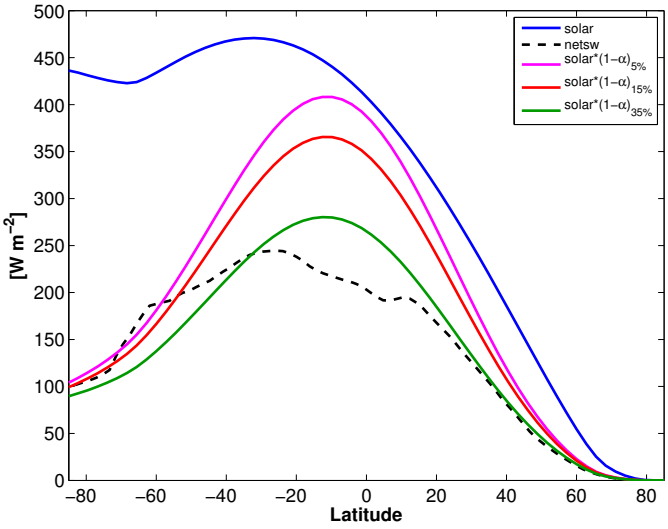

Figure 3.2: Prescribed incoming solar radiation (blue, W m^{-2}) averaged over DJF, computed according to the daily distribution (Hartmann, 1994), and the observed net shortwave radiation (dashed, W m^{-2}) at the top of the atmosphere based on NCEP reanalysis climatology, averaged between 1981-2010. The incoming solar radiation multiplied by TOA albedo parametrization (magenta, red and green, corresponding to A_{eq} of 5%, 15%, and 35%, respectively) demonstrates the effect of the TOA albedo on the idealized insolation profile. A_{pole} is set to 85%.

Fig. 3.2), the incoming solar radiation of Hartmann (1994) is reduced both at the equator and at the poles. This profile resembles the observed net incoming shortwave radiation in DJF (dashed black curve in Fig. 3.2). Larger percentage of TOA albedo leads to enhancement of the incoming radiation at all latitudes, with the largest increase at the equator. The incoming solar radiation for SON is shown in Fig. 3.3. Similarly to DJF, a TOA albedo profile of 35% at the equator (green curve in Fig. 3.3) resembles the meridional profile of the observed net incoming shortwave radiation (dashed black curve). The daily insolation, multiplied by TOA albedo, is shown in Fig. 3.4.

3.3.3 Seasonally-varying longwave absorption

Radiative transfer is represented by a two-stream gray radiation scheme. Optical depths of longwave and shortwave are a function of latitude ϕ, surface temperature and pressure. Unlike Frierson et al. (2006), we use seasonally-varying longwave optical thickness τ. At the surface, τ is centered around the latitude of maximum surface temperature (ϕ_{max}).

$$\tau_0(\phi) = \tau_{eq} + (\tau_{pole} - \tau_{eq}) \exp\left(\frac{-(\phi - \phi_{max})^2}{2\varsigma^2}\right) \tag{3.3}$$

where τ_{eq} and τ_{pole} are the values at the equator and at the poles for $\phi_{max} = 0$, respectively. ϕ_{max} is the latitude of maximum surface temperature, computed by the model at each time step. ς is the profile

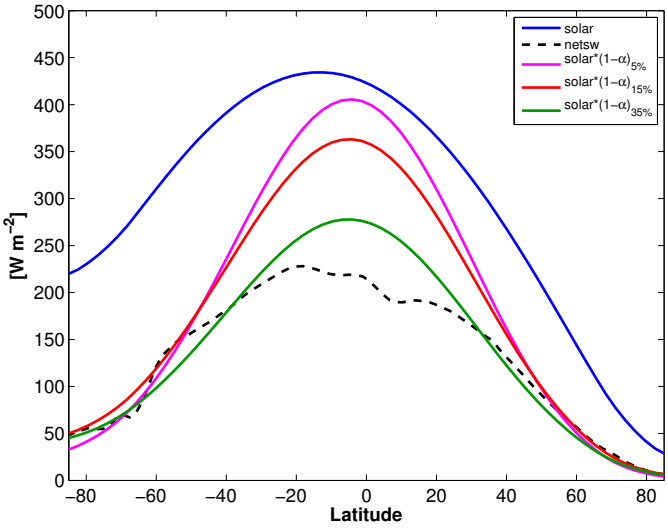

Figure 3.3: Same as Fig. 3.2 averaged over SON.

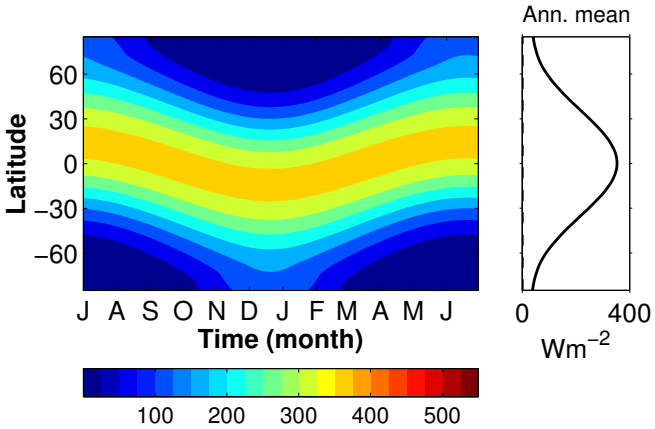

Figure 3.4: Left: Daily incoming solar radiation (W m^{-2}) at the top of the atmosphere multiplied by $(1-A_0)$ as a function of latitude and time. Right: zonally-averaged annual mean of solar insolation multiplied by $(1-A)$. A_{eq} and A_{pole} are set to 15% and 85%, respectively.

width, and taken as 1 in all simulations. The dependence of the optical thickness on pressure is given by (Frierson et al., 2006)

$$\tau = [f_1\sigma + (1-f_1)\sigma^4]\tau_0, \tag{3.4}$$

where $f_1 = 0.1$ and $\sigma = \frac{p}{p_s}$. The linear and quadratic terms in σ roughly represent absorption by a well mixed absorber (with weight f_1) and by water vapor (with weight $1-f_1$), respectively (see also Frierson et al., 2006; O'Gorman and Schneider, 2008).

3.3.4 Surface heat capacity

The depth of the ocean mixed layer controls the surface thermal inertia (Bordoni and Schneider, 2008). While thin mixed layer depth (1 m) corresponds to rapid changes in surface temperatures, a thick mixed layer (100 m) results in slow variations, particularly apparent during the transition seasons. We use an ocean mixed layer depth (δ) of 10 m, indicating an effective heat capacity[1] (κ) of 5×10^7 J K^{-1} m^{-2}. For comparison, in Frierson et al. (2006) the mixed layer depth is 2 m, corresponding to a heat capacity of 10^7 J K^{-1} m^{-2}.

3.3.5 Prescribed seasonally-varying ocean heat flux

The lower boundary of the GCM is a mixed-layer slab ocean of constant depth, in which surface temperatures are not prescribed but vary dynamically in response to changes in insolation, thermal radiative fluxes and surface fluxes of sensible and latent heat. In GCM studies with mixed layer ocean the ocean heat flux can either be prescribed or evaluated based on a control run driven by fixed SSTs (Bordoni, 2007).

Following Bordoni (2007), which have used prescribed time-independent meridional heat transport to match the observed annual-mean ocean heat transport in the tropics, we use ocean heat transport to control the strength of the Hadley circulation. An analytic Q-flux profile of a Gaussian of amplitude $\mathrm{Q_{max}}$ and width η centered around the latitude of maximum upward vertical velocity at 850 hPa (ϕ_{max}) is given by

$$\mathrm{Q_{flux}} = \mathrm{Q_{max}} \exp\left(\frac{-(\phi-\phi_{\mathrm{max}})^2}{2\eta^2}\right)$$

Here, an example of 16°-wide Q-flux profile is shown (Fig. 3.5). Unlike Bordoni (2007), we use a Gaussian Q-flux profile rather than the second derivative of a Gaussian, to avoid local heating at the subtropics which may create local meridional temperature gradients.

3.4 Surface temperature response to seasonal radiative forcing

Here, we present the simulation results of a series of sensitivity experiments, designed for obtaining a realistic climate in the zonally-symmetric idealized GCM. To achieve a seasonal cycle, we implement a seasonally-varying, daily insolation scheme, which varies with latitude and day of the year. In response, the simulated climate, shown in Fig. 3.6b, is rather similar to Earth's climate (Fig. 3.6a).

[1] Effective heat capacity (κ) can be computed by $\kappa = \delta\rho c_p$, where ρ is sea water density and c_p is sea water heat capacity.

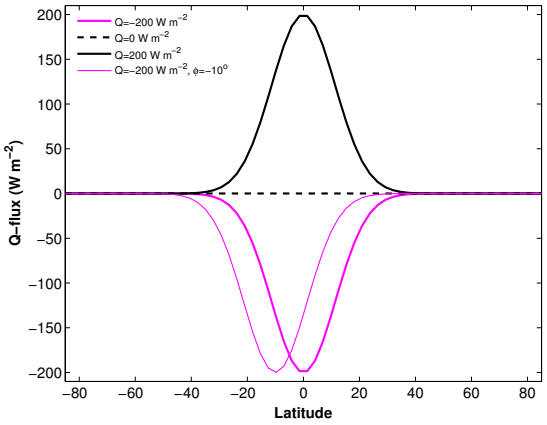

Figure 3.5: Meridional Q-flux profiles for simulations with prescribed ocean heat flux, with a minimum (or maximum) amplitude (Q_{max}) of -200 W m^{-2} (magenta line), 0 W m^{-2} (dashed black), 200 W m^{-2} (black) centered around the equator, and a -200 W m^{-2} profile centered off the equator at ϕ=-10° (thin magenta line).

Zonal surface temperatures are around 300 K in the tropics, and the equator-to-pole surface temperature gradient is nearly 30 K in the annual mean. However, the solstice temperature gradients are relatively weak, and polar temperatures are not captured by the model throughout the year.

Top of the atmosphere albedo We show results from three simulations, one without TOA albedo (Fig. 3.6b) and two simulations with TOA albedo profiles of 35% and 15% at the equator, respectively (Fig. 3.6c,d). At the poles, TOA albedo is set to 85%. When a TOA albedo is used, incoming solar radiation is decreased at all latitudes. As a result, surface temperature is decreased too, with the most prominent decrease during summer (since during the winter months no radiation reaches the poles and therefore any reflection has no direct effect). An increase of A_{pole} by 15%, leads to summer temperatures decrease near the poles by approximately 6-8 K. Therefore, with the absence of clouds and polar ice, introducing TOA albedo to the model is a useful method to prevent the poles from overheating during summer and equinox seasons, control the equator-to-pole insolation gradient, and obtain a more realistic seasonal temperature distribution.

Seasonally-varying longwave absorption To overcome the relatively cold climate that is a result of the TOA albedo implementation, we introduce a seasonally-varying longwave optical thickness (Fig. 3.7). While using a longwave optical thickness profile alone leads to a very high tropical surface temperature, implementing both longwave optical thickness and TOA profile parametrization (Fig. 3.7b,c) leads to a more realistic seasonal cycle. In particular, a realistic climate is obtained when a TOA albedo profile of 85% at the poles is used, with surface temperature of 300 K in the tropics and 240 K in the poles, during solstice seasons (Fig. 3.7).

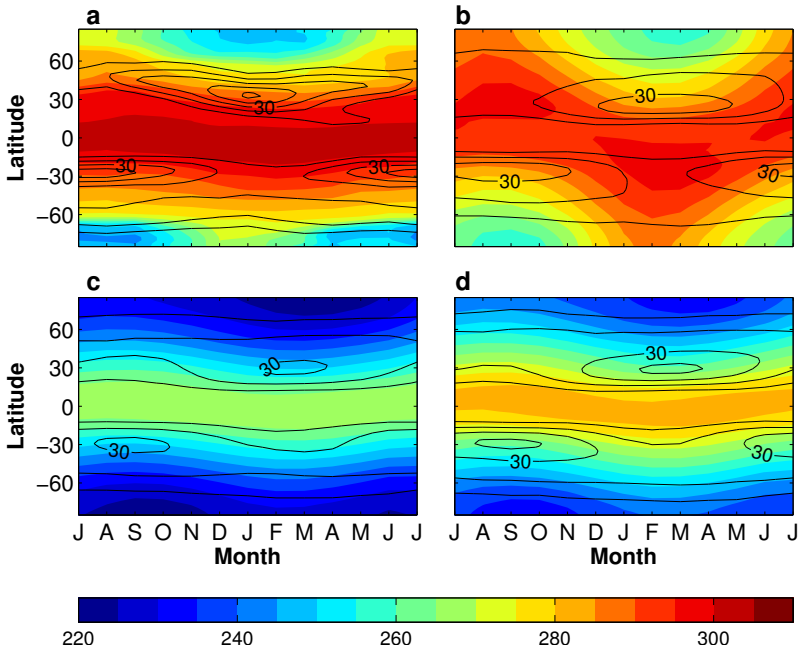

Figure 3.6: (a) Seasonal cycle of surface temperature (color contours, K) and zonally averaged zonal wind (black, m s^{-1}) based on NCEP reanalysis (averaged between 1981-2014) averaged over the Pacific sector. (b)-(d) The same fields from aquaplanet idealized GCM simulations in response to (b) daily, solar insolation, and with (c) TOA albedo profile of 35% at the poles and (d) TOA albedo profile of 15% at the equator. In all simulations, TOA albedo is set to 85% at the poles, longwave optical thickness is constant ($\tau = 6$), and mixed layer depth is set to 10 m.

Surface heat capacity Furthermore, we examine the effect of surface layer heat capacity, or mixed layer depth, on surface temperature seasonal cycle. Using a thin mixed layer depth (Fig. 3.8a), the zonal maximum surface temperature occurs in January, similar to observations. However, when a thicker depth is used, the peak is delayed by one to two months (Fig. 3.8b,c). Consistently, the same phase lag occurs for the peak of zonally-averaged zonal wind. Therefore, a mixed layer depth δ=10 m is chosen for the following seasonal simulations, in order to maintain a realistic seasonal time scale.

3.4.1 Equator-to-pole surface temperature structure

Fig. 3.9 shows the zonally-averaged surface temperature averaged over DJF for simulations with varying radiative parameters. As expected, the simulated changes in surface temperature are consistent with the insolation changes (Fig. 3.2). For insolation profile with TOA albedo of 35% at the equator, surface temperatures are relatively low, mimicking a colder climate, while for TOA albedo of 15% surface temperatures are higher. Implementing longwave absorption (with prescribed values as described in the figure legend) increases surface temperatures by nearly 10 degrees, yet the simulated temperature profile does not match the observed (black curve in Fig. 3.9). Applying the idealized

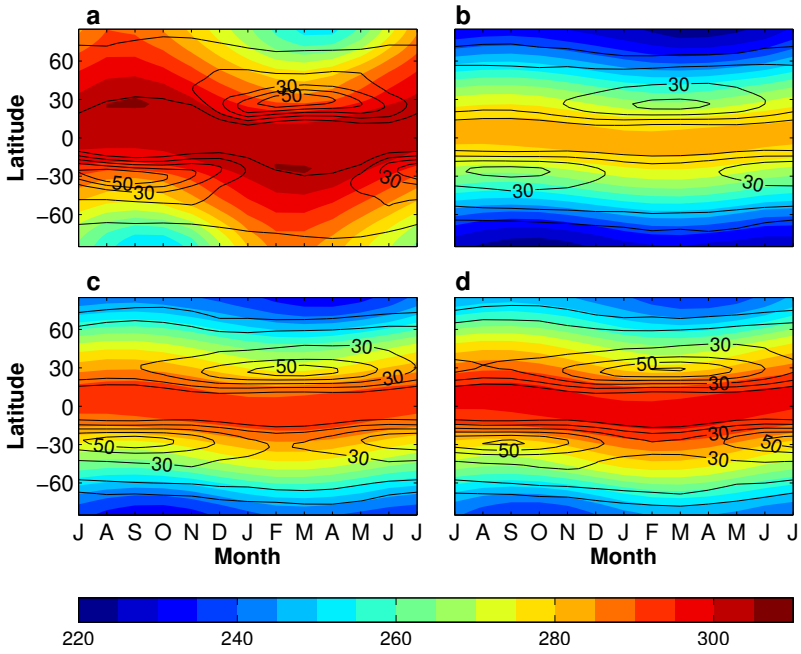

Figure 3.7: (a) Seasonal cycle of surface temperature (color contours, K) and zonally averaged zonal wind (black, m s^{-1}) in idealized GCM simulations in response to daily distribution of solar incoming radiation (Hartmann, 1994) and seasonally-varying longwave optical thickness (τ_{pole},τ_{eq}=[1.5, 16]). (b) Same as (a) with the addition of TOA albedo profile of 35%, (c) 15% and (d) 5% at the equator, and 85% at the poles. In all simulations, mixed layer depth is set to 10 m.

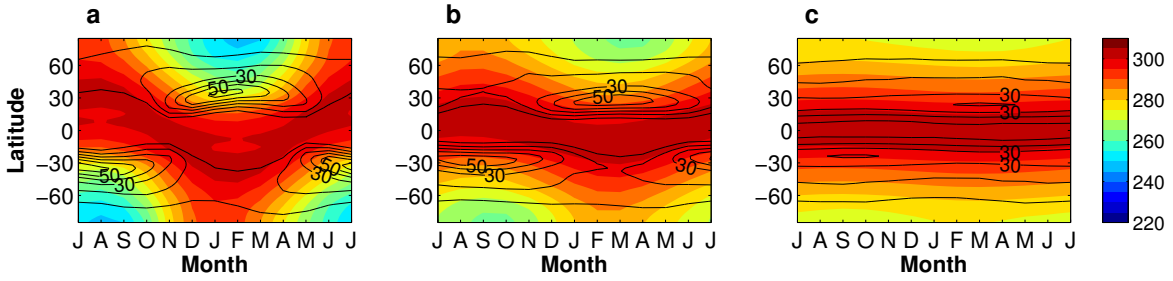

Figure 3.8: Seasonal cycle of surface temperature (color contours, K) and 300-hPa zonally averaged zonal wind (black, m s^{-1}) from idealized GCM simulations with mixed layer depth of (a) 1 m, (b) 10 m and (c) 100 m.

solar incoming radiation profile (blue), without TOA albedo or longwave absorption, leads to a relatively large discrepancy poleward of latitude 50°N. Simulated zonally-averaged surface temperatures are also compared for the northern hemisphere fall season (Fig. 3.10). These results suggest that the profile that best describes the meridional temperature structure is TOA albedo of 5% at the equator and 85% at the poles, applied together with time-dependent longwave absorption profile (magenta curve).

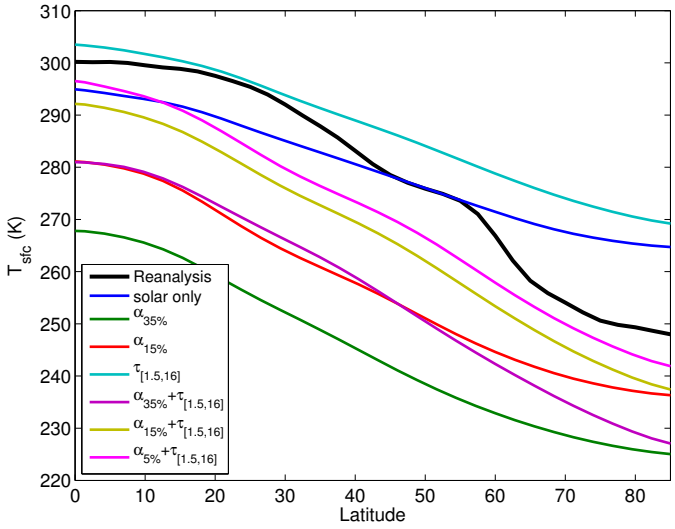

Figure 3.9: Surface temperature (K) averaged over DJF in idealized model simulations with varying radiative profiles, and the observed surface temperature (solid black, K) based on NCEP reanalysis dataset. All simulations are zonally-symmetric and hemispherically-symmetric.

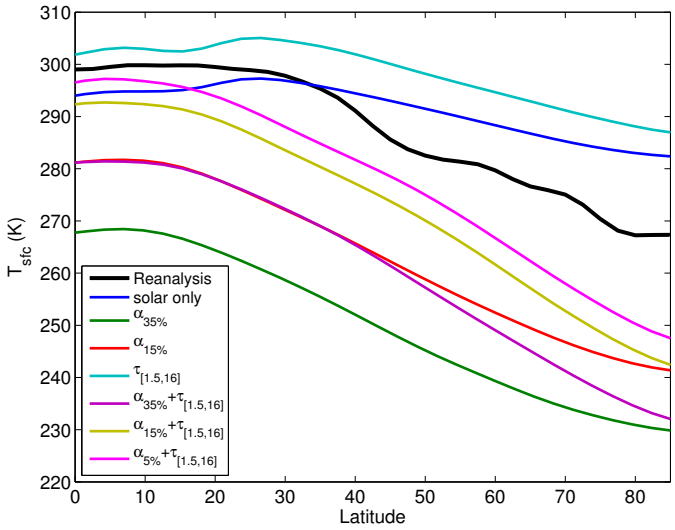

Figure 3.10: Same as Fig. 3.9 averaged over SON.

3.5 Model climatology

The model is spun-up until it reaches a statistical steady state. In this chapter, a zonally symmetric configuration of the idealized GCM is used, without zonal asymmetries (such as topography, land-sea contrast). Temperature variation with latitude is shown in Fig. 3.11a. Overall, the model captures the seasonal cycle of surface temperature rather well, with the highest resemblance to reanalysis in the Northern Hemisphere (Fig. 3.6a). Global mean temperature is 285.9 K, similar to the observed value.

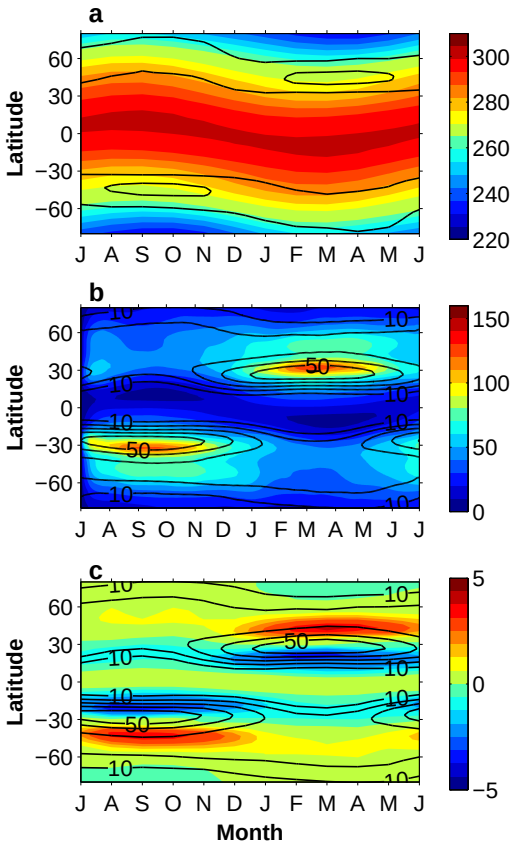

Figure 3.11: Reference simulation climatology. Seasonal cycle of (a) surface temperature (color, K) and lower-level zonal wind, averaged between 1000-850 hPa (black, m s^{-1}, contours every 4 m s^{-1}, starting from 4 m s^{-1}), (b) 300-hPa EKE (color, m^2 s^{-2}) and zonal wind at the same level (black, m s^{-1}, contours every 10 m s^{-1}) and (c) 300-hPa eddy momentum flux convergence (color, 10^{-5} m s^{-2}) and zonal wind at the same level (black, m s^{-1}, contours every 10 m s^{-1}).

For our purpose, the storm track is represented by transient eddy kinetic energy (EKE), computed by bandpass time filtering of daily horizontal winds using a Butterworth filter with a cutoff period of 3-10 days (Fig. 3.11b), matching the typical timescale of synoptic-scale storms in midlatitude. As in observations, most of the variability lays within the 3-10 days bandpass range, and is concentrated at the midlatitudes. Higher-frequency filters, such as the 2-4 days and 2-6 days filter, have similar characteristics and reach their maximal values in midlatitudes as well (Fig. 3.12), while lower-frequency filters reach their peak more equatorward.

As expected, the storm track is zonally- and hemispherically-symmetric. Both zonal wind and storm track have a delayed seasonal cycle, compared with observations (Fig 3.6a), reaching their maximum intensity in the Northern Hemisphere between February and April, rather than between December and February. The cause for this delay is the depth of the ocean mixed layer which controls the surface thermal inertia (see section 3.4). The maximum in storm track intensity occurs when jet is

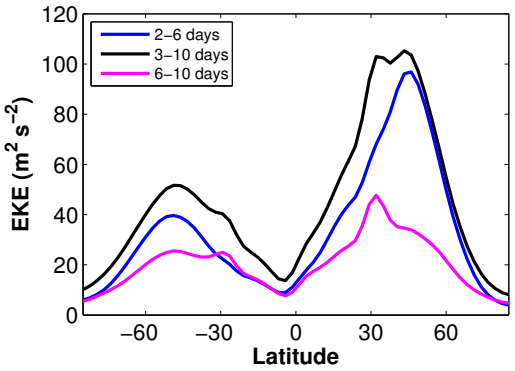

Figure 3.12: Variability of bandpass-filtered 300-hPa EKE (m^2 s^{-2}) in zonally-symmetric idealized GCM reference simulation, with cutoff periods of 2-6 days (blue), 3-10 days (black) and 6-10 days (magenta).

most intense, in consistence with classic linear theories of baroclinic instability (e.g., Charney, 1947; Eady, 1949).

3.5.1 Reference climate

The zonally-symmetric basic state produced by the reference simulation (driven by the zonally-symmetric solar radiation profile) is shown in Fig. 3.13. The meridional mass streamfunction (Fig. 3.13a) is defined as

$$\psi(\phi, \mathrm{p}) = 2\pi \mathrm{a} \int_0^{\mathrm{p}} \mathrm{v} \cos(\phi) \frac{\mathrm{dp}}{\mathrm{g}}, \tag{3.5}$$

where ϕ is latitude and a is the radius of the Earth. The subtropical jet is located at the poleward side of the Hadley circulation, around latitude 30°N, characterized by its more baroclinic structure, as well as a more barotropic component associated with eddy momentum flux convergence of the eddy-driven jet, around latitudes 40-45°N (Fig. 3.13c).

Lower-level baroclinicity, measured by the Eady growth rate (Fig. 3.13d), exhibits a double peak structure, similarly to Brayshaw et al. (2009). The first maximum occurs between latitudes 25-30°N, and the second is in midlatitudes, around 50°N. While the first peak is associated with the subtropical jet, the second peak is associated with the temperature gradients in this region. Eddy activity, measure by the 3-10 days bandpass-filtered EKE, is strongest in midlatitudes, around 35°N. This peak in eddy activity is associated with the peak in upper-level baroclinicity.

The long-term mean of the meridional circulation and zonal wind during selected months in the reference simulation is shown in Fig. 3.14. Similar to reanalysis, in solstice seasons (represented by January and July for NH and SH, respectively) the jet is located at the edge of the cross-equatorial cell. During this period, the cells are suggested to be less strongly influenced by eddy momentum fluxes

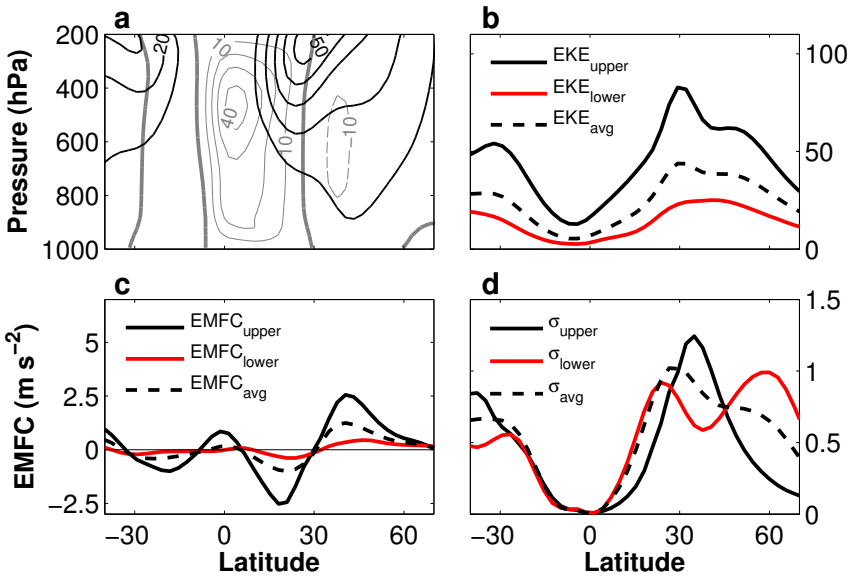

Figure 3.13: Reference simulation averaged over the period of maximum jet intensity (JFM). (a) Meridional mass streamfunction (gray contours, 10^8kg s^{-1}, contour interval 10×10^8 kg s^{-1}. Dashed contours denote negative values) and zonal winds (black contours, contour interval 10 m s^{-1}). (b) Zonally-averaged EKE (m^2 s^{-2}), vertically-averaged over the upper levels of the atmosphere (black curve, between 300-250 hPa) and near the surface (red, between 925-700 hPa). (c) Eddy momentum flux convergence (EMFC, m s^{-2}), averaged over the same levels as EKE. (d) Eady growth rate averaged between 500-850 hPa (black, s^{-1}) and near the surface (red). In panels (b)-(d), the vertically-averaged fields between 925-250 hPa are plotted as well (dashed curve).

(Walker and Schneider, 2006). In equinox seasons (April and October for NH and SH, respectively), the circulation is close to symmetric around the equator and the jet is located further poleward.

3.6 Series of simulations

The standard radiative parameters we use are a meridional TOA albedo profile, set to 85% at the poles and 15% at the equator, and time-dependent longwave absorption profile, set to 16 at the equator and 1.5 at the poles (in equinox). In a series of simulations, we investigate the storm track seasonal cycle and examine its response to strengthening of the subtropical jet, controlled in the idealized GCM by variation of the ocean heat flux forcing. Additional set of simulations explores the storm track seasonal variability in response to variation of the ratio between the seasonal and synoptic time scale, which in the idealized GCM is achieved by changing the planet's orbital period while maintaining the timescale of synoptic eddies.

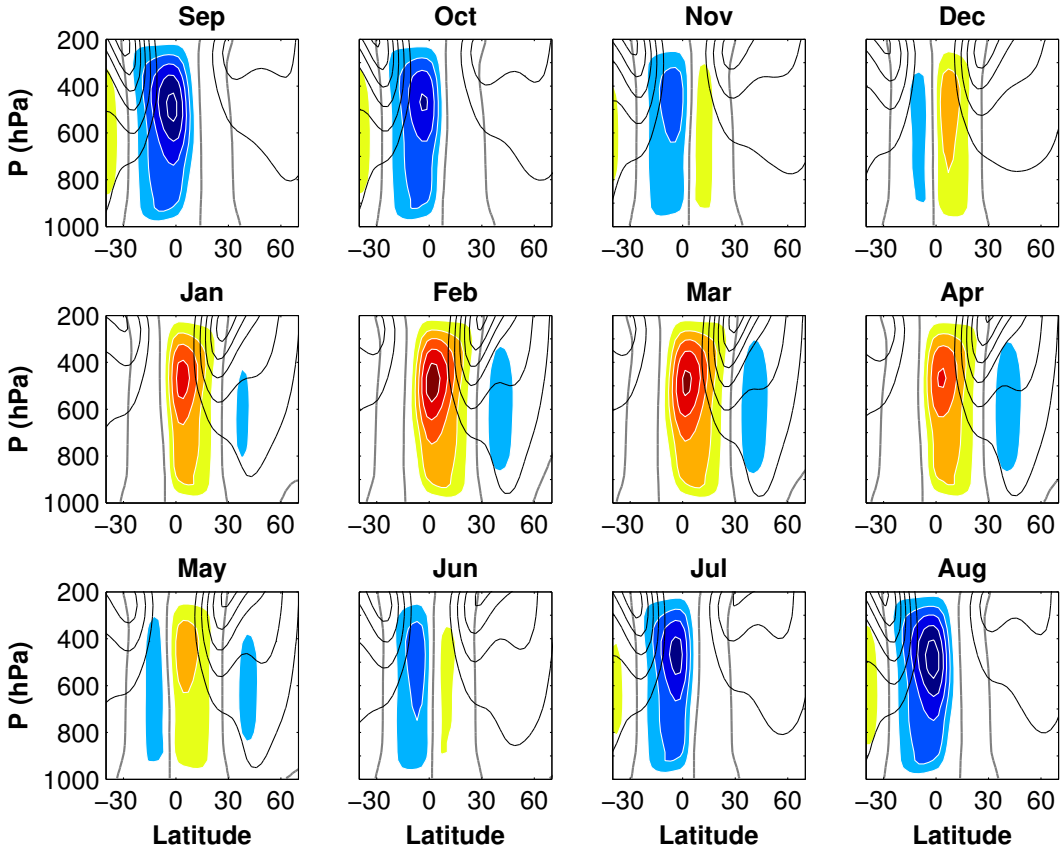

Figure 3.14: Reference simulation between September and August. Streamlines of the meridional mass streamfunction (filled contours, kg s^{-1}, contour interval 1×10^9 kg s^{-1}, zero value is denoted in gray) and zonal winds (black contours, contour interval 10 m s^{-1}).

3.7 Storm track response to variations in subtropical jet strength

3.7.1 Model description

Observations show that years of a midwinter minimum are characterized by a stronger Pacific jet during winter and early spring relative to years without a minimum (Nakamura, 1992). To examine the response of the storm track to variations in the strength of the subtropical jet, we vary the amplitude of the ocean heat flux, which allows us to control the strength of the Hadley circulation and as a result the strength of the subtropical jet. Lee and Kim (2003) have used a similar approach to study the differences between the Pacific jet, which is largely subtropical in nature, and the eddy-driven Atlantic jet. In their simulations, the strength of the subtropical jet is determined by the amplitude of tropical heating. They suggested that a strong subtropical jet would lead to eddy activity in the vicinity of

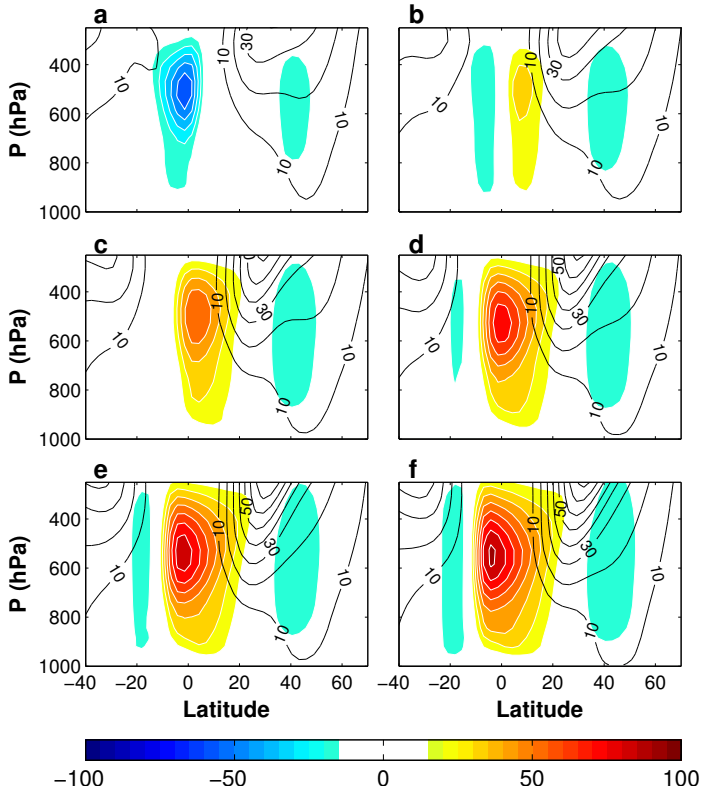

Figure 3.15: (a-f) Meridional mass streamfunction (color contours, kg s^{-1}, contour interval 1×10^9 kg s^{-1}) in idealized model simulations with varying ocean heat flux amplitude of (a) 200 W m^{-2}, (b) 100 W m^{-2}, (c) 0 W m^{-2}, (d) -100 W m^{-2}, (e) -200 W m^{-2} and (f) -300 W m^{-2}. The ocean heat flux Gaussian profile is centered in the tropics, at the same latitude as the upward branch of the Hadley circulation. Eddy momentum flux convergence (red contours, 10^{-5} m s^{-2}, contour interval 2×10^{-5} m s^{-2}) and zonally-averaged zonal wind (black, m s^{-1}) are plotted for each simulation. All fields are averaged during JFM.

the subtropical jet (on the northward flank of the jet), leading to a single jet structure, while a weaker subtropical jet will result in eddy activity extending poleward, creating a double jet structure. The inclusion of a seasonally-varying prescribed Q-flux in the ocean mixed layer provides a method for systematically controlling the strength of the Hadley circulation and the subtropical jet as they shift with the seasons. Furthermore, in idealized GCM simulations the Hadley cell is relatively strong, with a maximum strength of 8×10^{11} kg s^{-1}, which is approximately 10 times the observed annual mean strength. Strong Hadley cell also appears in previous studies using a similar model configuration (Bordoni, 2007; Frierson et al., 2006). A seasonally-varying ocean heat flux, as described above, can be used for this purpose and be adjusted to systematically control the strength of the cell.

Simulation results, presented in Fig. 3.15, show the idealized model response to variation of the ocean heat flux amplitude (Q-flux). The range of Q-flux amplitude is varied between 200 to -300 W m^{-2}. Here, we present results from six experiments. In response to a positive ocean heat

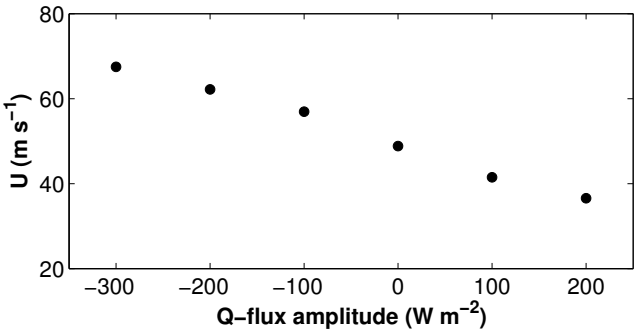

Figure 3.16: 300-hPa zonally-averaged zonal wind (m s^{-2}) as a function of ocean heat flux amplitude (in W m^{-2}). Zonal wind speed is averaged over jet maximum, between 25°-40°N and during JFM.

flux forcing (Fig. 3.15a,b), the Hadley circulation is relatively weak in the NH, associated with a relatively weak subtropical jet. As the ocean heat flux amplitude becomes more strongly negative, the Hadley circulation is enhanced, and the associated subtropical jet becomes stronger (Fig. 3.15d-f). Eddy momentum flux convergence is increased in the poleward flank of the jet. The relation between the subtropical jet strength and the Q-flux amplitude is monotonically decreasing, as demonstrated in Fig. 3.16.

3.7.2 Simulated storm track seasonal cycle

The seasonal cycle of storm track intensity in simulations with varying subtropical jet strength is shown in Fig. 3.17. In all cases, the jet reaches its maximal intensity between January and April, which is the peak of the cold season in the northern hemisphere in these simulations (for more details on the cause of this delay, see section 3.4). In winter, EKE is enhanced in the vicinity of the intensified subtropical jet, while in midlatitudes EKE is weaker relative to spring and fall. During the transition seasons, EKE in midlatitudes becomes relatively strong, with an increase of 20-25% in fall and spring compared to midwinter. In spring, EKE forms a double storm track structure, with a distinct separation between two regions of EKE enhancement (Fig. 3.17e,f). While strengthening of the subtropical jet reaches its peak between January and May, most of the increase in storm track intensity occurs in spring (Fig. 3.18), suggesting that the sensitivity of the strength of the subtropical jet is larger in spring, and therefore the storm track response is more pronounced, relative to earlier seasons. In terms of its latitudinal position, strengthening of the subtropical jet occurs around latitude ∼30°N, with very little variation in latitude as it strengthens (Fig. 3.19a). As a result, EKE increases in the vicinity of the jet but also in midlatitudes (Fig. 3.19b).

Fig. 3.20 shows the seasonal cycle of lower-level baroclinicity, averaged between 850-700 hPa, in zonally-symmetric simulations with weak, medium and strong subtropical jet. Following Lee and Kim (2003), we identify two branches of maximum Eady growth rate, one along the subtropical

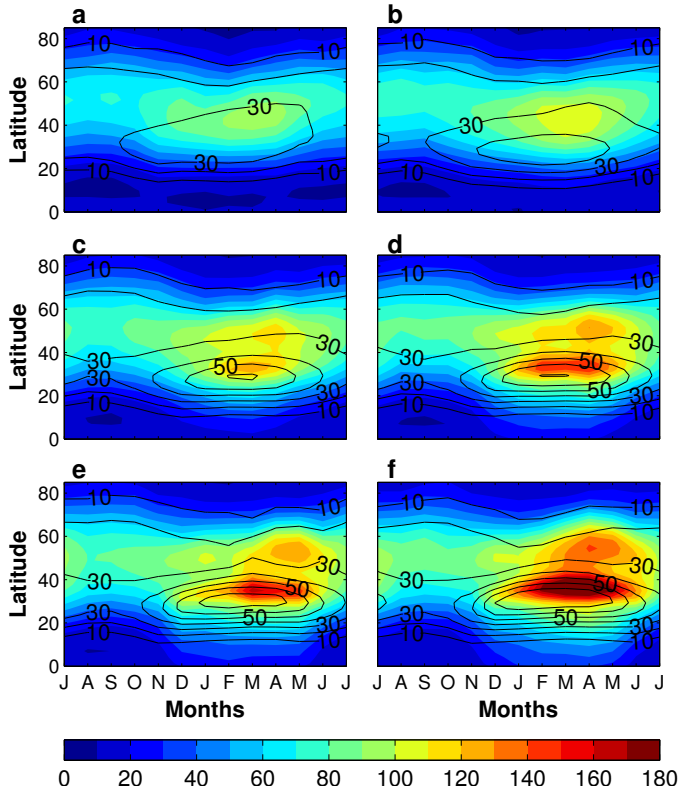

Figure 3.17: Seasonal cycle of (a-f) zonally-averaged 300-hPa EKE (color contours, m^2 s^{-2}) and zonal wind (black, m s^{-1}) at the same vertical level in idealized model simulations with varying subtropical jet strength (same as in Fig. 3.15).

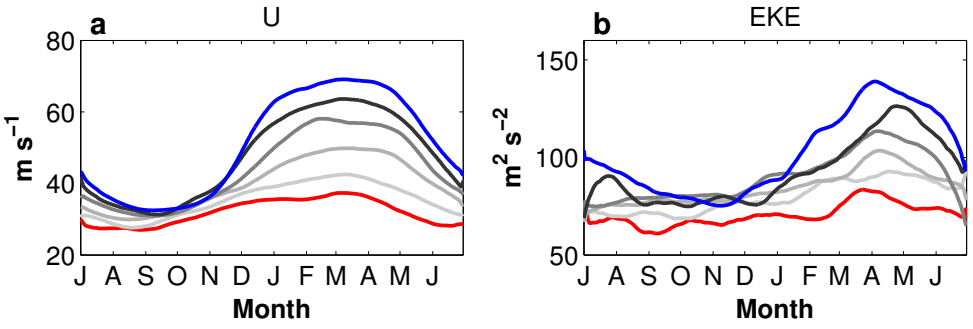

Figure 3.18: Seasonal cycle of 300-hPa (a) zonal wind (m s^{-1}) and (b) EKE (m^2 s^{-2}) in idealized model simulations with varying subtropical jet strength (same as in Fig. 3.15) between weak subtropical jet (Q=200 W m^{-2}, red curve), medium-strength jet (from Q=100 W m^{-2} to Q=-200 W m^{-2}, gray curves) and strong subtropical jet (Q=-300 W m^{-2}, blue). Zonal wind is averaged between 20°-40°N, and EKE between 40°-60°N. Results are smoothed using a 31-day running average.

jet and the other in the midlatitudes, where the midlatitude branch is not necessarily located where there is a preexisting jet (Lee and Kim, 2003). As the strength of the subtropical jet increases, the

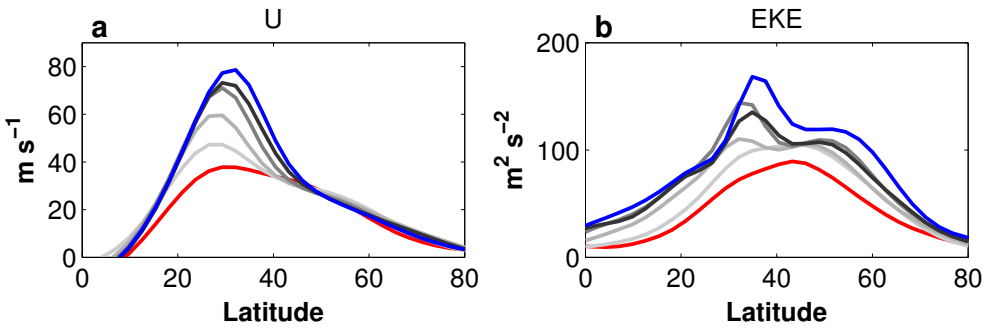

Figure 3.19: A comparison of wintertime 300-hPa (a) zonal wind (m s^{-1}) and (b) EKE (m^2 s^{-2}) in idealized model simulations with varying subtropical jet strength (same as in Fig. 3.15) between weak subtropical jet (Q=200 W m^{-2}, red curve), medium-strength jet (from Q=100 W m^{-2} to Q=-200 W m^{-2}, gray curves) and strong subtropical jet (Q=-300 W m^{-2}, blue). Winter season is represented by February-March average.

maximum Eady growth rate shifts from midlatitudes to the latitude of subtropical jet. This transition also occurs throughout the seasonal cycle; maximum baroclinicity moves from midlatitude branch in fall to the subtropical branch in winter, and then back to the midlatitude branch in spring (Fig. 3.20c). In simulation with strong subtropical jet, baroclinicity is reduced in midlatitudes by nearly 30% during midwinter relative to simulation with weak jet (Fig. 3.20c), suggesting that despite the lack of a clear midwinter minimum of eddy activity, lower-level baroclinicity exhibits a significant reduction in midlatitudes during midwinter, as the strength of the subtropical jet is increased. Under these conditions, baroclinic wave growth in midlatitudes is expected to be suppressed during midwinter even in a zonally-symmetric configuration.

In response to the increase in the strength of the jet, EKE is mostly increased close to the subtropical jet (Fig. 3.21). Baroclinic wave growth in midlatitudes is decreased and a weaker eddy-driven jet is formed. On the other hand, in the case of a relatively weak subtropical jet, baroclinic wave growth mostly occurs in more poleward latitudes. According to (Lee and Kim, 2003), if the subtropical jet is sufficiently strong, there will be a transition from double, well-separated jets to a single jet structure. In our simulations, the double jet structure is mostly apparent in middle-levels of the atmosphere (between 600-500 hPa, Fig. 3.21a-c), and its transition to a single jet when the subtropical jet strengthens is reproduced as well. Yet, despite the transition to a single jet, EKE in simulations with strong subtropical jet has a double storm track structure, indicating that some of the baroclinic wave growth still takes place in midlatitudes.

During winter, the maximum Eady growth rate is strongest near the jet maximum (Fig. 3.22). However, in the lower levels of the atmosphere, as also demonstrated in Fig. 3.20, Eady growth rate is reduced in midlatitdues as the strength of the subtropical jet is increased. This reduction of baroclinicity is most pronounced in the lower levels of the atmosphere, between 600-800 hPa. At

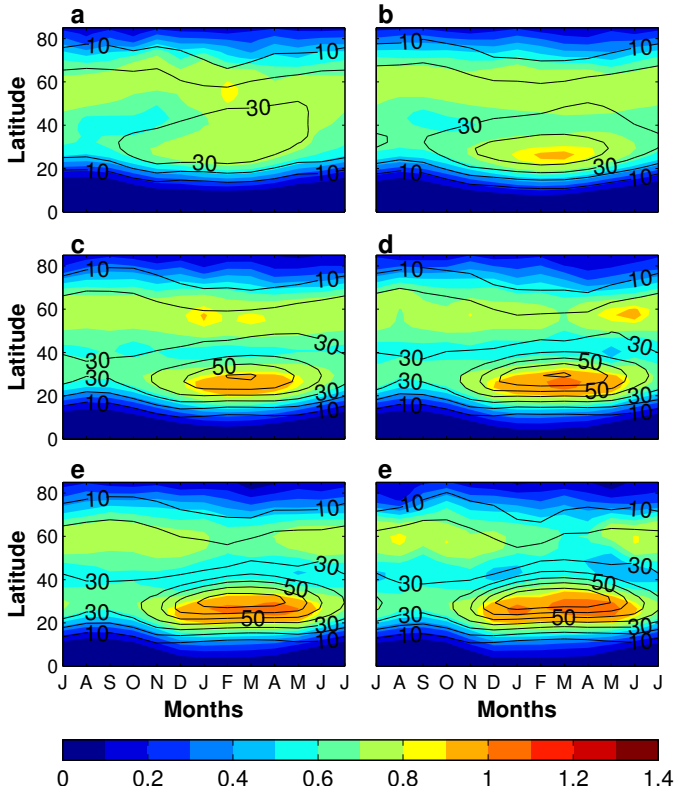

Figure 3.20: Seasonal cycle of lower-level Eady growth rate (color, day^{-1}) averaged between 850-700 hPa in zonally-symmetric simulations with varying subtropical jet strength (amplitudes as in Fig. 3.19). Zonal wind at 300-hPa (black, m s^{-1}) is shown for reference. The fields are zonally-averaged, and smoothed using a 31-day running average.

the same time, in the subtropics baroclinicity in enhanced (particularly in the upper-levels of the atmosphere, but not only), which leads to baroclinic wave growth in the vicinity of the subtropical jet. Weakening of baroclinicity in midlatitudes is consistent with weakening of the eddy-driven jet and transition to a single jet structure.

To better understand the relationship between storm track intensity and jet strength in the zonally-symmetric configuration, we plot vertically-averaged EKE at different levels of the atmosphere as a function of subtropical jet strength (defined here as the averaged zonal wind in the subtropics, between 20°-40°N) (Fig. 3.23a). At all pressure levels, there is a positive relation between the intensity of midlatitude eddies the strength of the jet in the subtropics, in agreement with previous studies that showed a linear growth of baroclinic eddies in response to strengthening of the subtropical jet (Lee and Kim, 2003). However, when the relation between EKE and near-surface baroclinicity (represented by the Eady growth rate) in midlatitudes is examined (Fig. 3.23b), we find an inverse relation which resembles the interannual variability of the Pacific storm track (Nakamura, 1992), where years of strong jet and enhanced baroclinicity are associated with weaker eddies.

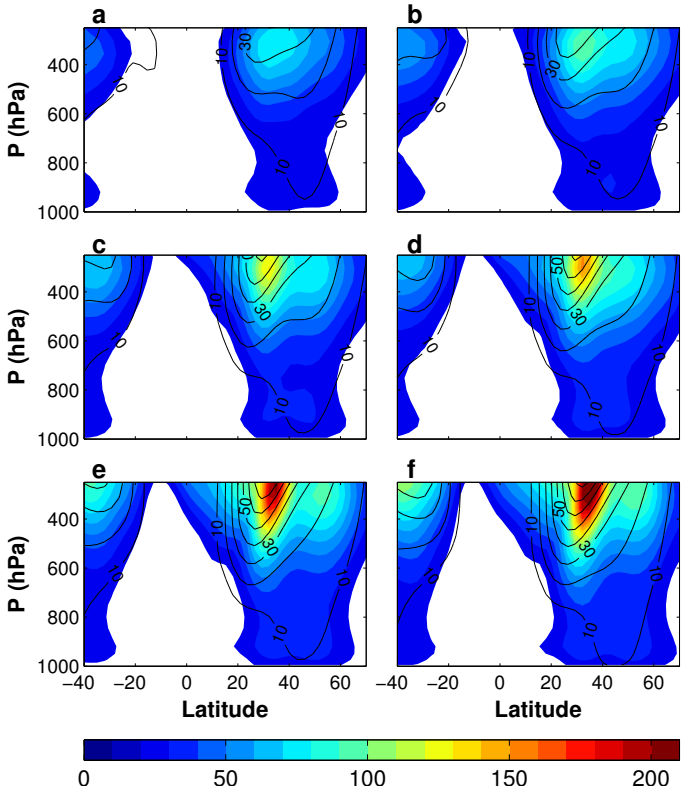

Figure 3.21: (a-f) Vertical structure of JFM-mean, zonally-averaged EKE (color contours, $m^2\ s^{-2}$) and zonal wind (black, m s^{-1}, starting from 10 m s^{-1}) in idealized model simulations with varying subtropical jet strength (same as in Fig. 3.15).

3.7.3 Seasonal variation of baroclinicity, shear and static stability

The reduction in near-surface Eady growth rate during winter (Fig. 3.22) suggests less favorable conditions for baroclinic growth, which may help to explain the observed midwinter suppression. The Eady growth rate depends on both vertical shear of zonal wind and static stability. Following Penny et al. (2010), we examine the seasonal cycle of each variable, relative to its annual mean (Fig. 3.24). Eady growth rate can be expressed in terms of static stability and vertical wind shear as follows (Penny et al., 2010)

$$\frac{\Delta\sigma}{\overline{\sigma}} \approx \frac{\Delta\lambda}{\overline{\lambda}} - \frac{\Delta N}{\overline{N}} \tag{3.6}$$

where σ indicates the maximum Eady growth rate, λ represents vertical wind shear, and N is static stability. An overbar denotes the annual mean and Δ implies departure of each variable from its annual mean.

In simulations with a relatively weak subtropical jet, Eady growth rate maximizes in winter (JFM), while static stability is strongly negative and the shear is either zero or negative. In contrast, in the

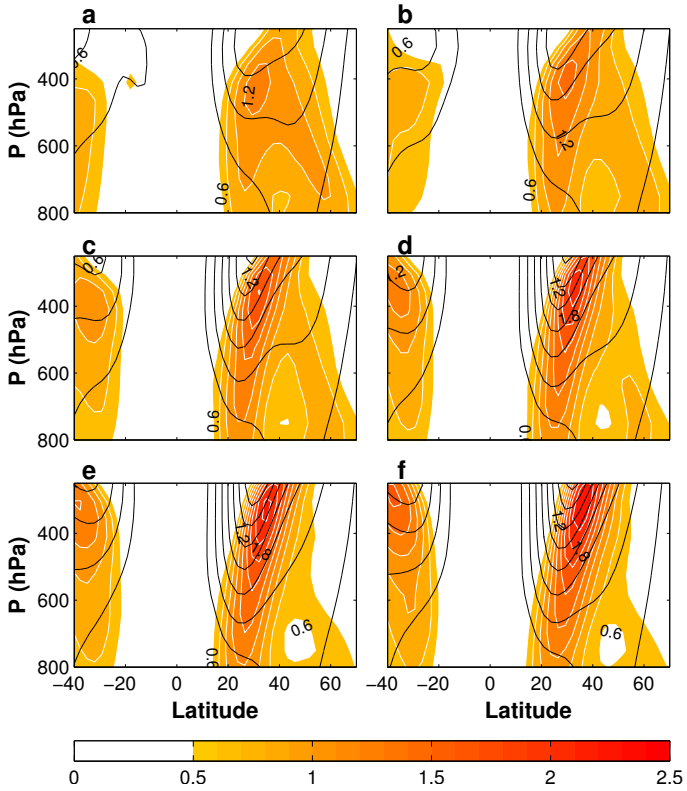

Figure 3.22: (a-f) Vertical structure of zonally-averaged Eady growth rate (color contours, s^{-1}) in idealized model simulations with varying subtropical jet strength (same as in Fig. 3.15).

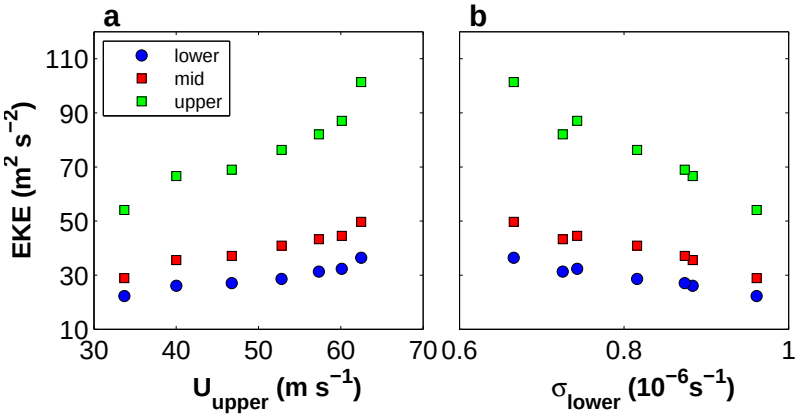

Figure 3.23: Scatter plot of (a) vertically-averaged EKE (m^2 s^{-2}), averaged between 800-950 hPa ("lower"), 400-750 hPa ("mid"), and 250-400 hPa ("upper") and between 40°-60°N, as a function of upper-level zonal wind (m s^{-1}), averaged over the subtropics (between 20°-40°N) in idealized model simulations with varying strength of the subtropical jet (controlled by the ocean heat flux, see Fig. 3.15). (b) Same as (a) but as a function of lower-level Eady growth rate (s^{-1}), averaged between 700-850 hPa and between 40°-60°N. All fields are averaged over JFM, consistent with the delayed winter season in the model.

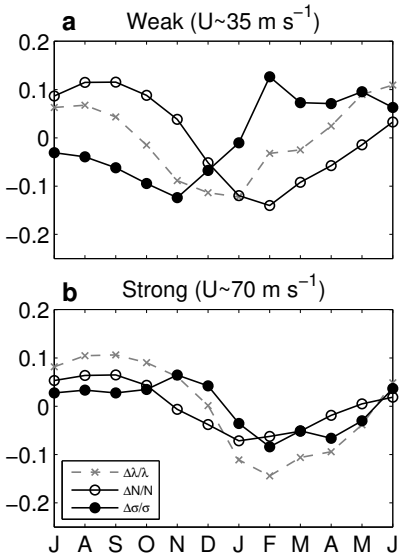

Figure 3.24: Seasonal cycle of zonally-averaged baroclinicity (thick solid line, s^{-1}), defined as the maximum Eady growth rate (Lindzen and Farrell, 1980), vertical wind shear (dashed, s^{-1}) and static stability (thin black, s^{-1}) in model simulations with (a) weak, and (b) strong subtropical jet. Each variable is averaged between 850-700 hPa and between latitudes 40°-70°N. Units correspond to the fractional departure of each variable from its annual mean.

case of a strong subtropical jet, the growth rate follows the shear with a minimum in winter, when static stability is increased. These results suggest that in simulations with a strong subtropical jet the static stability has a more stabilizing effect, similarly to observational analysis of Penny et al. (2010). This reduction of the Eady growth rate in simulations with strong subtropical jet occurs in JFM, at the same period of EKE reduction relative to spring peak (Fig. 3.17e,f). Lee et al. (2013) have suggested that strong static stability and weak wind shear in midwinter leads to a minimum in baroclinicity over the northern part of the Tibetan Plateau, in consistency with feature-tracking analysis of Penny et al. (2010). Yet, we show that a reduction in baroclinicity during midwinter can also occur in a zonally-symmetric configuration, without topography or land-sea contrast, and can be attributed to the change in the subtropical jet strength.

3.8 Model simulations with longer orbital period

On Earth, the oceans provide a long-term memory to the climate system by storing and releasing heat on longer time scales than the atmosphere. By using an ocean with a shallow mixed layer depth (as discussed in the previous section), we reduce the long-term memory of the system and obtain a shorter atmospheric response to solar forcing. An alternative method for controlling the seasonal time-scale and separating the temporal scale of the storm tracks from the seasonal time scale is by varying the

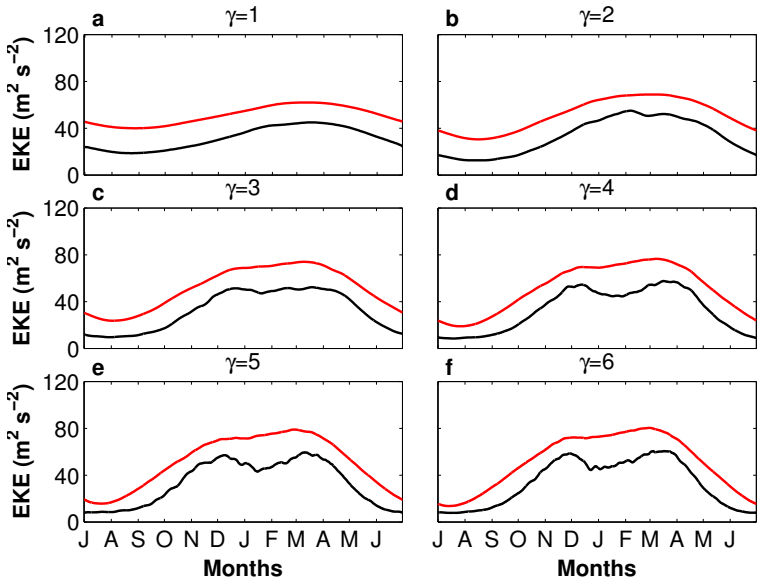

Figure 3.25: Upper-level EKE (black, in $m^2\ s^{-2}$) and upper-level zonal wind (red, in $m\ s^{-1}$, scaled by a factor of 3) in model simulations with a varying orbital period, specified by the factor γ. For all simulations, EKE is averaged between latitudes 20°-70°N. A 31-day running average is used for smoothing. The time axis is scaled by the number of days in a year (γ) in each simulation (i.e., for 365 days for γ=1, 730 days for γ=2, etc).

planetary orbital period, while maintaining an ocean mixed layer depth of 10m and keeping the rest of the radiative parameters of the model unchanged. The ratio between the seasonal timescale (τ_s) and the timescale of transient eddies (τ_e) is given by

$$\alpha = \frac{\tau_s}{\tau_e} \tag{3.7}$$

where τ_e is the synoptic eddy timescale of 3-10 days. In terms of bandpass variability, the longer seasonal timescale (τ_s) does not seem to affect the range of maximum variance, and the eddies maintain their largest variance between 3-10 days (consistent with Christoph et al., 1997).

Although the zonal wind does not vary much throughout the winter season (Fig. 3.25), eddy activity exhibits significant changes as the planetary orbital period is varied. In simulations with a lower orbital period, EKE reaches its maximum in midwinter, consistent with the maximum strength of the zonal wind. However, for the cases of longer orbital period the storm tracks exhibit a midwinter minimum with a distinct decrease in EKE in midwinter relative to fall or spring, despite a peak in the jet strength. This midwinter suppression is not limited to upper-level EKE, and occurs in the vertically-integrated EKE as well. As the orbital period is increased, the temperature gradient between the equator and the pole becomes stronger, due to the longer winters and the temperature decrease at the poles. In addition, the latitudinal distribution of EKE varies over the course of the seasonal cycle.

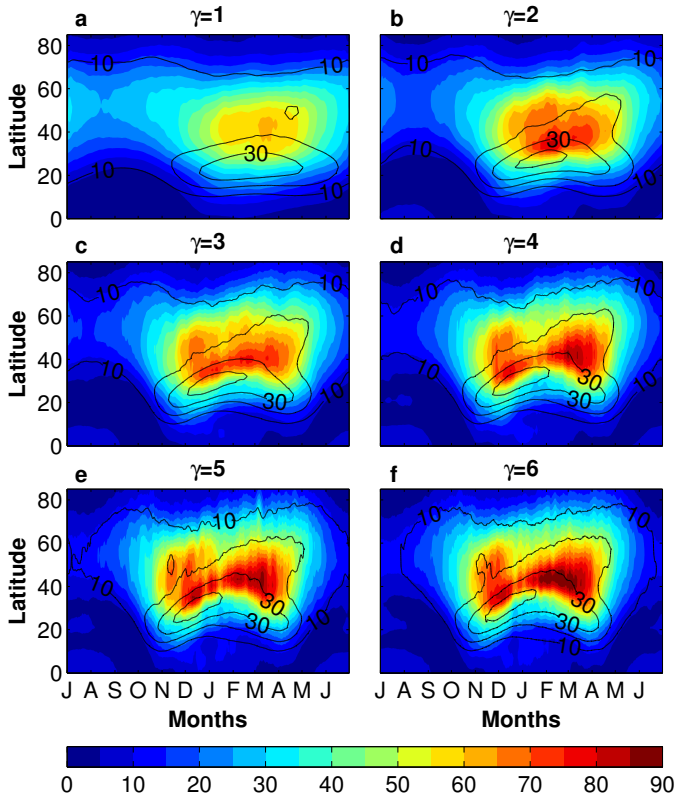

Figure 3.26: Seasonal cycle of (a-f) zonally-averaged EKE (color contours, $m^2\ s^{-2}$) and zonal wind (black, $m\ s^{-1}$) in idealized model simulations with varying orbital period (same as in Fig. 3.25). Both EKE and zonal wind are at the same vertical level of 300 hPa. Daily results are smoothed using a 31-day running average.

Narrowing of the storm tracks during midwinter contributes to the reduction in average EKE over the midlatitudes (Fig 3.26). In simulations with an orbital periods beyond 6γ the seasonal cycle does not change much in amplitude and resembles the midwinter suppression in 6γ.

In addition to the reduction of EKE in midwinter, there is an increase of EKE during fall and spring as the orbital period is increased. While in simulations with a lower orbital period EKE is strongest in midwinter, as the orbital period is increased EKE is enhanced in the shoulder seasons, resulting in larger differences between midwinter and fall or spring (Fig 3.26). During the shoulder seasons, and particularly in spring, the jet strengthens in midlatitudes, similar to the poleward shift of the Pacific jet during these seasons (Fig. 1.4c). In addition to the poleward branch of the jet, in simulations with higher orbital period there is also a subtropical branch of the jet, that is more intense in fall and spring (unlike Earth, where the subtropical jet is less intense in fall and spring due to the weakening of the Hadley cell).

These results suggest that separating the temporal scale of the storm tracks from the seasonal time scale by varying the planetary orbital period, is a useful method for understanding the effects of the

seasonal time scale. As the seasonal timescale is increased, the seasonal cycle of the storm track is significantly changed. It is found that when the same radiative gradient is forced in a slower rate, the seasonal contrast between midwinter and the transition seasons is increased. While eddy intensity is enhanced in the midlatitudes during fall and spring, it is reduced in midwinter. This seasonal variation in storm track intensity is associated with a latitudinal shift of the jet and the development of a more poleward branch of the jet in fall and spring, reaching latitude 60°N. In midwinter, the poleward branch is less intense (this transition is most apparent between midwinter and spring).

Recently, Robert et al. (2017) have found that on the short timescale (i.e., a few days) synoptic waves exert energy from the mean flow when the jet is accelerated, by increasing the rate of decay of EKE by barotropic conversion. They show that due to strong barotropic decay, there is an abrupt reduction of the total energy of synoptic eddies, occurring just after the maximum intensity of the jet. While this feedback occurs on short timescales, extending the seasonal timescale, as done in this set of experiments, may lead to this "short-term dynamics" being more prevalent. Strengthening of the jet in early-winter leads to stronger meridional shear of the jet, and results in reduction of EKE. While this feedback may last for a few days (Robert et al., 2017), in simulations with higher seasonal timescale, this process may last longer (intensified subtropical jet leads to an abrupt reduction of EKE, that in turn decelerates the eddy-driven jet, while the subtropical jet is intensified again due to external solar forcing).

3.9 Discussion

In this chapter, we perform a series of sensitivity experiments, designed for obtaining a realistic climate in the zonally-symmetric idealized GCM. To achieve a seasonal cycle, we implement a seasonally-varying daily insolation profile based on Hartmann (1994), with a latitude-dependent TOA albedo, and a time-dependent longwave absorption profile. Simulation results show that a realistic seasonal variability of the climate system can be obtained in the zonally-symmetric idealized GCM, without topography and land-sea contrast.

We conduct a series of simulations in which we vary the strength of the subtropical jet by changing the amplitude of the ocean heat flux forced at the upward branch of the Hadley cell. Simulation results show that as the strength of the subtropical jet is increased, EKE is enhanced in the vicinity of the jet, in agreement with dry model simulations of Lee and Kim (2003). In midlatitudes, EKE is increased mostly during spring, relative to winter and fall. In addition, we find that strengthening of the subtropical jet is related to weakening of near-surface baroclinicity in the midlatitude region in winter. These results suggest a possible link between the strengthening of the subtropical jet, which leads to baroclinic growth around latitude 30°N, and the reduction of midlatitudes eddies during this period. The occurrence of a late peak of EKE during spring, relative to the weaker EKE in midwinter,

resembles the second peak of EKE of the Pacific storm track (Nakamura, 1992).

The low-level baroclinicity plays an important role in controlling the jet position (Orlanski, 2003). According to Orlanski (2003), the final jet position in a series of baroclinic lifecycle experiments is determined by the characteristics of wave breaking; equatorward or poleward jet position corresponds to whether the waves break cyclonically or anticyclonically, respectively. For a weak eddy forcing, anticyclonic wave breaking occurs, leading to a poleward shift of the jet. However, above a certain threshold, the eddies become more intense and there is an abrupt shift from anticyclonic (LC1 type) to cyclonic (LC2 type) wave breaking (Thorncroft et al., 1993; Orlanski, 2003). Further work is needed to determine whether periods of midwinter minimum of storm track activity in winters of strong jet can be explained by the transition to cyclonic wave breaking.

It has been shown that in winters of strong jet disturbances rarely become mature systems, and therefore their amplitude is weaker (Penny et al., 2013). We find that the minimum becomes more pronounced as the ratio between the eddy time-scale and the seasonal time-scale is increased, which in the idealized GCM we explore by increasing the planetary orbital period. Taken together, these results suggest that when the eddies travel under slowly-changing conditions for a longer time, adjustment of the background gradients (due to the eddies activity) occurs faster than the external forcing of the meridional temperature gradient (i.e., by the sun), resulting in weaker amplitudes and less mature systems. Furthermore, these results suggest that when we increase the seasonal time-scale, while keeping the synoptic time-scale unchanged, eddy dynamics is dominated by short-term processes (Robert et al., 2017) which normally last only a few days.

In summary, we find that the zonally-symmetric model captures certain realistic aspects of the observed storm track and its seasonal cycle, including the inverse relation between the strength of the subtropical jet and midlatitude baroclinicity. In fact, the storm track seasonal cycle in the zonally-symmetric idealized GCM resembles that of the southern hemisphere. Storm track in the southern hemisphere tends to coincide with the oceanic frontal zone (also known as the Antarctic polar frontal zone) around latitude 50°N (Nakamura and Shimpo, 2004). It has been found that baroclinic growth of transient eddies is weaker in midlatitudes when the subtropical jet is intensified, suggesting that an intense subtropical jet in the southern hemisphere is not necessarily associated baroclinic growth of eddies (see also Nakamura and Shimpo, 2004; Sampe et al., 2010).

Chapter 4

The seasonal cycle of midlatitude storm tracks. Part II: zonally-asymmetric idealized GCM

4.1 Introduction

Lee et al. (2013) studied the role of topography on the seasonal cycle of the storm track using a full coupled ocean-atmosphere model with realistic orography. They found that the presence of the Tibetan Plateau tends to suppress Pacific storm track activity during midwinter despite the fact that it intensifies the upper-level jet and strengthens baroclinicity along the Pacific jet.

Consistently, Yun et al. (2016) found that during winter the Tibetan Plateau uplift intensifies the stationary EKE along the mid-latitude region except for the downstream of the Tibetan Plateau, whereas the transient EKE is substantially reduced. This suppression of transient EKE has been suggested to be partly caused by the weakening of the downstream eddy development and baroclinic energy conversion (Park et al., 2010).

While the link between the presence of the Tibetan Plateau and the Pacific midwinter minimum has been shown by previous studies, understanding the underlying mechanisms in a full GCM is rather complex. Therefore, we use an idealized GCM to isolate the main factors that affect the storm track seasonal cycle. To examine the occurrence of a midwinter minimum of transient EKE, we use the seasonal zonally-symmetric configuration, with the addition of a Gaussian mountain range at longitude 90°E and latitude 30°N. This mountain represents the Tibetan Plateau, with similar dimensions; half-width is 10° in longitude and 4° in latitude. Different from Lee et al. (2013), we do not use realistic orography, and the Gaussian mountain is the only asymmetric feature in the model. The Gaussian mountain does not modify surface properties (an aquamountain, e.g., Wills and Schneider, 2016)

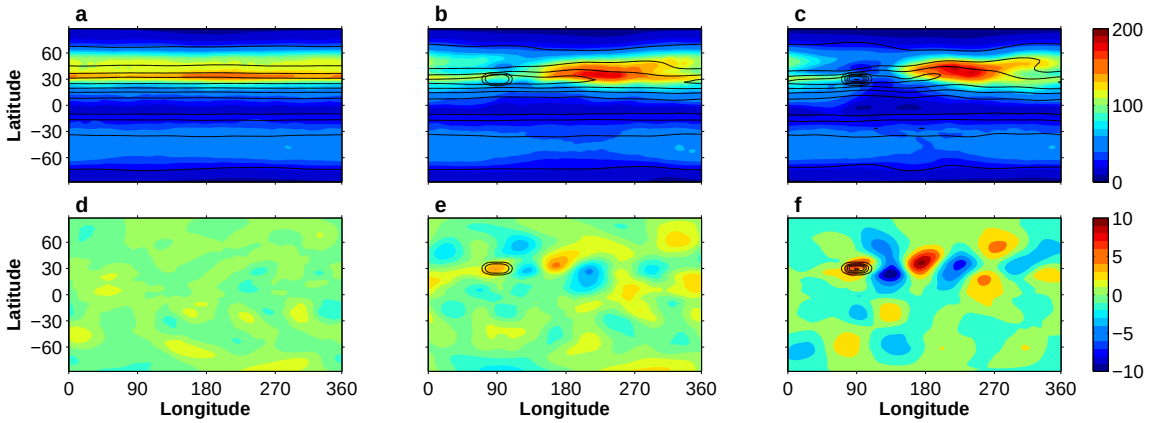

Figure 4.1: Response to the Gaussian mountain in the zonally-asymmetric reference simulation. (Upper row) JFM maps of 300-hPa EKE (color, $m^2\ s^{-2}$) and zonal wind at the same level (black, $m\ s^{-1}$) from zonally-asymmetric simulations with (a,d) flat orography, and with the addition of a Gaussian-shaped mountain with height of (b,e) 2000m and (c,f) 4500m. (Lower row) Meridional stationary velocity at 300-hPa (color, $m\ s^{-1}$), averaged over JFM. Gaussian topography is centered around longitude 90°E and latitude 30°N. The height of the Gaussian mountain is marked for reference (thick black contours, contour interval is 500m).

4.2 Idealized GCM with a Gaussian mountain

The presence of the Gaussian mountain in the model affects both the shape and the seasonality of transient eddies. As shown in Fig. 4.1a, without zonal asymmetry the storm track occupies a zonally-symmetric band of enhanced EKE in midlatitdues as expected. However, with zonal asymmetries in the form of a Gaussian mountain, stationary eddies contribute to a localized storm track (i.e., increase in transient EKE) downstream of the Gaussian mountain. For our reference, we define a Gaussian mountain with height of 4500m, representing the Tibetan Plateau (Fig. 4.1c,f). In the reference simulation, the localized zonal asymmetry results in a localized storm track (i.e., increase in transient EKE) downstream of the Gaussian mountain. The upper-level stationary-eddy meridional velocity response to the mountain is shown in Fig. 4.1f. There is a series of positive and negative meridional velocities, indicating a stationary wave train propagating in the zonal direction. Winter season is represented by JFM average, due to a delayed seasonal cycle, compared with observations. The cause for this delay is the depth of the ocean mixed layer in the model, which controls the surface thermal inertia (see section 3.4).

The seasonal cycle of the storm track, averaged downstream of the Gaussian mountain, (Fig. 4.2) shows that a midwinter minimum of transient EKE appears only in the simulation using a 4500m-high mountain. Using a lower configuration does not result in a midwinter minimum. These results are consistent with previous studies (Park et al., 2010; Lee et al., 2013), however rather than using a full, comprehensive GCMs, we use an idealized model with the exception of a Gaussian mountain,

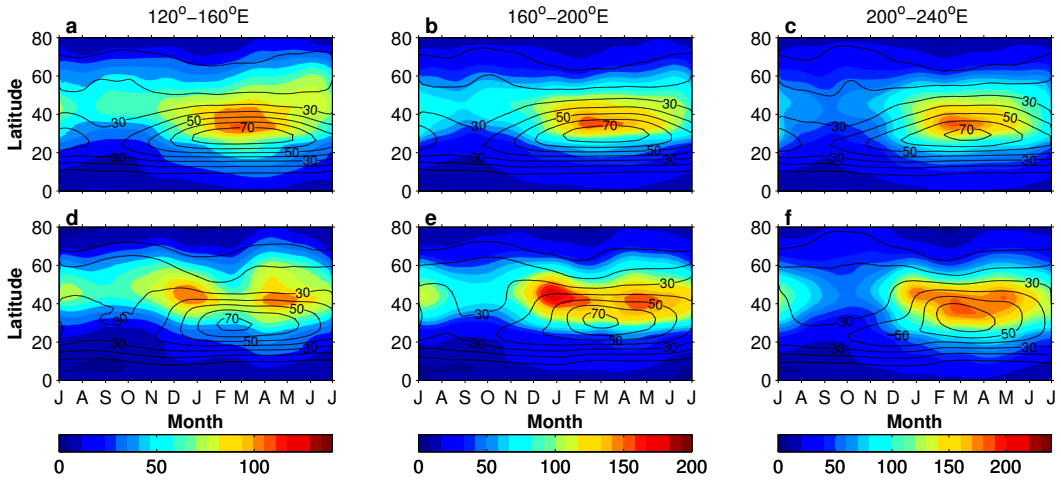

Figure 4.2: Seasonal cycle of 300-hPa EKE (color, $m^2\ m^{-2}$) and zonally averaged zonal wind at the same level (black, $m\ s^{-1}$) from idealized GCM simulations with Gaussian mountain height of (a-c) 2000m, and (d-f) 4500m, averaged downstream of the mountain, between longitudes: (left column) 120°-160°E, (central column) 160°E-160°W, and (right column) 200°-240°E.

and yet obtain a midwinter minimum of eddy activity. To further examine the downstream region, transient EKE is averaged over three longitudinal sectors in the downstream domain of the reference simulation (Fig. 4.2d-f). Results indicate that the midwinter suppression of EKE is most pronounced in the downstream region that is closest to the mountain (Fig. 4.2d,e). Further downstream, as EKE becomes more enhanced, the minimum disappears and EKE exhibits a single maximum in winter (Fig. 4.2f). For comparison, in downstream-averaged EKE in simulation with lower topography no midwinter minimum was found (Fig. 4.2a-c), as well as in the upstream region (not shown).

4.2.1 Sensitivity to the longitudinal width of the mountain

We conduct a series of simulations with varying mountain longitudinal width. Simulations with varying ridge size (i.e., longitudinal width) are presented in Fig. 4.3. For all three cases, zonal wind is strongest in winter, yet the jet is stronger in the case of a narrow Gaussian mountain (Fig. 4.3a) relative to the case of a wider ridge (Fig. 4.3c), reaching only 10 $m\ s^{-1}$ in the wide ridge case relative to 70 $m\ s^{-1}$ for the narrow ridge. However, despite the strong jet, EKE exhibits a midwinter suppression with EKE decreasing, on average, from 30 $m^2\ s^{-2}$ in November to 25 $m^2\ s^{-2}$ in January and February, and increasing again for a second peak in spring (Fig. 4.4), similar to the Pacific storm track seasonal cycle (Nakamura, 1992). As we increase the width of the mountain, the midwinter minimum becomes more pronounced further downstream of the mountain (Fig. 4.4). In addition, the seasonal cycle of the jet in the downstream region has a more realistic structure, in terms of its latitudinal position (i.e., a more poleward jet in fall and spring, and a more equatorward jet in winter) in simulations with a

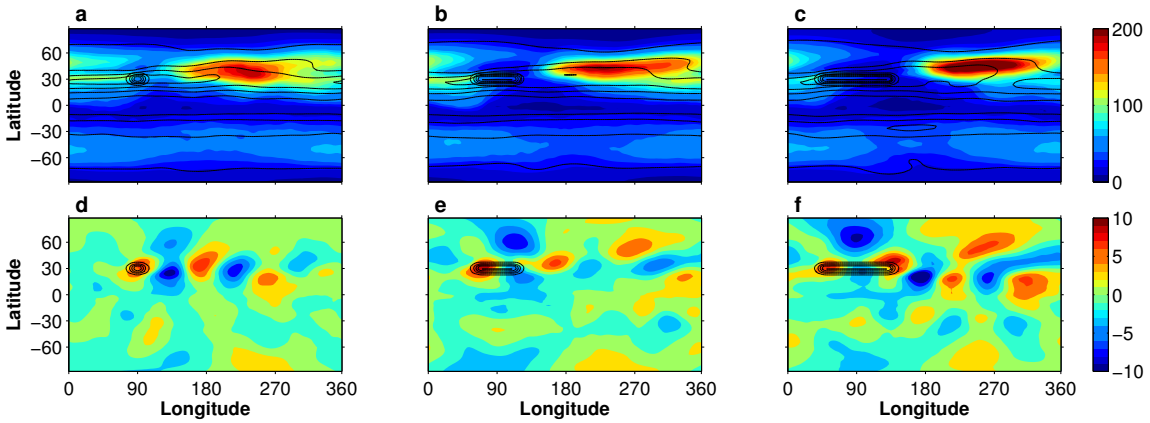

Figure 4.3: Response to extending Gaussian mountain width in the zonally-asymmetric reference simulation. (Upper row) JFM maps of 300-hPa EKE (color, $m^2\ s^{-2}$) and zonal wind at the same level (black, m s^{-1}, contour interval 20 m s^{-1}) from zonally-asymmetric simulations with varying ridge longitudinal width of (a,d) 0°, (b,e) 20° and (c,f) 40°. (Lower row) Meridional stationary velocity at 300-hPa (color, m s^{-1}), averaged over JFM. Gaussian topography is centered around longitude 90°E and latitude 30°N. The height of the Gaussian mountain is marked for reference (thick black contours, contour interval is 500m).

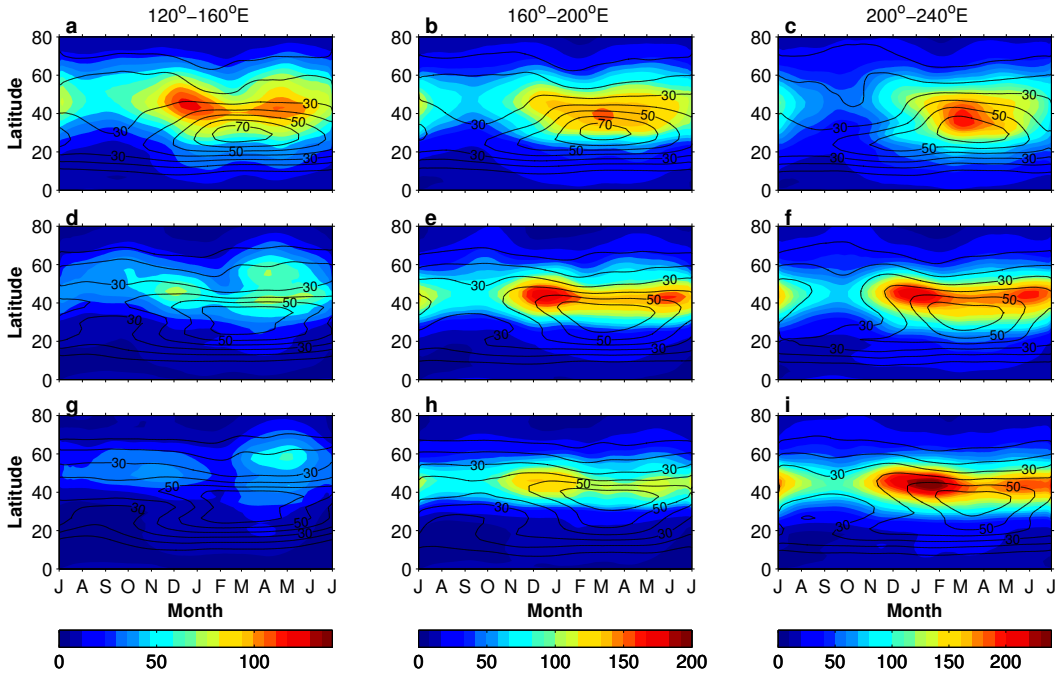

Figure 4.4: Seasonal cycle of 300-hPa EKE (color, $m^2\ m^{-2}$) and zonally averaged zonal wind at the same level (black, m s^{-1}) from idealized GCM simulations with varying Gaussian mountain longitudinal width of (a-c) 0°, (d-f) 20°, and (g-i) 40°, averaged downstream of the mountain, between longitudes: (left column) 120°-160°E, (central column) 160°E-160°W, and (right column) 200°-240°E.

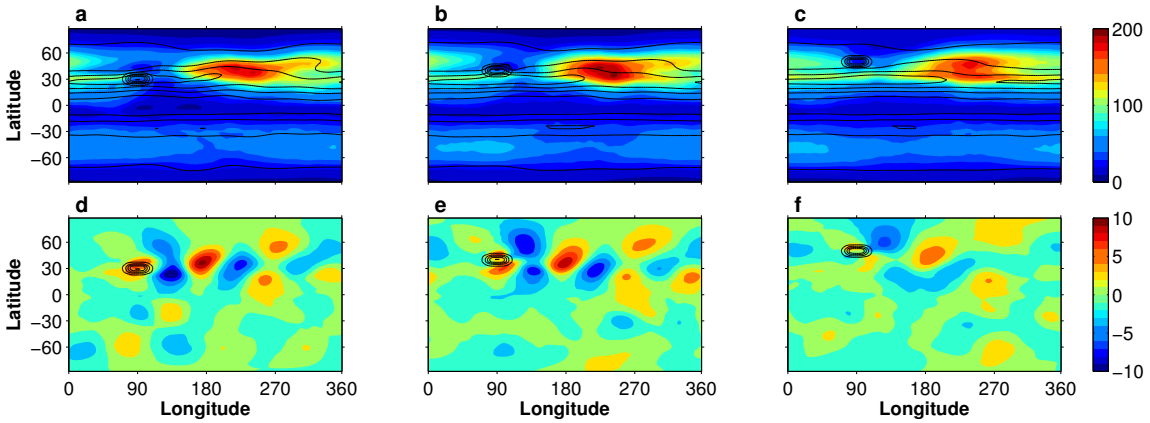

Figure 4.5: Response to the Gaussian mountain in the zonally-asymmetric reference simulation. (Upper row) JFM maps of 300-hPa EKE (color, $m^2\ s^{-2}$) and zonal wind at the same level (black, m s^{-1}, contour interval 20 m s^{-1}) from zonally-asymmetric simulations with varying Gaussian mountain position, centered at (a,d) 30°N, (b,e) 40°N, and (c,f) 50°N. (Lower row) Meridional stationary velocity at 300-hPa (color, m s^{-1}), averaged over JFM. Gaussian topography is centered around longitude 90°E. The height of the Gaussian mountain is marked for reference (thick black contours, contour interval is 500m).

wider ridge widths, suggesting that the seasonal cycle of the jet is captured in the model when the Gaussian mountain resembles a plateau, similar to the Tibetan Plateau in the upstream of the Pacific storm track.

4.2.2 Sensitivity to the latitudinal position of the mountain

In a series of simulations, we vary mountain latitudinal position and examine the storm track response to this change. Simulations with mountain centered at latitude 30°N, 40°N, and 50°N are shown in Fig. 4.5. In all three cases, zonal wind is strongest in winter. Yet, despite the strong jet, when the mountain is located at latitude 30°N, EKE is decreased during midwinter downstream of the mountain (Fig. 4.6). When the mountain in located more poleward, at latitude 40°N, the midwinter minimum is less pronounced in the downstream region that is close to the mountain, although it appears to be more robust further downstream, eastward of longitude 240°E (Fig. 4.6f). When the mountain is located at 50°N, the midwinter minimum disappears. These results show that the midwinter minimum is more pronounced when the idealized mountain is located at the latitude of the subtropical jet in the simulation, suggesting that similarly to the Pacific storm track, where the midwinter minimum occurs downstream of the Tibetan Plateau, the presence of a Gaussian mountain at a latitude 30°N contributes to the occurrence of the midwinter minimum in the model.

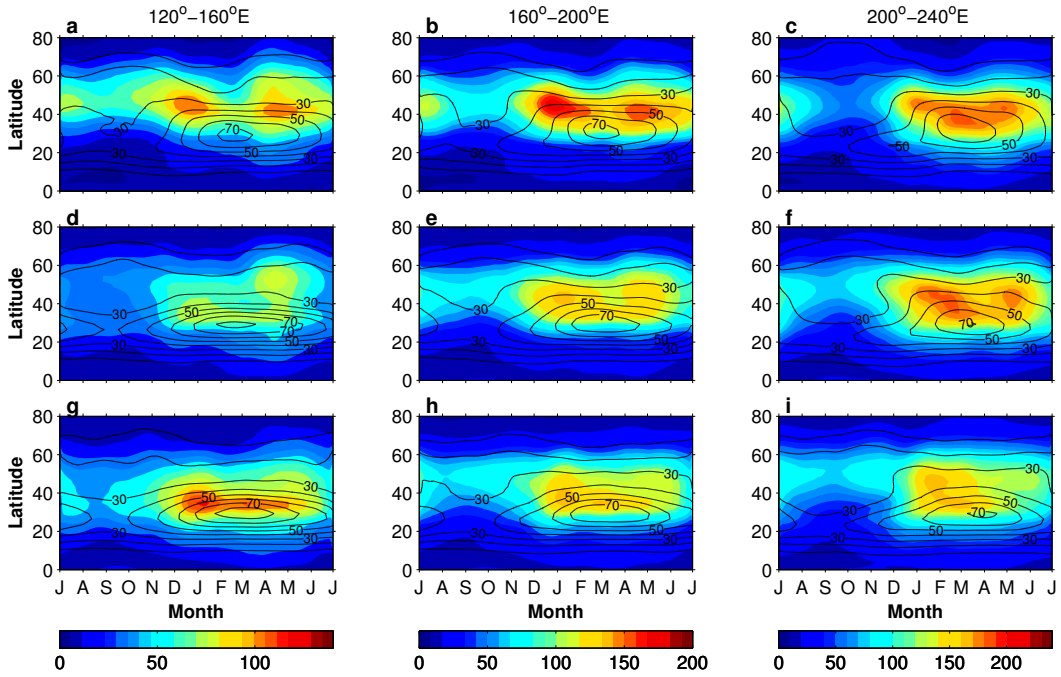

Figure 4.6: Seasonal cycle of 300-hPa EKE (color, $m^2\ m^{-2}$) and zonally averaged zonal wind at the same level (black, $m\ s^{-1}$) from idealized GCM simulations with varying Gaussian mountain position at (a-c) 30°N, (d-f) 40°N, and (g-i) 50°N, averaged downstream of the mountain, between longitudes: (left column) 120°-160°E, (central column) 160°E-160°W, and (right column) 200°-240°E.

4.3 Storm track response to variations in subtropical jet strength

Observations show that years of midwinter minimum are characterized by a stronger Pacific jet during winter and early spring relative to years without a minimum (Nakamura, 1992). To understand the relative contribution of strengthening the subtropical jet to the transient storm tracks and energy budget, we run a series of experiments in which we vary the amplitude of the ocean heat flux, which allows us to control the strength of the Hadley circulation and as a result the strength of the subtropical jet. This approach is similar to Lee and Kim (2003), where the response of baroclinic eddies to strengthening of the subtropical jet is examined. Unlike to Lee and Kim (2003), we use an idealized model forced by a daily, time-dependent insolation, rather than a perpetual forcing.

Simulation results show that in response to strengthening of the subtropical jet, the storm track becomes more intense (as shown by JFM-averaged EKE in Fig. 4.7), and the location of the storm track maximum shifts further downstream. To examine the storm track seasonal cycle, we define three longitudinal sectors in the downstream domain of the reference simulation (Fig. 4.8). As the strength of the subtropical jet is increased (associated with a negative ocean heat flux), the midwinter minimum of EKE becomes more pronounced. For the relatively strong subtropical jet presented in Fig. 4.8g,h, the eddies weaken by nearly 30% in February-March relative to their maximum intensity, despite a

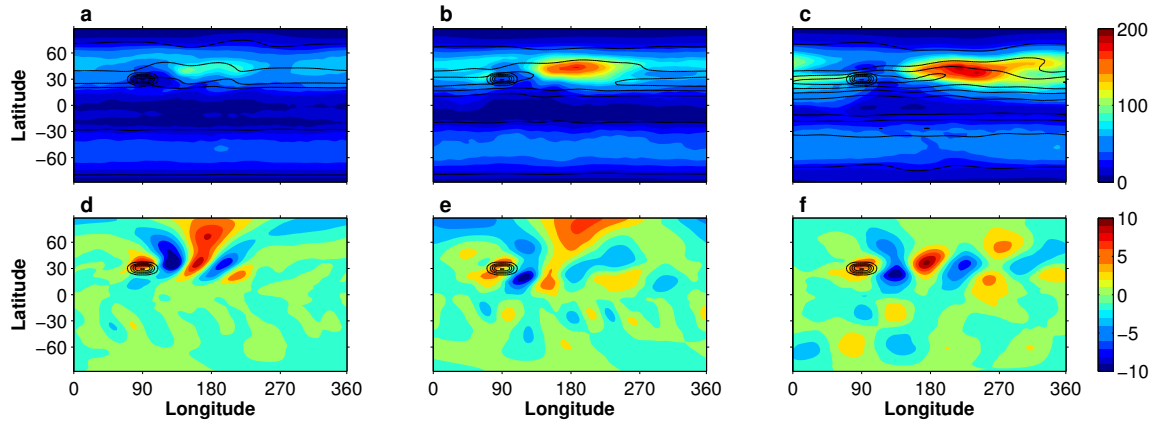

Figure 4.7: Response to the Gaussian mountain in the zonally-asymmetric reference simulation. (Upper row) JFM maps of 300-hPa EKE (color, $m^2\ s^{-2}$) and zonal wind at the same level (black, m s^{-1}, contour interval 20 m s^{-1}) from zonally-asymmetric simulations with varying subtropical jet strength of (a,d) weak jet (Q=200 W m^{-2}), (b,e) medium-strength jet (Q=0 W m^{-2}) and (c,f) strong jet (Q=-200 W m^{-2}). (Lower row) Meridional stationary velocity at 300-hPa (color, m s^{-1}), averaged over JFM. Gaussian topography is centered around longitude 90°E. The height of the Gaussian mountain is marked for reference (thick black contours, contour interval is 500m).

relatively strong jet of $\sim$70 m s^{-1} during this period. A weak midwinter minimum also occurs in simulation without ocean heat flux forcing, and is more pronounced in the downstream region that is closest to the mountain (Fig. 4.8d). Further downstream, as the subtropical jet weakens, the minimum disappears and EKE exhibits a single maximum in winter (Fig. 4.8i).

Strengthening of the subtropical jet is also associated with an equatorward shift of the jet (Fig. 4.9a). While for weak and medium jet intensities the jet is located around 40°N, a strong subtropical jet is found around 30°N. For all three cases, EKE is maximized in midlatitudes, around 40°N (Fig. 4.9b), in contrast to the zonally symmetric case where the storm track intensified in the vicinity of the subtropical jet itself. Furthermore, for weak and medium jet intensities, jet location implies that this is an eddy-driven or a merged jet, which coexists in the same latitudes as the storm track eddies (Lachmy and Harnik, 2014), while in the case of strong subtropical jet EKE maximum is found nearly 10°-15° poleward of the jet peak.

Next, we extend our set of simulations and systematically examine a wider range of ocean heat flux amplitudes. Results show that for stronger ocean heat flux amplitude, the midwinter minimum becomes more pronounced. In all simulations, the midwinter minimum (or maximum) occurs in March. The month of maximum EKE in fall changes as the amplitude of the heating becomes stronger (negative sign stands for heat transport into the atmosphere) (Fig. 4.10), with an earlier peak by $\sim$2 months for enhanced heating, hence with a stronger subtropical jet.

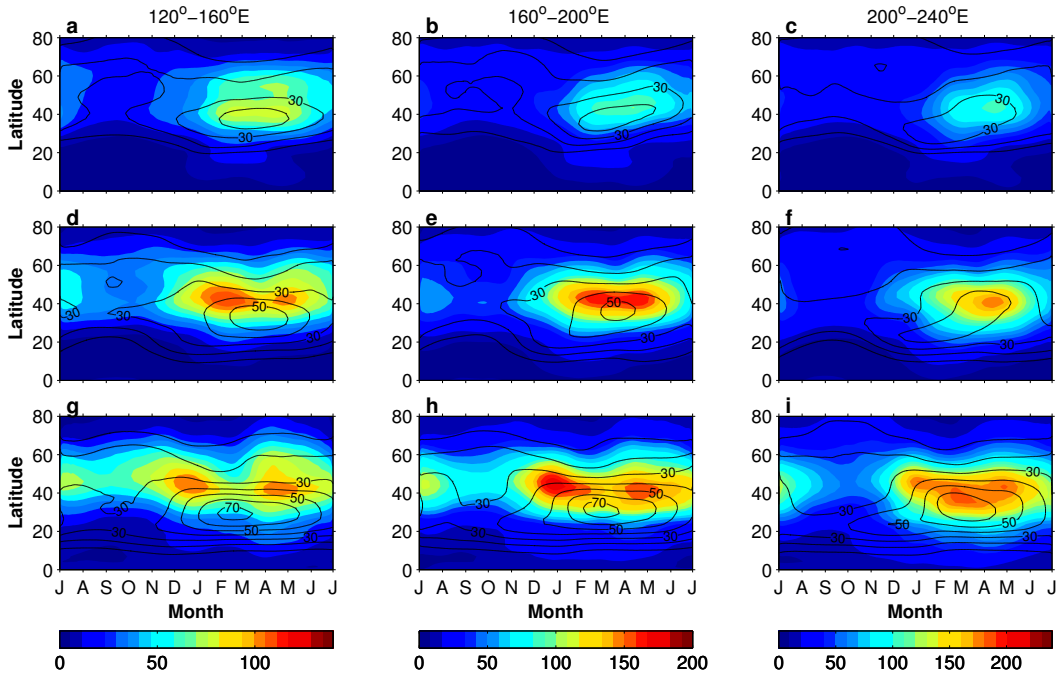

Figure 4.8: Seasonal cycle of 300-hPa EKE (color, $m^2\ m^{-2}$) and zonally averaged zonal wind at the same level (black, m s^{-1}) from zonally-asymmetric simulations with varying subtropical jet strength of (a,b) weak jet (Q=200 W m^{-2}), (c,d) medium-strength jet (Q=0 W m^{-2}) and (e,f) strong jet (Q=-200 W m^{-2}), averaged downstream of the mountain, between longitudes: (left column) 120°-160°E, (central column) 160°E-160°W, and (right column) 200°-240°E.

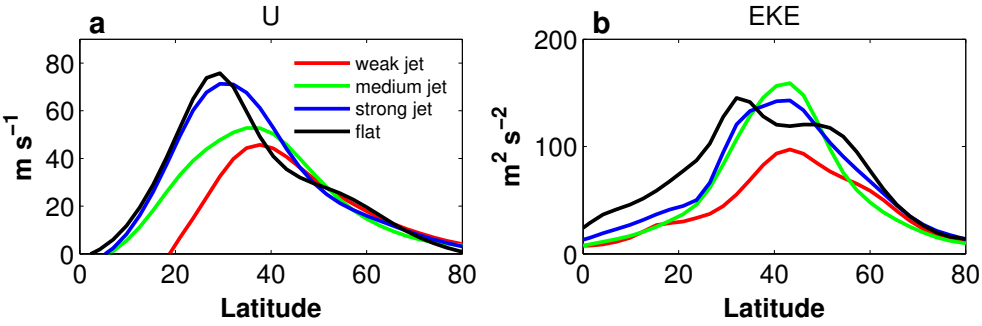

Figure 4.9: A comparison of wintertime 300-hPa (a) zonal wind (m s^{-1}) and (b) EKE ($m^2\ s^{-2}$) between idealized model simulations with weak subtropical jet (red), medium-strength jet (green) and strong subtropical jet (blue). Fields are averaged downstream of the mountain, between 160°E-160°W. Winter season is represented by February-March average.

4.4 Eddy-mean flow energy cycle

The mean meridional circulation in midlatitudes (and the global atmosphere) can be described by the eddy-mean energy cycle (Lorenz, 1955). While the solar radiative forcing maintains a zonally-symmetric flow, eddies in midlatitudes tend to deform the zonally-symmetric temperature structure

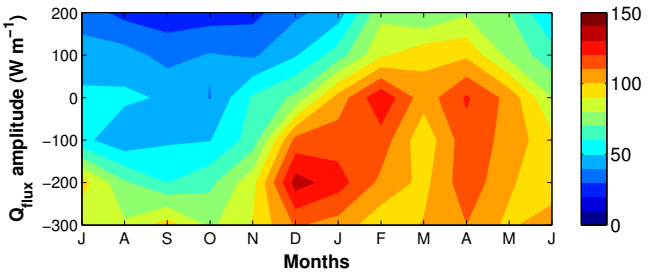

Figure 4.10: Seasonal cycle of zonally-averaged 300-hPa EKE (color contours, m^2 s^{-2}) as a function of ocean heat flux amplitude, in zonally-asymmetric simulations with varying ocean heat flux amplitude of 200, 100, 0, -100, -200 and -300 W m^{-2}, averaged between latitudes 30°-60°N and between longitudes 160°E-160°W).

(Peixoto and Oort, 1992). Mechanisms such as baroclinic instability can transform some of the eddy available potential energy into kinetic energy of the eddies. These eddies, in turn, transport momentum in midlatitudes, and transfer energy into the kinetic energy of the mean. Other, more barotropic, mechanisms, such as transport of momentum by the eddies up the gradient of the mean flow, can lead to conversion of the eddy kinetic energy back into mean kinetic energy (from the small scale into the large scale). Analyzing the energy transfer between the mean flow and the eddies, and between the potential energy and kinetic energy, can shed light on the underlying mechanisms controlling the amplitude of eddy kinetic energy in midlatitudes and specifically the midwinter minimum. This approach is particularly relevant for the midwinter minimum, where eddy kinetic energy is decreased in midwinter despite the intense zonal mean flow and the enhanced baroclinicity during this season.

We examine the eddy kinetic and available potential energy budgets as presented by the Lorenz energy cycle (Lorenz, 1955). The equation for the evolution of EKE (K_e) can be written as follows

$$\frac{\partial K_e}{\partial t} = -\nabla \cdot \overline{\left(\mathbf{v}\mathrm{K_e} + \mathbf{v_a'}\Phi\right)} - \overline{\omega'\alpha'} - \overline{\mathbf{v}' \cdot \left(\mathbf{v_3'} \cdot \nabla_3\right)\overline{\mathbf{v}}} - \frac{\partial}{\partial \mathrm{p}}\overline{\omega \mathrm{K_e}} - \frac{\partial}{\partial \mathrm{p}}\overline{\omega'\Phi'} + \overline{\mathrm{R}} \tag{4.1}$$

where $\mathbf{v} = (\mathrm{u}, \mathrm{v})$ is the horizontal wind velocity, $\mathbf{v_3}$ the three-dimensional velocity. K_e is kinetic energy of the eddies ($\mathrm{EKE} = \frac{\overline{\mathrm{u'^2}}+\overline{\mathrm{v'^2}}}{2}$). The eddy components (primed) are defined as deviations from the mean flow, and the mean is denoted by an overbar. The eddy fields are obtained by time filtering of daily horizontal winds (with cutoff frequency of 3-10 days). [1]

The first term on the rhs represents the convergence of the total energy flux, due to advection by the

[1] Chang (2001) defines the eddies as deviation from the time mean (monthly mean). However, in this case we use time filtering as an alternative definition of the storm track (Blackmon, 1976; Blackmon et al., 1977). Similar to Drouard et al. (2015), we can write the eddy energy equations for the high-frequency eddies, where overbars and primes indicate the low-frequency and high-frequency parts of the flow. In this case, the contributions from lowpass (>10 days) eddies are usually small compared to the others and their time mean is zero (see also Riviere et al., 2015; Drouard et al., 2015). The medium-range bandpass used for this analysis (3-10 days) captures the same variability of synoptic-scale signal as the high-frequency range (of <10 days) used in (Drouard et al., 2015).

mean flow and the eddies, and due to dispersion. The second term represents conversion from eddy available potential energy (EAPE) to EKE. The third term is the barotropic conversion between the kinetic energy of the mean (MKE) to EKE. The fourth and the fifth terms are the energy vertical flux convergence (these terms vanish when vertically integrated over the entire atmospheric column). The residue term R contains contributions from friction and additional terms (e.g., first-order correlations between the mean and the eddies) that become zero when applying a climatological mean. A similar interpretation of these terms has been discussed by previous studies (e.g., Orlanski and Katzfey, 1991; Chang and Orlanski, 1993; Chang, 2001).

The eddy potential energy equation (P_e) can be written as follows

$$\frac{\partial P_e}{\partial t} = -\nabla \cdot \overline{\mathbf{v}\mathrm{P_e}} - \overline{\omega'\theta'\frac{\partial \Theta(\mathrm{p})}{\partial \mathrm{p}}} - \overline{\theta'\left(\mathbf{v_3'}\cdot\nabla_\mathbf{3}\right)\left[\overline{\theta}-\Theta(\mathrm{p})\right]} + \overline{Q'\theta'} - \frac{\partial}{\partial \mathrm{p}}\overline{\omega P_e} \tag{4.2}$$

where θ is the potential temperature and $\Theta(\mathrm{p})$ is the reference potential temperature. The first term on the rhs is convergence of eddy potential energy due to advection, the second term is the conversion between EAPE and EKE, and the third term is baroclinic conversion between the available potential energy of the mean flow (MAPE) and EAPE, also referred to as the baroclinic generation term (Chang, 2001). The fourth term represents diabatic sources or sinks of potential energy. The fifth term is vertical energy flux convergence.

We examine the meridional profiles of the dominant terms in the eddy kinetic and potential energy balances (Fig 4.11). We find that in all seasons eddies lose energy in the subtropics, and gain energy in more poleward latitudes through barotropic conversion (Fig 4.11a). During the winter season, eddies gain EKE through barotropic conversion mostly around latitude 40°N (negative values in Fig 4.11a), while losing EKE in the subtropics. Both the energy gain and loss are stronger in winter relative to fall and spring. Conversion of EAPE to EKE occurs around latitude 30°N (Fig 4.11b) and indicates that EKE is mostly gained in this region. Convergence of total energy flux has the opposite sign than that of $-\overline{\omega'\alpha'}$ (Fig 4.11c), and their magnitude is quite similar. Baroclinic conversion of transient MAPE to EAPE (Fig 4.11d) is responsible for eddy energy gain in midlatitudes, with the largest conversion rate in winter. However, in addition to its increase, we note that the maximum of baroclinic conversion shifts equatorward in winter, relative to the transition seasons.

To investigate how the presence of topography in the model affects the eddy energy budget, and specifically the baroclinic and barotropic conversion during midwinter, we compute the vertically-integrated barotropic and baroclinic conversion rates in a simulation with flat topography (i.e., zonally-symmetric configuration) and compare these results to that of a simulation with a Gaussian mountain (i.e., zonally-asymmetric configuration). Results are shown in Fig. 4.12. As expected, in a simulation without a Gaussian mountain, all terms have a zonally symmetric pattern (gray curves in Fig. 4.12). We note that the barotropic conversion is negative downstream of the mountain, indicating that eddies

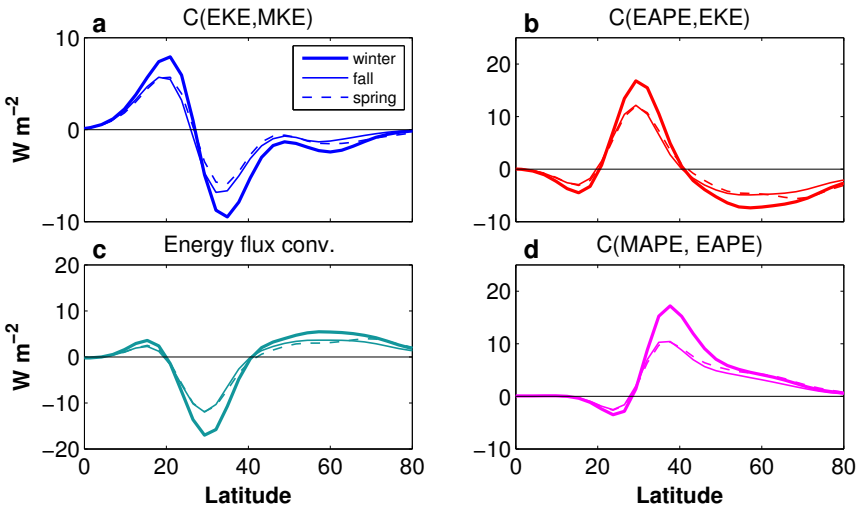

Figure 4.11: Energy conversions in the eddy energy budget as a function of latitude. Vertically integrated (a) barotropic conversion rate (W m^{-2}, following Eq. 4.1), (b) conversion between EAPE to EKE (W m^{-2}, second term on rhs in Eq. 4.1) and (c) energy flux convergence (W m^{-2}, first term on rhs in Eq. 4.1) for winter (thick line), fall (thin) and spring (dashed), from zonally-symmetric simulation with intensified subtropical jet (obtained by ocean heat flux of -200 W m^{-2}). Conversion rates are vertically-integrated between 250-850 hPa, and zonally-averaged over all longitudes. Seasons are represented according to their period in simulation (Dec-Jan, Feb-Mar and Apr-May for fall, winter and spring, respectively). (d) Baroclinic conversion term (W m^{-2}, following Eq. 4.2).

gain energy, on average, in this region. In winter, barotropic conversion becomes strongly negative, relative to fall and spring, and more kinetic energy is transferred from of the mean flow to the eddies. This term becomes closer to zero further downstream, yet it does not become positive until upstream of the mountain (in this context, we note that positive barotropic conversion in the downstream region, around 60°W, occurs when near-surface levels are included in the vertical integration). On the other hand, the baroclinic conversion, shown in Fig. 4.12d, is strongly positive in the downstream of the mountain, however it also indicate eddy energy gain. This term is stronger in winter, relative to the other seasons, indicating a positive contribution to the available potential energy budget of the eddies. In addition, the peak of baroclinic energy conversion is located further downstream in winter, possibly related to a more effective energy redistribution by advection (Chang and Orlanski, 1993). The other two terms in the EKE equation, conversion from EAPE to EKE and energy flux convergence (Fig. 4.12b and Fig. 4.12c, respectively) are smaller than the baroclinic and barotropic conversion terms and change their sign multiple times further downstream.

To understand how strengthening of the subtropical jet influences the eddy energy budget during midwinter, we compare the zonally-averaged, vertically-integrated conversion rate between three simulations with weak, medium and strong subtropical jets. First, we examine the zonally-symmetric model configuration (Fig. 4.13). While baroclinic conversion is almost identical between all three

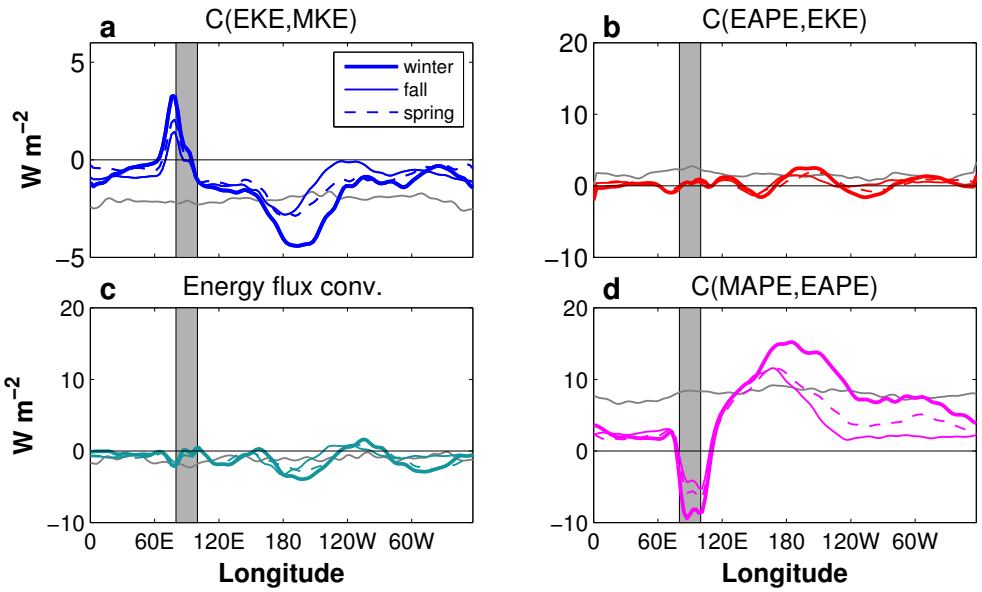

Figure 4.12: Eddy energy budget as a function of longitude. Vertically integrated (a) barotropic conversion rate (W m^{-2}), (b) conversion between EAPE to EKE (W m^{-2}), (c) energy flux convergence (W m^{-2}), and (d) baroclinic conversion term (W m^{-2}) for winter (thick line), fall (thin) and spring (dashed) in a zonally-asymmetric simulation, with a Gaussian mountain. Conversion rates are vertically-integrated between 250-850 hPa, and meridionally-averaged between 20°-70°N. Winter mean of each term in a simulation with a zonally-symmetric configuration (i.e., flat topography) is denoted in gray. Shaded area marks the extent of the mountain.

simulations (Fig. 4.13b), indicating an increasing eddy energy in midlatitudes, there are significant differences in the intensity of barotropic conversion (Fig. 4.13a). For a weak subtropical jet, bartropic conversion is rather weak, with only a small maximum of eddy energy loss in the subtropics. However, as the strength of the subtropical jet is increased, eddies tend to lose more energy to the mean flow in the subtropics, as indicated by the positive contribution of barotropic conversion equatorward of 30°N, yet gain more energy poleward of 30°N.

Next, we compare the baroclinic and barotropic conversion rates in a zonally-asymmetric model simulations with weak, medium and strong subtropical jets (Fig. 4.14). Similar to the zonally-symmetric case, baroclinic conversion shifts more equatorward as the subtropical jet is increased (Fig. 4.14b). Increasing the subtropical jet strength does not influence the amplitude of baroclinic conversion and it remains quite similar despite the change in the mean flow. Barotropic conversion becomes more strongly negative as the subtropical jet strengthens, and the peak of barotropic energy conversion shifts further equatorward (Fig. 4.14a). The positive contribution (i.e., eddy energy loss) shifts from around 30°N to almost 20°N. Consequently, less energy is gained in the midlatitudes due to the equatorward shift of the conversion peaks, consistent with the shift of EKE maximum to the vicinity of the subtropical jet in simulations with strong jet (Fig. 4.9).

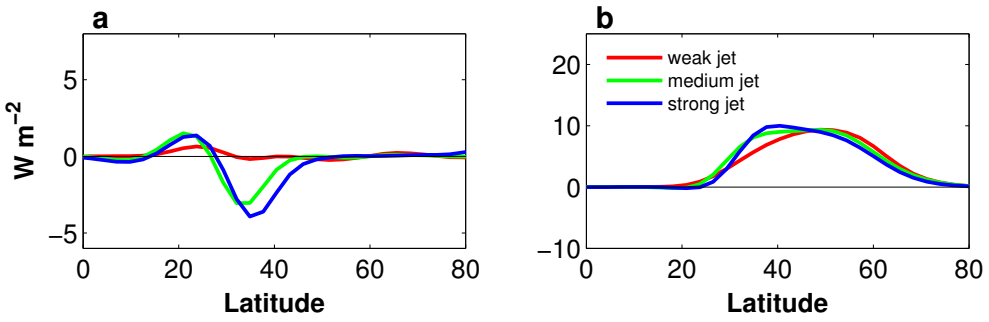

Figure 4.13: A comparison of wintertime vertically-integrated (a) barotropic conversion rate (W m^{-2}) and (b) baroclinic conversion (W m^{-2}) between idealized model simulations with weak subtropical jet (Q=200 W m^{-2}) (red line), medium-strength jet (Q=0 W m^{-2}) (green), strong subtropical jet (Q=-200 W m^{-2}) (blue), and strong jet without topography (black). Conversion rates are vertically-integrated between 250-850 hPa, and averaged over all longitudes. Winter season is represented by February-March average. Simulations are described in section 3.7.

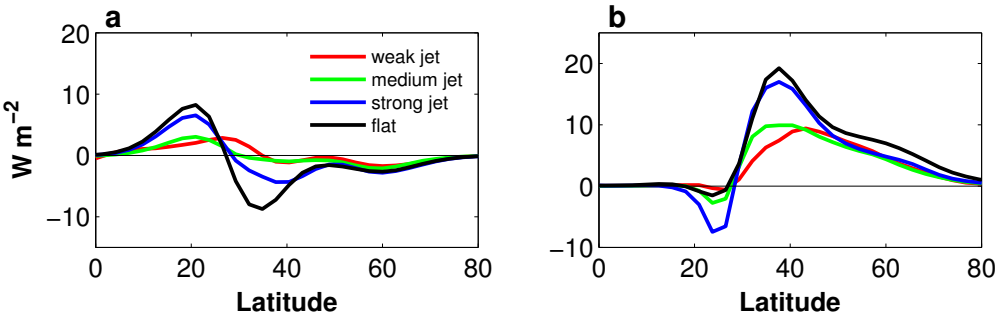

Figure 4.14: Same as Fig. 4.13 for a zonally-asymmetric model configuration. A comparison of wintertime vertically-integrated (a) barotropic conversion rate (W m^{-2}) and (b) baroclinic conversion (W m^{-2}) between idealized model simulations with weak subtropical jet (red line), medium-strength jet (green) and strong subtropical jet (blue). Conversion rates are vertically-integrated between 250-850 hPa, and averaged over all longitudes. Winter season is represented by the February-March average.

Furthermore, examining the energy budget in simulation with flat topography (in black) reveals that in the zonally-symmetric case eddies tend to gain more energy through barotropic conversion in the subtropics, between 30°-40°N. Hence, the addition of a Gaussian mountain to the model is associated with reduced zonally-averaged barotropic conversion, despite the intense subtropical jet (Fig. 4.14a). In midlatitudes, barotropic conversion gradually goes to zero, indicating that energy is neither gained or lost by barotropic process, while baroclinic conversion is maximized in this region (Fig. 4.14b).

In summary, the main difference between these simulations is the amplitude of the eddy-mean flow energy conversions. As subtropical jet intensity is increased, the eddies gain more energy in

midlatitdues through baroclinic conversion to EAPE, and more energy is gained in winter relative to fall or spring. In addition, in winter the eddies gain more energy poleward of 30°N through barotropic conversion to EKE, but also losing more EKE equatorward of 30°N (Fig 4.11). The implementation of a Guassian mountain leads to less EKE gain in the downstream area that is closest to the mountain, westward of 160°E, relative to the zonally-symmetric case (Fig. 4.12a), and may suggest that the midwinter minimum can be explained by the reduction in barotropic conversion in simulations with zonal asymmetry. In addition, while baroclinic conversion rate in midwinter indicates that more energy is transferred to the eddies, relative to fall and spring, most of this increase takes place around the subtropical jet in simulations with strong subtropical jet, and the change in midlatitudes is very small (Fig. 4.14b). Similarly, more eddy energy loss through barotropic conversion occurs more equatorward as the subtropical jet strengthens (Fig. 4.14a).

Relation to the Pacific storm track Chang (2001) has shown that over the Pacific storm track, baroclinic growth (associated with horizontal structure of eddy geopotential flux) occurs in midlatitudes, and contributes to the EKE budget. In midwinter this contribution is larger than the annual mean (see also Peixoto and Oort, 1992), indicating that the eddies gain more energy in winter. On the other hand, eddies tend to lose energy in the subtropics (through barotropic conversion), and this reduction is more pronounced in midwinter (Peixoto and Oort, 1992). While this reduction could provide a potential explanation for the midwinter suppression of EKE, over the Pacific eddies actually tend to lose less energy in midwinter, relative to fall and spring (Chang, 2001; Yin, 2002; Chang and Zurita-Gotor, 2007), which does not explain the observed midwinter minimum of EKE. We find that in a zonally-asymmetric idealized model, two processes contribute to the reduction in the eddy energy budget. First, during the winter season baroclinic energy conversion occurs further equatorward relative to fall and spring, leading to less energy gained by the eddies in midlatitudes during this period. Second, during midwinter eddies indeed gain more energy in the midlatitudes as was found over the Pacific by previous studies (Chang, 2001; Yin, 2002; Chang and Zurita-Gotor, 2007), but this contribution is smaller than that of the zonally-symmetric case (Fig. 4.12a).

4.5 Atlantic storm track response

While the midwinter suppression is a robust feature of the Pacific storm track both in model and in observations, there has been less attention to the possibility of an Atlantic midwinter minimum. Over the Atlantic storm track, a midwinter minimum of transient EKE is less frequent, although it occurs in nearly 30% of the years (particularly, years of strong jet can be associated with favorable conditions for an Atlantic midwinter minimum, see section 2.4 for discussion). To examine the differences between the Pacific and the Atlantic storm track, we run the model using a topography configuration

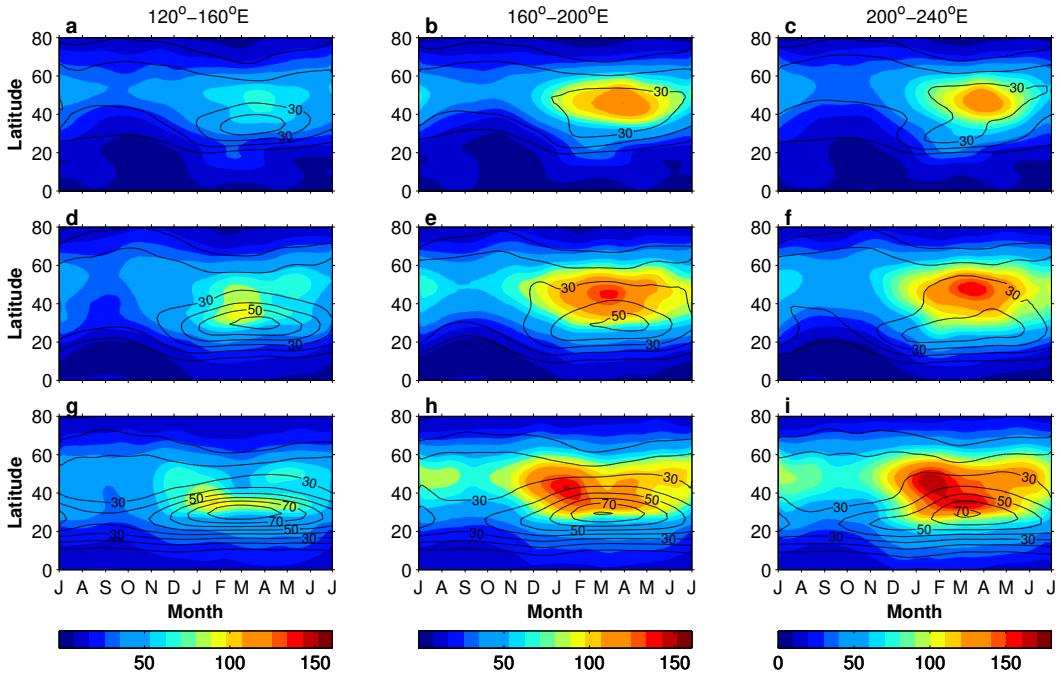

Figure 4.15: Storm track response to "Rocky Mountains" topography. Seasonal cycle of 300-hPa EKE (color, $m^2\ m^{-2}$) and zonally averaged zonal wind at the same level (black, $m\ s^{-1}$) from zonally-asymmetric simulations with a Gaussian mountain located at latitude 45°N, and varying ocean heat flux of (a-c) 200 $W\ m^{-2}$, (d-f) 0 $W\ m^{-2}$ and (g-i) -200 $W\ m^{-2}$, averaged downstream of the mountain, between longitudes (left column) 120°-160°E, (central column) 160°E-160°W, and (right column) 200°-240°E.

that resembles the Rocky Mountains (Wills and Schneider, 2016), and thus the downstream "Atlantic" storm track. When the zonal-asymmetry is located at latitude 45°N, rather than at latitude 30°N, the storm track seasonal cycle reaches its maximum intensity in winter (Fig. 4.15, middle row), without a midwinter suppression of EKE as occurs in simulations with a mountain at 30°N.

Variation of the subtropical jet strength in the "Atlantic" model configuration indicates that similarly to the Pacific storm track the Atlantic EKE is also influenced by the strength of the subtropical jet (controlled by the magnitude and the sign of ocean heat-flux in the model). When the subtropical jet is weaker (Fig. 4.15, upper row) there is a single maximum of EKE, comparable to the winter peak in the reference case (middle row of Fig. 4.15). However, when the subtropical jet is stronger, transient EKE is suppressed in late winter and early spring despite the relatively strong jet and enhanced baroclinicity (Fig. 4.15g-i). Interestingly, the storm track seasonal cycle in simulations with strong subtropical jet resembles the Atlantic EKE in years of negative NAO, shown in Fig. 2.9a, with a weakening of EKE in late-winter and spring. The jet in these simulations in more equatorward, centered around latitude 30°N, suggesting a link between the pronounced late-winter suppression of EKE and the equatorward, zonal jet in years of negative NAO.

4.6 Discussion

While the storm track midwinter minimum is a robust feature of midlatitude dynamics over the Pacific, there is no agreement on what is the dominant underlying mechanism. Here we study the midwinter minimum using an idealized GCM, by implementing a Gaussian mountain to form a zonally-asymmetric configuration. We show that a midwinter minimum occurs in simulations with Gaussian mountain of 4500 m, which resembles the Tibetan Plateau. The minimum is most pronounced when the mountain is located around latitude 30°N, suggesting that the minimum occurs due to an interaction between the subtropical jet and topography, which causes a suppression of midlatitude EKE during winter.

Our results imply that the midwinter minimum is associated with relatively strong subtropical jet. Below a certain threshold of subtropical jet strength, the storm tracks will not exhibit a midwinter minimum, yet as the subtropical jet intensifies, a pronounced midwinter minimum of storm track intensity will occur in the downstream region of the mountain. The presence of a Gaussian mountain leads to more reduction in lower-level baroclinicity in midlatitudes during midwinter. Baroclinicity decreases significantly when the subtropical jet is intensified, and as a result baroclinic wave growth is suppressed in midwinter and the midlatitude, eddy-driven jet weakens.

Seasonal variation of the eddy-mean flow interaction, represented using the Lorenz energy cycle, may potentially explain the source of the midwinter suppression. We find that two processes may be responsible for the reduction in EKE. First, baroclinic energy conversion peaks further equatorward in midwinter as the subtropical jet becomes stronger, indicating less energy gained by the eddies in midlatitudes. Second, while barotropic conversion contributes to stronger energy gain by the eddies poleward of latitude 30°N), an equatorward shift of the barotropic conversion results in less eddy energy gained. Hence, the reduced energy conversion from the mean to the eddies could potentially explain part of the observed midwinter minimum of transient EKE.

We find that barotropic energy conversion from the mean flow to transient eddies is weaker during midwinter in simulations with Gaussian mountain, despite the stronger jet. The inefficiency of barotropic energy conversion can be attributed to a change in the eddy structure in the presence of the Tibetan Plateau (Lee et al., 2013). As the westerly jet strengthens, eddy structure tends to become less efficient in converting the mean flow energy into eddy energy (Chang, 2001; Nakamura et al., 2002).

Recently, Robert et al. (2017) have found that synoptic waves also exert energy from the mean flow when the jet strengthens, by increasing the rate of decay of EKE by barotropic conversion. When jet intensity is increased, horizontal wind shear is increased and the rate of EKE decay by barotropic conversion will become more strongly negative. As a result, there is an abrupt reduction of the total energy of synoptic eddies, occurring just after the maximum intensity of the jet. Furthermore, Robert et al. (2017) propose a negative feedback: due to the reduction in EKE, the synoptic eddies will

deposit less momentum into the jet core, resulting in deceleration of the eddy-driven jet.

4.7 Appendix A: MWM Index and subtropical jet strength

To compare the seasonal variation of EKE between simulations, we define an index Δ, which is the difference between fall and spring averages and midwinter, normalized relative to fall and spring average

$$\Delta E = \frac{< E_{\text{winter}} > - < E_{\text{fall,spring}} >}{< E_{\text{fall,spring}} >} \tag{4.3}$$

where angle brackets denote a horizontal mean. The relation between Δ and the strength of the jet is presented in Fig. 4.16. A weak jet is associated with larger, positive ΔEKE, indicating that EKE in these simulations is stronger in midwinter than in fall and spring, on average. As the strength of the subtropical jet is increased, ΔEKE becomes negative and its absolute value is increased as well, indicating a midwinter minimum of EKE relative to fall and spring (Fig. 4.16a). Furthermore, examining the relation between EKE and jet strength reveals that when the subtropical jet is stronger, the absolute intensity of EKE is increased as well, relative to the reference simulation (Fig. 4.16b), indicating a positive relation between storm track intensity and jet strength, unlike the observed inverse relation of the Pacific for jet speeds exceeding 45 m s^{-1} (Nakamura, 1992). Interestingly, the relation between EKE and jet strength is not increasing linearly, and reaches a saturation beyond a certain threshold on 55 m s^{-1}.

Therefore, while these simulations capture the seasonal variability of the storm tracks, with the midwinter minimum becoming more pronounced as the subtropical jet strengthens, the intra-model variability seems to be different from the interannual variability of the Pacific storm tracks.

4.8 Appendix B: Seasonal variability of lower-level baroclinicity

A systematic variation of the strength of the subtropical jet shows that the midwinter minimum of storm track intensity becomes more pronounced when the jet strength is increased. Fig. 4.17 shows the seasonal cycle of lower-level Eady growth rate, averaged between 850-700 hPa, in zonally-asymmetric simulations (i.e., with a Gaussian mountain) with weak, medium and strong subtropical jet. In all simulations there are two branches of maximum Eady growth rate, one along the subtropical jet ($\sim$ 30°N) and the other in the midlatitudes ($\sim$50°N), similarly to Lee and Kim (2003). For a weak subtropical jet case, baroclinicity branches are located more poleward, around 60°N (Fig. 4.17a). The maximum Eady growth rate moves from midlatitudes in fall to the latitude of the jet ($\sim$ 40°N) in winter and back to midlatitudes in spring. As the strength of the subtropical jet increases, a similar tran-

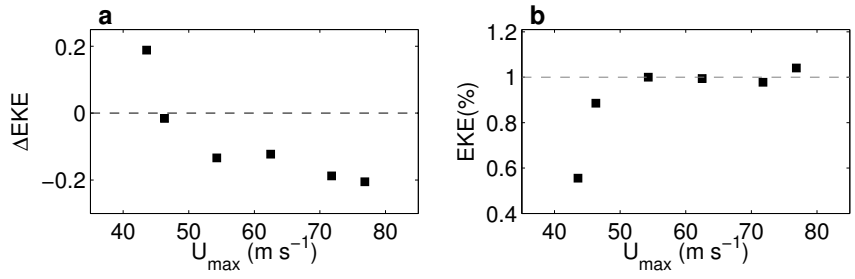

Figure 4.16: (a) ΔEKE as a function of jet maximum (m s^{-1}) in a series of model simulations with varying subtropical jet strength. ΔEKE is defined as the difference between fall and spring average value, and midwinter. The difference is then normalized relative to fall and spring average. (b) EKE in percentage relative to the reference simulation (without ocean heat flux forcing). Both zonal wind and EKE are zonally averaged over the downstream region (between 160°E-160°W). Subtropical jet strength is defined according to the maximum of zonally-averaged zonal wind between 20°-40°N. EKE is averaged over a 10° latitude interval centered around jet maximum. Seasonal EKE is based on monthly-averaged EKE.

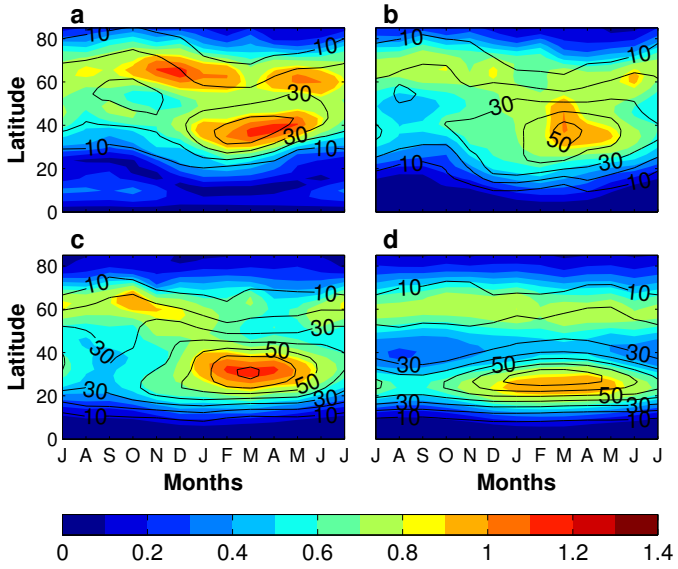

Figure 4.17: Seasonal cycle of lower-level baroclinicity (color, day^{-1}) and zonally averaged zonal wind at 300 hPa (black, m s^{-1}) from zonally-asymmetric simulations with varying subtropical jet strength of (a) weak subtropical jet, (b) medium-strength jet, (c) strong subtropical jet, and (d) same as (c) with flat-topography configuration. The fields are averaged downstream of the mountain (160°E-160°W), and smoothed using a 31-day running average.

sition occurs from midlatitudes in fall/spring to the latitude of subtropical jet in winter (Fig. 4.17c). However, for the strong jet case, baroclinicity is reduced in midlatitudes by nearly 30% during mid-winter relative to simulation with weak jet, corresponding to the reduction in EKE shown in Fig. 4.8h.

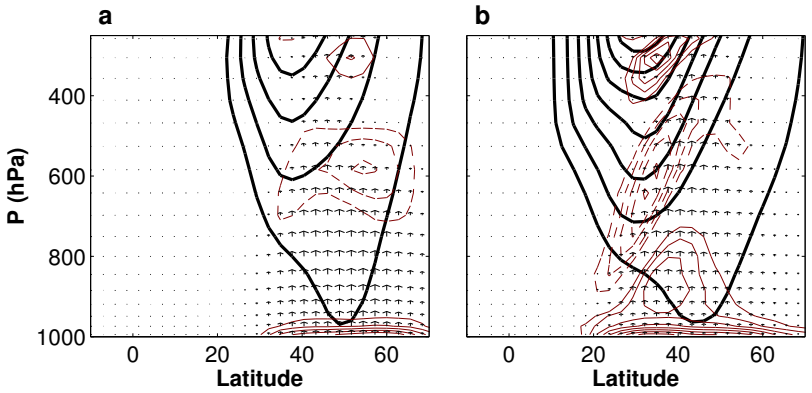

Figure 4.18: The Eliassen-Palm flux in a zonally-asymmetric idealized GCM, with the presence of a Gaussian mountain. The EP flux (arrows) and its divergence (red contours, with intervals of 0.4 m s^{-1} day^{-1}) during winter in simulations with (a) weak subtropical jet, and (b) strong subtropical jet. The solid contours indicates flux divergence and eastward flow acceleration, and the dashed contours indicate flux convergence and flow deceleration. All fields are zonally averaged downstream of the mountain (between 160°E-160°W). The zonal wind is denoted for reference (black contours, m s^{-1}).

Note that in the medium-jet strength case, a midwinter reduction in midlatitude baroclinicity is more robust in the downstream area which is closest to the mountain (120°-160°E). These results suggest that the presence of zonal asymmetry leads to reduction in lower-level baroclinicity in midlatitudes during midwinter. When the subtropical jet is stronger, this reduction in midlatitude baroclinicity becomes even more pronounced, leading to a suppression baroclinic growth in midwinter. Comparing these results with the zonally-symmetric case (Fig. 4.17d), indicates that without topography two branches of baroclinicity co-exist, yet the Eady growth rate has a relatively weak amplitude along the subtropical branch (∼25°N) and along the poleward midlatitude branch (∼60°N).

Therefore, the midwinter minimum of EKE becomes more pronounced in simulations with a Gaussian topography as a result of the reduced localized baroclinicity in midlatitudes during midwinter, and the corresponding suppression of the baroclinic growth. Strengthening of the subtropical jet leads to strengthening of baroclinicity further downstream of the mountain, and to an equatorward, eastward-extended baroclinic zone (not shown).

4.9 Appendix C: Seasonal variation of the EP Flux

The Eliassen-Palm flux acts to decelerates the flow in the upper troposphere, where it is balanced by the Coriolis force, while accelerating the flow at the surface, where it is mostly balanced by friction (Vallis, 2007).

Convergence of the EP flux is most dominant in the midlatitudes, and is stronger when the sub-

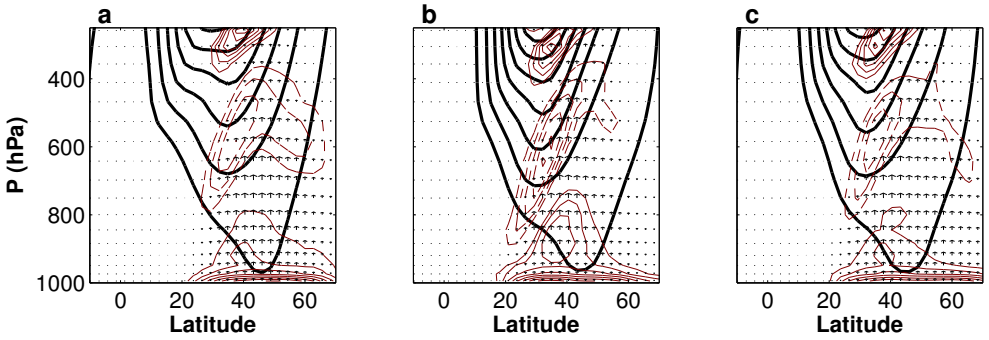

Figure 4.19: The seasonal variation of the Eliassen-Palm flux. Fields are the same as in Fig. 4.18 for fall, winter and spring, in zonally-asymmetric simulation with a strong subtropical jet.

tropical jet is more intense (Fig. 4.18). Divergence of the EP flux occurs at the surface and at upper levels of the atmosphere, and is substantially weaker in simulations with a weak jet. For the case of a strong jet, maximal divergence takes place poleward of the jet core and near the surface, acting to accelerate of the mean flow in these regions. Interestingly, both convergence and divergence of the EP flux shift further equatorward in the case of a strong subtropical jet, extracting momentum from upper and lower levels, and depositing at the mid-level troposphere.

In regions where EP flux divergence acts to accelerate the flow, eddies transfer momentum upgradient (Vallis, 2007). In simulations with a strong subtropical jet, such acceleration of the mean flow occurs in midwinter, mostly poleward of the subtropical jet core at the upper levels, as well as in the midlatitudes (around latitude 40°N) in the lower levels (Fig. 4.18b).

Therefore, analysis of the EP flux indicates that as the subtropical jet strengthens and shifts more equatorward, extraction of momentum from the subtropics becomes more intense, both near the surface and at the upper levels of the atmosphere, poleward of the jet core. Throughout the seasonal cycle, the most striking feature is the absence of EP flux convergence in midlatitudes during midwinter, relative to fall or spring (Fig. 4.19), indicating that less momentum is being deposited by the eddies at these latitudes in midwinter, thus driving a weaker eddy-driven jet.

Chapter 5

Summary and conclusions

In this thesis we study the mechanisms that control the seasonal cycle of midlatitude storm tracks using both an observational analysis and numerical modeling. Specifically, we focus on the occurrence of a distinct minimum of storm track intensity during midwinter relative to fall and spring, known as the midwinter minimum. First observed over the Pacific basin (Nakamura, 1992), the midwinter minimum has been discussed in several previous studies. Yet, there is no agreement in the literature on what is the dominant underlying mechanism causing the midwinter minimum.

This work aims to identify the source of the midwinter minimum of storm track intensity and its relation to the jet variability throughout the seasonal cycle. The main questions that are addressed are as follows:

- How does the nature of the jet and its seasonal variability (in terms of acceleration and north-south shifts) affect the storm track intensity? Specifically, what is the influence of subtropical jet strength?

- How does the midwinter minimum change the eddy energy balance? Is it of a barotropic or baroclinic nature?

- What is the role of topography in the midwinter minimum occurrence? Does interaction with topography play a role in the transition seasons only? or also in midwinter?

The midwinter minimum is considered to be an intriguing phenomena, as it occurs despite an intense wintertime jet and enhanced baroclinicity, and raises questions regarding the applicability of linear theory predictions. On one hand, an intense subtropical jet (as found over the Pacific in winter) is considered favorable for the growth of baroclinic eddies due to its strong vertical shear (e.g., Lee and Kim, 2003). On the other hand, observational studies indicate that a strong subtropical jet is not necessarily associated with intense baroclinic growth, as occurs in the North Pacific (Nakamura, 1992;

Nakamura and Sampe, 2002), and in the southern hemisphere, where baroclinic growth of eddies has been shown to be weaker along an intense subtropical jet (Nakamura and Shimpo, 2004).

We find that similar to the well-known Pacific midwinter minimum, eddy kinetic energy over the North Atlantic is also reduced during winter relative to fall and spring, despite the stronger wintertime jet and its increased vertical shear (Fig. 2.1). The reduction over the Atlantic is smaller and persists for a shorter period. When the wintertime jet is stronger, this midwinter suppression of eddy activity is more pronounced (Fig. 2.5). Since the climatological Atlantic jet is weaker relative to the Pacific jet, the conditions for a midwinter suppression in the Atlantic are generally less favorable, yet a midwinter suppression often occurs in years of a strong jet (Afargan and Kaspi, 2017).

Next, we approach these questions by using an idealized GCM with moist dynamics and a seasonal cycle that we implemented in the model. Strengthening of the subtropical jet in winter leads to baroclinic growth of eddies primarily in the vicinity of the subtropical jet (Fig. 3.17), similar to the numerical experiments of Lee and Kim (2003). Throughout the seasonal cycle, the jet maximum shifts further equatorward (in winter) relative to its more poleward position in fall and spring (Fig. 3.19). Consequently, due to thermal wind balance, near-surface baroclinicity in the midlatitudes is reduced in winter (Fig. 3.22), resulting in a weaker baroclinic growth of transient eddies at these latitudes. These results verify the conclusion in Penny et al. (2013), which has not been emphasized in previous studies, that storm track intensity is not reduced throughout the entire Pacific domain, but mostly in the midlatitudes. These results are also consistent with Afargan and Kaspi (2017), showing that most of the midwinter suppression of EKE occurs in midlatitudes. In the zonally-symmetric model, a midwinter minimum-like behavior is simulated in winter and spring, which resembles the second half of the seasonal cycle in reanalysis data.

A more realistic seasonal cycle is obtained when a Gaussian mountain is implemented in the idealized model. We find that as the strength of the subtropical jet is increased, the midwinter minimum becomes more pronounced (Fig. 4.8), and resembles observations of the Pacific storm track (Nakamura, 1992), where below a certain threshold of subtropical jet strength, the storm track will exhibit a midwinter maximum of EKE, yet as the subtropical jet intensifies EKE will be reduced in midwinter. Using analysis of the eddy-mean energy budget, we are able to clarify some on the mechanisms leading to the midwinter minimum. We find that during midwinter, when the subtropical jet becomes stronger, the decay rate of EKE by barotropic conversion becomes strongly negative due to the increases barotropic shear, which should result in more energy for the eddies. However, the peak of the barotropic conversion shifts further equatorward as the subtropical jet is intensified, resulting in a smaller contribution of barotropic conversion to the EKE budget in midlatitudes (Fig. **??**). A similar equatorward shift occurs for the peak of baroclinic conversion, reducing the potential energy transfer from the mean flow to the eddies. It is found that this reduction in the contribution to the kinetic energy of the eddies through barotropic conversion may play an important role in the seasonal

variability of the transient eddies. Recently, Robert et al. (2017) have found that in the short term (i.e., within a few days after the jet maximum) synoptic eddies lose energy to the mean flow, by increasing the rate of decay of EKE by barotropic conversion which leads to a faster depletion of synoptic eddy total energy. Taken together, these findings suggest an explanation on why the midwinter minimum is more pronounced in midlatitudes: When subtropical jet intensity is increased, horizontal wind shear is increased, and the rate of EKE decay by barotropic conversion will become larger due to the increased shear. Due to the equatorward shift of the jet (which is a direct result of strengthening of the zonal wind in the subtropics), more kinetic energy of the eddies will be converted into kinetic energy of the mean flow in the subtropics, leading to a reduction of the energy of synoptic eddies, occurring just after the jet reaches its maximum intensity. In addition, Robert et al. (2017) also propose a negative feedback: due to the reduction in EKE, the synoptic eddies will deposit less momentum into the jet core, leading to deceleration of the eddy-driven jet. While this feedback can be relevant for years of midwinter minimum in the Atlantic domain (Afargan and Kaspi, 2017), in the case of the Pacific storm track (as also shown in our simulations), there is a distinction between the subtropical (or merged) jet which is more prominent in winter, and the eddy-driven jet which mostly develops during the shoulder seasons. A more intense subtropical jet, as occurs in winter, will lead to increased horizontal wind shear and therefore to weaker eddies. Less momentum will be deposited in midlatitudes, resulting in a weakening of the eddy-driven jet and midlatitude baroclinicity (see also EP flux analysis in section 4.9).

Baroclinic eddies propagate upward and equatorward of the baroclinic zone, before they break and dissipate (e.g., Edmon et al., 1980; Robinson, 2000). As a result, the eddies gain energy in midlatitudes (where they also converge momentum and generate an eddy-driven jet), while dissipating and losing energy in the subtropics. Strengthening of the subtropical jet in midwinter leads to a stronger horizontal wind shear and increased rate of barotropic decay of EKE into mean kinetic energy in the subtropics. In addition, an equatorward shift of the jet leads to a reduction of the meridional temperature gradient in midlatitudes and weakens the near-surface baroclinicity. As a result, less baroclinic growth occurs in midlatitudes, which in turn weakens the eddy-driven jet. The equatorward shift of the storm track also shifts the baroclinic zone to a more "stable" region in the subtropics, where baroclinicity does not act as in the midlatitudes (Nakamura and Shimpo, 2004; Sampe et al., 2010; Lachmy and Harnik, 2014). Lachmy and Harnik (2014) have shown that when the jet is more subtropical and located more equatorward, eddies tend to be weaker than in a case of a dominant eddy-driven jet, due to the lower-level potential vorticity structure.

Similarly, from momentum balance perspective, when the subtropical jet is more intense, the horizontal component of the EP flux acts to extract momentum from the subtropics and deposit in midlatitudes, in order to accelerate the mean flow poleward of the a subtropical jet and generate a more barotropic jet. In simulations with strong subtropical jet, such acceleration takes place in midlatitudes

during midwinter, either in the upper levels of the atmosphere or at the surface. Throughout the seasonal cycle, one of the main differences between midwinter and the shoulder seasons in simulations with strong subtropical jet is the absence of EP flux convergence in midlatitudes in midwinter, indicating that the eddies deposit less momentum into the midlatitudes, which decelerates the midlatitude jet and sustains the intense subtropical jet at the edge of the Hadley cell.

We find that an equatorward shift of the jet, as occurs in midwinter over the North Pacific, is associated with reduced EKE and a more pronounced midwinter minimum of storm track intensity. When the jet shifts more equatorward, meridional temperature gradient in midlatitudes is reduced, as well as the baroclinicity. Consequently, midlatitudes eddies become weaker, and their momentum flux convergence drives a weaker jet.

Note that the occurrence of a midwinter minimum of storm track intensity in response to strengthening of the subtropical jet is more robust when a localized asymmetry, in the form of a Gaussian mountain, is present. In the zonally symmetric case, EKE is enhanced only during spring, and resembles only the second peak of EKE of the Pacific storm track (Nakamura, 1992). There are several explanations for this. First, in the zonally symmetric configuration, storms are being generated everywhere, and their temporal average is zonally-symmetric. The presence of a localized asymmetry results in a localized baroclinic zone, where cyclones are being generated at the same location and decay in another (Kaspi and Schneider, 2013; Tamarin and Kaspi, 2017). Therefore, a temporal average in the zonally-asymmetric case will show a longitudinal separation between regions of baroclinic growth and regions of barotropic decay, enabling us to capture the midwinter suppression of EKE in the downstream region of the mountain. Further downstream, EKE is enhanced, similar to observations where storm track is enhanced over the Atlantic domain, which is often seeded by storms that originate over the western Pacific (Hakim, 2003). Similarly, Lachmy and Harnik (2014) have noticed that a mechanism for the weakening of baroclinic instability in the subtropical jet regime is found to be relevant for local zonal sections but not for the zonal mean.

We find that an addition of a Gaussian mountain to the idealized model mostly affects the shoulder seasons, by increasing midlatitude baroclinicity in fall and spring, essential for obtaining a realistic, Pacific-like, seasonal cycle. The main difference in the storm tracks between the zonally-symmetric and the zonally-asymmetric simulation lays in the generation of an intense, eddy-driven jet in midlatitudes during fall and spring, and its associated synoptic eddies. In our recent work (Yuval et al., 2018) we found that both in reanalysis data and in idealized simulations the seasonal differences in jet characteristics play an important role in the occurrence of the midwinter minimum. By simulating the Pacific temperature distribution it is found that forcing of a subtropical-like jet in winter leads to EKE being decreased, while forcing of an eddy-driven jet in the shoulder seasons results in EKE being increased. These results are consistent with the results presented earlier, indicating that reproducing the exact climatological conditions and the characteristics of the jet throughout the seasonal cycle is

essential for capturing seasonal features, such as the midwinter minimum.

Furthermore, it has been shown that in winters of strong subtropical jet, disturbances rarely become mature systems, and therefore their amplitude is weaker (Penny et al., 2013). We find that the midwinter minimum becomes more pronounced as the ratio between the eddy time-scale and the seasonal time-scale is increased (Fig. 3.25, see also section 3.8). Taken together, these results suggest that when the seasonal time-scale changes in a slower rate (i.e, longer orbital period), while keeping the synoptic time-scale unchanged, synoptic eddy dynamics are dominated by short-term processes (Robert et al., 2017) which usually persists only for a few days. When the eddies travel under slowly-changing conditions for a longer time, adjustment of the background gradients (due to the eddy activity) occurs faster than the external forcing of the meridional temperature gradient, resulting in weaker amplitudes and less mature systems during winter.

Bibliography

Afargan, H., and Y. Kaspi, 2017: A midwinter minimum in North Atlantic storm track intensity in years of a strong jet. *Geophys. Res. Lett.*, **44**.

Ambaum, M. H., B. J. Hoskins, and D. B. Stephenson, 2001: Arctic oscillation or north atlantic oscillation? *J. Climate*, **14 (16)**, 3495–3507.

Blackmon, M., J. Wallace, N. Lau, and S. Mullen, 1977: An observational study of the Northern Hemisphere wintertime circulation. *J. Atmos. Sci.*, **34 (7)**, 1040–1053.

Blackmon, M. L., 1976: A climatological spectral study of the 500 mb geopotential height of the northern hemisphere. *Journal of the Atmospheric Sciences*, **33 (8)**, 1607–1623.

Bordoni, S., 2007: On the role of eddies in monsoonal circulations: Observations and theory. Ph.D. thesis, University of California, Los Angeles.

Bordoni, S., and T. Schneider, 2008: Monsoons as eddy-mediated regime transitions of the tropical overturning circulation. *Nature Geoscience*, **1 (8)**, 515–519.

Brayshaw, D. J., B. Hoskins, and M. Blackburn, 2008: The storm-track response to idealized sst perturbations in an aquaplanet gcm. *J. Atmos. Sci.*, **65 (9)**, 2842–2860.

Brayshaw, D. J., B. Hoskins, and M. Blackburn, 2009: The basic ingredients of the north atlantic storm track. part i: Land–sea contrast and orography. *J. Atmos. Sci.*, **66 (9)**, 2539–2558.

Chang, E. K. M., 2001: GCM and observational diagnoses of the seasonal and interannual variations of the Pacific storm track during the cool season. *J. Atmos. Sci.*, **58**, 1784–1800.

Chang, E. K. M., and Y. Guo, 2011: Comments on"The source of the midwinter suppression in storminess over the North Pacific". *J. Climate*, **24**, 5187–5191.

Chang, E. K. M., and Y. Guo, 2012: Is Pacific storm-track activity correlated with the strength of upstream wave seeding? *J. Climate*, **25**, 5768–5776.

Chang, E. K. M., S. Lee, and K. L. Swanson, 2002: Storm track dynamics. *J. Climate*, **15**, 2163–2183.

Chang, E. K. M., and I. Orlanski, 1993: On the dynamics of a storm track. *J. Atmos. Sci.*, **50 (7)**, 999–1015.

Chang, E. K. M., and P. Zurita-Gotor, 2007: Simulating the seasonal cycle of the Northern Hemisphere storm tracks using idealized nonlinear storm-track models. *J. Atmos. Sci.*, **64 (7)**, 2309–2331.

Charney, J., 1947: The dynamics of long waves in a baroclinic westerly current. *J. Meteor*, **4 (5)**, 135–161.

Christoph, M., U. Ulbrich, and P. Speth, 1997: Midwinter suppression of Northern Hemisphere storm track activity in the real atmosphere and in gcm experiments. *J. Atmos. Sci.*, **54 (12)**, 1589–1599.

Deng, Y., and M. Mak, 2005: An idealized model study relevant to the dynamics of the midwinter minimum of the Pacific storm track. *J. Atmos. Sci.*, **62 (4)**, 1209–1225.

Drouard, M., G. Rivière, and P. Arbogast, 2015: The link between the north pacific climate variability and the north atlantic oscillation via downstream propagation of synoptic waves. *Journal of Climate*, **28 (10)**, 3957–3976.

Eady, E., 1949: Long waves and cyclone waves. *Tellus*, **1 (3)**, 33–52.

Edmon, H., B. Hoskins, and M. McIntyre, 1980: Eliassen-palm cross sections for the troposphere. *J. Atmos. Sci.*, **37 (12)**, 2600–2616.

Eichelberger, S. J., and D. L. Hartmann, 2007: Zonal jet structure and the leading mode of variability. *J. Climate*, **20 (20)**, 5149–5163.

Frierson, D., I. Held, and P. Zurita-Gotor, 2006: A gray-radiation aquaplanet moist gcm. part i: Static stability and eddy scale. *J. Atmos. Sci.*, **63 (10)**, 2548–2566.

Gerber, E. P., and G. K. Vallis, 2009: On the zonal structure of the north atlantic oscillation and annular modes. *J. Atmos. Sci.*, **66 (2)**, 332–352.

Hakim, G., 2003: Developing wave packets in the North Pacific storm track. *Mon. Weather Rev.*, **131 (11)**, 2824–2837.

Harnik, N., and E. K. M. Chang, 2004: The effects of variations in jet width on the growth of baroclinic waves: Implications for midwinter Pacific storm track variability. *J. Atmos. Sci.*, **61**, 23–40.

Harnik, N., E. Galanti, O. Martius, and O. Adam, 2014: The anomalous merging of the African and North Atlantic jet streams during the Northern Hemisphere winter of 2010. *J. Climate*, **27 (19)**, 7319–7334.

Hartmann, D., 1994: *Global physical climatology*, Vol. 56. Academic Pr.

Hurrell, J. W., 1995: Decadal trends in the North Atlantic oscillation: regional temperatures and precipitation. *Science*, **269 (5224)**, 676–679.

James, I., 1987: Suppression of baroclinic instability in horizontally sheared flows. *J. Atmos. Sci.*, **44 (24)**, 3710–3720.

James, I., and L. Gray, 1986: Concerning the effect of surface drag on the circulation of a baroclinic planetary atmosphere. *Q. J. ROY. METEOR. SOC.*, **112 (474)**, 1231–1250.

Kalnay, E., and Coauthors, 1996: The ncep/ncar 40-year reanalysis project. *Bull. Am. Meteor. Soc.*, **77 (3)**, 437–471.

Kanamitsu, M., W. Ebisuzaki, J. Woollen, S.-K. Yang, J. Hnilo, M. Fiorino, and G. Potter, 2002: Ncep–doe amip-ii reanalysis (r-2). *Bull. Am. Meteor. Soc.*, **83 (11)**, 1631–1643.

Kaspi, Y., and T. Schneider, 2013: The role of stationary eddies in shaping midlatitude storm tracks. *J. Atmos. Sci.*, **(2013)**.

Lachmy, O., and N. Harnik, 2014: The transition to a subtropical jet regime and its maintenance. *J. Atmos. Sci.*, **71 (4)**, 1389–1409.

Lee, S., and S. Feldstein, 1996: Mechanism of zonal index evolution in a two-layer model. *J. Atmos. Sci.*, **53 (15)**, 2232–2246.

Lee, S., and H.-k. Kim, 2003: The dynamical relationship between subtropical and eddy-driven jets. *J. Atmos. Sci.*, **60 (12)**, 1490–1503.

Lee, S.-S., J.-Y. Lee, K.-J. Ha, B. Wang, A. Kitoh, Y. Kajikawa, and M. Abe, 2013: Role of the tibetan plateau on the annual variation of mean atmospheric circulation and storm-track activity. *J. Climate*, **26 (14)**, 5270–5286.

Lindzen, R., and B. Farrell, 1980: A simple approximate result for the maximum growth rate of baroclinic instabilities. *J. Atmos. Sci.*, **37 (7)**, 1648–1654.

Lorenz, E. N., 1955: Available potential energy and the maintenance of the general circulation. *Tellus*, **7**, 157–167.

Merlis, T. M., 2012: The general circulation of the tropical atmosphere and climate changes. Ph.D. thesis, California Institute of Technology.

Nakamura, H., 1992: Midwinter suppression of baroclinic wave activity in the Pacific. *J. Atmos. Sci.*, **49**, 1629–1642.

Nakamura, H., T. Izumi, and T. Sampe, 2002: Interannual and decadal modulations recently observed in the Pacific storm track activity and east asian winter monsoon. *J. Climate*, **15 (14)**, 1855–1874.

Nakamura, H., and T. Sampe, 2002: Trapping of synoptic-scale disturbances into the North-Pacific subtropical jet core in midwinter. *Geophys. Res. Lett.*, **29 (16)**, 1761.

Nakamura, H., and A. Shimpo, 2004: Seasonal variations in the southern Hemisphere storm tracks and jet streams as revealed in a reanalysis dataset. *J. Climate*, **17 (9)**, 1828–1844.

O'Gorman, P., and T. Schneider, 2008: The hydrological cycle over a wide range of climates simulated with an idealized gcm. *J. Climate*, **21 (15)**, 3815–3832.

Orlanski, I., 2003: Bifurcation in eddy life cycles: Implications for storm track variability. *J. Atmos. Sci.*, **60 (8)**, 993–1023.

Orlanski, I., and J. Katzfey, 1991: The life cycle of a cyclone wave in the southern Hemisphere. part i: Eddy energy budget. *J. Atmos. Sci*, **48 (17)**, 1972–1998.

O'Rourke, A. K., and G. K. Vallis, 2013: Jet interaction and the influence of a minimum phase speed bound on the propagation of eddies. *J. Atmos. Sci*, **70 (8)**, 2614–2628.

Park, H., J. Chiang, and S. Son, 2010: The role of the central Asian mountains on the midwinter suppression of North Pacific storminess. *J. Atmos. Sci.*, **67 (11)**, 3706–3720.

Peixoto, J., and A. Oort, 1992: *Physics of climate*. New York, NY (United States); American Institute of Physics.

Penny, S., G. Roe, and D. Battisti, 2010: The source of the midwinter suppression in storminess over the North Pacific. *J. Climate*, **23 (3)**, 634–648.

Penny, S., G. Roe, and D. Battisti, 2011: Reply to Comments on "The source of the midwinter suppression in storminess over the North Pacific". *J. Climate*, **24 (19)**, 5192–5194.

Penny, S. M., D. S. Battisti, and G. H. Roe, 2013: Examining mechanisms of variability within the Pacific storm track: Upstream seeding and jet-core strength. *J. Climate*, **26 (14)**, 5242–5259.

Ren, H.-L., F.-F. Jin, and J.-S. Kug, 2014: Eddy-induced growth rate of low-frequency variability and its mid-to late winter suppression in the Northern Hemisphere. *J. Atmos. Sci.*, **71 (7)**, 2281–2298.

Ren, X., X. Yang, and C. Chu, 2010: Seasonal variations of the synoptic-scale transient eddy activity and polar front jet over east asia. *J. Climate*, **23 (12)**, 3222–3233.

Riviere, G., P. Arbogast, and A. Joly, 2015: Eddy kinetic energy redistribution within idealized extratropical cyclones using a two-layer quasi-geostrophic model. *Quarterly Journal of the Royal Meteorological Society*, **141 (686)**, 207–223.

Riviere, G., and I. Orlanski, 2007: Characteristics of the Atlantic storm-track eddy activity and its relation with the North Atlantic oscillation. *J. Atmos. Sci.*, **64 (2)**, 241–266.

Robert, L., G. Rivière, and F. Codron, 2017: Positive and negative eddy feedbacks acting on midlatitude jet variability in a three-level quasigeostrophic model. *J. Atmos. Sci.*, **74 (5)**, 1635–1649.

Robinson, W. A., 2000: A baroclinic mechanism for the eddy feedback on the zonal index. *J. Atmos. Sci.*, **57 (3)**, 415–422.

Sampe, T., H. Nakamura, A. Goto, and W. Ohfuchi, 2010: Significance of a midlatitude sst frontal zone in the formation of a storm track and an eddy-driven westerly jet. *J. Climate*, **23 (7)**, 1793–1814.

Seager, R., N. Harnik, Y. Kushnir, W. Robinson, and J. Miller, 2003: Mechanisms of hemispherically symmetric climate variability. *J. Climate*, **16 (18)**, 2960–2978.

Seager, R., N. Naik, M. Ting, M. Cane, N. Harnik, and Y. Kushnir, 2010: Adjustment of the atmospheric circulation to tropical Pacific SST anomalies: Variability of transient eddy propagation in the Pacific–North America sector. *Q. J. R. Meteorol. Soc.*, **136 (647)**, 277–296.

Son, S.-W., and S. Lee, 2005: The response of westerly jets to thermal driving in a primitive equation model. *J. Atmos. Sci.*, **62 (10)**, 3741–3757.

Tamarin, T., and Y. Kaspi, 2017: Mechanisms controlling the downstream poleward deflection of midlatitude storm tracks. *J. Atmos. Sci.*, **74 (2)**, 553–572.

Thorncroft, C., B. Hoskins, and M. McIntyre, 1993: Two paradigms of baroclinic-wave life-cycle behaviour. *Q. J. R. Meteorol. Soc.*, **119 (509)**, 17–55.

Vallis, G., 2007: Atmospheric and oceanic fluid dynamics: Fundamentals and large-scale circulation. UK: Cambridge University Press; ISBN 978-0-521-84969-2.

Walker, C. C., and T. Schneider, 2006: Eddy influences on Hadley circulations: Simulations with an idealized GCM. *J. Atmos. Sci.*, **63 (12)**, 3333–3350.

Wills, R. C., and T. Schneider, 2016: How stationary eddies shape changes in the hydrological cycle: Zonally asymmetric experiments in an idealized gcm. *J. Climate*, **29 (9)**, 3161–3179.

Woollings, T., A. Hannachi, and B. Hoskins, 2010: Variability of the North Atlantic eddy-driven jet stream. *Q. J. R. Meteorol. Soc.*, **136 (649)**, 856–868.

Yin, J., 2002: The peculiar behavior of baroclinic waves during the midwinter suppression of the Pacific storm track. Ph.D. thesis, University of Washington, 121 pp.

Yun, K.-S., Y.-W. Seo, K.-J. Ha, J.-Y. Lee, and A. Kitoh, 2016: The seasonally varying effect of the tibetan plateau on Northern Hemispheric blocking frequency and amplitude. *Clim. Dyn.*, **47 (7-8)**, 2527–2541.

Yuval, J., H. Afargan, and Y. Kaspi, 2018: The seasonal subtropical to eddy-driven jet transition leading to Pacific midwinter minimum in eddy activity. *Geophys. Res. Lett.*

Yuval, J., and Y. Kaspi, 2016: Eddy activity sensitivity to changes in the vertical structure of baroclinicity. *J. Atmos. Sci.*, **73 (4)**, 1709–1726.

Yuval, J., and Y. Kaspi, 2017: The effect of vertical baroclinicity concentration on atmospheric macroturbulence scaling relations. *J. Atmos. Sci.*, **74 (5)**, 1651–1667.

Zhang, Y., and I. Held, 1999: A linear stochastic model of a gcm's midlatitude storm tracks. *J. Atmos. Sci.*, **56 (19)**, 3416–3435.